INAUGURAL-DISSERTATION
zur
Erlangung der Doktorwürde

der
Naturwissenschaftlich-Mathematischen
Gesamtfakultät

der
Ruprecht-Karls-Universität
Heidelberg

Graduiertenkolleg 273
Einwirkung Fluider Phasen auf
locker- und Festgesteine

vorgelegt von
Dipl. Geophysiker Thierry Marbach
aus Strasbourg / Frankreich

2002

Fluid/rock Interaction History of a Faulted Rhyolite-Granite Contact, Eastern Rhine Graben Shoulder, SW-Germany:

Alteration Processes Determined by Sr- Pb-Isotopes, Th/U-Disequilibria and Elemental Distributions.

Gutachter: Prof. Dr. Augusto Mangini

Priv. Doz. Dr. Laurence N. Warr

Zusammenfassung

Die Verwitterungsgeschichte der Schauenburg Störung, ist anhand des gestörte Granit-Rhyolith Kontaktes, mit Isotopen- und Elementverteilungen erforscht worden. Die Schauenburg Störungszone befindet sich entlang der östlichen Rheingrabenschulter, in der Nähe von Heidelberg (SW-Deutschland).

Haupt- und Spurenelementanalysen geben Informationen über die chemischen Umwandlungen, die durch Verwitterungen verursacht werden. Es bestehen petrografische Unterschiede, weil das Profil den Granit-Rhyolith Kontakt kreuzt. Die Unterschiede werden aber auch durch den unterschiedlichen Verwitterungsgrad durch die Fluid-Zirkulation entlang der Störung verursacht. Der Granit-Rhyolith Kontakt setzt die Primärstruktur fest. Nur die inkompatibelsten Elemente (Si, Al, Zr, Hf) behalten ihre ursprünglichen Signatur und zeugen von einer Mischung zwischen typischen Granit- und Rhyolith- Lithologie über den verwitterten Zonen (cataclasite). Die beweglicheren Elemente zeigen einen anderen Aufbau innerhalb der verwitterten Zonen (cataclasite), vornehmlich ein starkes Auslaugen der Kationen. Die geochemischen Indikatoren deuten auf mindestens ein starkes hydrothermales Ereignis hin, mit reduzierenden Bedingungen in den verwitterten Zonen.

Die isotopischen Analysen ergaben die qualitativen und zeitlichen Informationen. Die verschiedenen isotopischen Systeme (Rb/Sr -, U/Pb-Isotope und Th/U-Ungleichgewicht) zeigen eine komplizierte Geschichte der mehrphasigen Fluid/Rock Verwitterung im Laufe der Permischen Extrusion, bemerkenswerte Störungen während des hydrothermalen Ereignisses im späten Jura, das tertiäre Rifting des Rheingrabens und die rezente quartäre Verwitterung. Die Granitzone zeigt eine neue, zurückgestellte Rb-Sr Isotopen Signatur, die das ursprüngliche Karbon Alter ersetzt hat. Die Rb-Sr Daten der Granitproben produzieren ein Isochronenalter des Gesamtaufschlusses von ± 152 5,7 Ma (2σ Fehler) im Einklang mit dem weithin bekannten hydrothermalen Ereignis im späten Jura (135-160 Ma). Die Felsenentwicklungslinien für Pb stützen ein tertiäres hydrothermales Ereignis (54 Ma ± 16; 1σ Fehler), möglicherweise in Anschluss an die Entwicklung des Rheingrabens. Die

Profilproben haben Uran- und Thorium- Wiederverteilungprozesse erfahren, die innerhalb der letzten ~ 10^6 Jahre aufgetreten sind. Die Proben der verwitterten Zonen deuten auf eine kompliziertere Geschichte des Uran Austausches mit der wäßrigen Phase hin. Dieser Uran-Austausch ist proportional zur Porosität. Der beste Näherungswert wird für einen Uran-Austauschkoeffizienten (λe) erreicht, der von 2,5 E-06 [a^{-1}] in der Mitte der verwitterten Zonen bis 2,5 E-05 [a^{-1}] auf den Seiten der verwitterten Zonen reicht.

Résumé

Cette étude géochimique et isotopique a été mené à travers un contact faillé entre granite et rhyolite afin d'étudier l'altération de la faille Schauenburg située sur l'épaulement Est du graben rhénan, près de Heidelberg (SO Allemagne).

L'analyse des éléments majeurs et traces permet d'obtenir des informations concernant les changements induit par l'altération. Les différences sont d'abord d'ordre pétrographique puisque le profil traverse un contact faillé entre granite et rhyolite. Les différences sont également dues à différent degré d'altération causé par la circulation de fluides le long du système faillé qui a drainé les processus d'altération. Le contact faillé granite-rhyolite constitue la structure primaire. Seul les éléments les plus incompatibles (Si, Al, Zr, Hf) ont préservé leur signature qui reflète dans les zones altérées (cataclasite) un mélange constitué de granite et de rhyolite. Les éléments plus mobiles affichent différentes compositions pour les zones altérées (cataclasite) notamment une forte perte en cations. Les traceurs géochimiques suggèrent également au moins un processus hydrothermal accompagné par des conditions réductrices dans les zones altérées.

Les analyses isotopiques donnent une information qualitative et temporelle. L'utilisation de plusieurs systèmes isotopiques (Rb/Sr, U/Pb, déséquilibre U-Th) révèlent une altération complexe eau-roche durant le volcanisme au Permien, montrant des effets notables pendant l'hydrothermalisme tardif du Jurassique, durant la formation tertiaire du rift rhénan et de plus récente altération quaternaire. Le granite du profil présente une signature isotopique Rb-Sr qui remplace la signature originelle acquise durant l'intrusion au Carbonifère. L'isochrone Rb-Sr roche totale du granite donne un âge de 152 ± 5,7 Ma (2σ erreur) en accord avec l'hydrothermalisme tardif du Jurassique. Les régression des données du Pb s'accordent avec des processus hydrothermaux tertiaire (54 Ma ± 16; 1σ erreur), connectés au développement du graben rhénan. Les échantillons étudiés montrent un processus de redistribution d'uranium et de thorium qui s'est effectué durant les dernières ~ 10^6 années. Les échantillons des zones altérées ont subit un échange d'uranium avec la phase aqueuse plus complexe. Cet échange d'uranium est proportionnel à la porosité. La meilleure

approximation est obtenue pour une coefficient d'échange pour l'uranium (λ_E) allant de 2,5 E-06 [a^{-1}] au centre des zones altérées à 2,5 E-05 [a^{-1}] sur les cotés des zones altérées.

Abstract

The alteration history of the Schauenburg fault has been investigated with isotope and element distributions across the faulted granite-rhyolite contact. The Schauenburg fault zone is situated along the eastern Rhine Graben shoulder, close to Heidelberg (SW-Germany).

Major and trace element analyses allow to obtain information concerning the chemical changes induced by alteration. Differences are partly petrographic because the profile crosses the granite-rhyolite contact, but they are also due to different alteration levels induced by fluid circulation along the fault system which has drained the alteration processes. The granite-rhyolite contact constitutes the primary structure. Only the most incompatible elements (Si, Al, Zr, Hf) retain their original signatures and reflect a mixing between typical granite and rhyolite lithologies across the altered zones (cataclasite). The more mobile elements show a different composition within the altered zones (cataclasite) notably a high leaching of cations. The geochemical tracers also suggest at least one strong hydrothermal event with reducing conditions in the altered zones.

The isotopic analyses delivered qualitative and temporal information. The use of several isotopic systems, Rb/Sr -, U/Pb-isotopes and Th/U disequilibria, reveals a complex history of polyphase fluid/rock interaction following the Permian volcanic extrusion, showing notable disturbances during the late Jurassic hydrothermal activities, the Tertiary rifting of the Rhine Graben and more recent Quaternary alteration. The granite zone of the sampling profile has underwent an event which set up a new Rb-Sr isotopic composition and reset the Rb/Sr system which originatly corresponded to the Carboniferous intrusion ages. The Rb-Sr data of the granite samples produce a whole rock isochron of 152 ± 5,7 Ma (2σ error) in good agreement with the well-known late Jurassic hydrothermal event (135-160 Ma). The rocks evolution lines for Pb support a Tertiary hydrothermal event (54 Ma ± 16; 1σ error), potentially connected with the development of the Rhine Graben. The profile samples have undergone uranium and thorium redistribution processes which have occurred within the last ~ 10^6 years. The samples of the altered zones record a more

complex history of uranium exchange with the aqueous phase. This uranium exchange is proportional to the porosity. The best approximation is reached for an exchange coefficient (λ_E) for uranium ranging from 2,5 E-06 [a^{-1}] in the middle of the altered zones to 2,5 E-05 [a^{-1}] on the sides of the altered zones.

Table of Contents

Chapter 1
Introduction

The mobility and transport of fluids are important processes for the migration of ions and the formation of mineral deposits. It is of economical and scientific interest to investigate zones of high fracture permeability like fault structures on a large and smaller scale to observe and better understand the evolution of fluid-rock interaction processes. Estimates of the change in isotopic composition and concentration during fluid-rock interaction and fluid circulation are central to several areas of the earth and environmental sciences, including waste management (e.g. nuclear waste), ore exploration, and evaluation of nutrient migration and the erosion rate.

The alteration of rocks at the Earth's surface and at depth occurs in response to circulating fluids of various origins, such as ground waters, basinal brines, or hydrothermal fluids. Faults are therefore important as sites of fluid migration and mineral alteration and it is possible to study both surface and subsurface fluids alteration on the same location (fig. 1.1). Such rock alteration, in this case granite alteration, involves physical and mineralogical changes, which occur in response to shifts in the kinetics caused by the surrounding milieu (e.g. hydrothermal behavior of the fault) and leads to fundamental changes in chemical and isotopic properties.

1.1 The alteration of granite

Alteration of granite occurs by a complex interaction of physical and chemical processes that modifies the rock in some general or specific way. The minerals may be broken down, dissolved or converted to new minerals by a variety of processes which can be separated into two groups.

Mechanical alteration is the disintegration of rock by physical processes and involves no change in chemical composition; the rock is broken down by fracturing (brittle response to stress) into smaller fragments by physical means:

- Granite is an igneous intrusive rock that forms under high pressure and high temperature. It cools slowly, forming large crystals. As a silica-rich rock, it shows considerable resistance to alteration (Sausse et al., 2001). As the granite rises to the surface, it loses external pressure inducing an exfoliation (peeling off in sheet layers). Decompression and cooling produce fractures in the granite batholith structure (fig. 1.1).

- Frost action in the form of freeze/thaw cycles, occurs when pore water freezes to ice. It has been estimated that water expands between 8 to 11 percent during the freezing process (Sausse et al., 2001). This increase of internal pressure combined with repeated freeze/thaw cycles produces micro-fissures, cracks, flaking and spalling.

Chemical alteration is the decomposition of rocks by chemical alteration of the constituent minerals. The internal structure of the mineral is dissolved, and new minerals are formed by precipitation or replacement and recrystallization processes. This kind of alteration is important for this study because it occurs during the fluid-rock interaction, especially during hydrothermal circulation:

- Hydrolysis is the dissolution and alteration process that affects silicate minerals in granite-type rocks. Hydrolysis reactions add water to the new products. feldspars are an important silicate mineral group in granite and granite-type stones, with their general formulas containing potassium, sodium and calcium (Sausse, 2002). These soluble elements are leached during the chemical reaction with acidicly charged waters and carried away. This process promotes permeability increases, producing more reactive surface area. Under certain conditions clay minerals are formed (kaolinite) while the colloidal silica is removed by the solution (Goldich, 1938). This process is irreversible.

- Oxidation is an important process in the alteration of iron and magnesium rich minerals. It is accelerated by moisture and high temperatures. Mineralogically iron occurs in three states: metallic, ferrous (Fe^{2+}) and ferric (Fe^{3+}). During the oxidation process Iron II is converted to Iron III resulting in color changes and a weakening of

the mineral structure. Ferrousmagnesian silicate minerals that undergo oxidation are responsible for the appearance of rust spots on some granite-type rocks. During the oxidation process the volume of the mineral structure may increase, usually making it softer and weaker and rendering it more vulnerable to further chemical alteration.

In nature, mechanical and chemical alteration occur simultaneously. While one process may dominate in a given area, depending on the climatic variation and rock composition, mechanical and chemical alteration processes generally attack the rock at the same time. The mechanical processes generally lead to a weakening of the rock, increasing its permeability providing greater penetration of water and increasing the areas for the chemical alteration processes. The rate of alteration is determined by the intensity and duration of the reactions involved (Sausse, 2002).

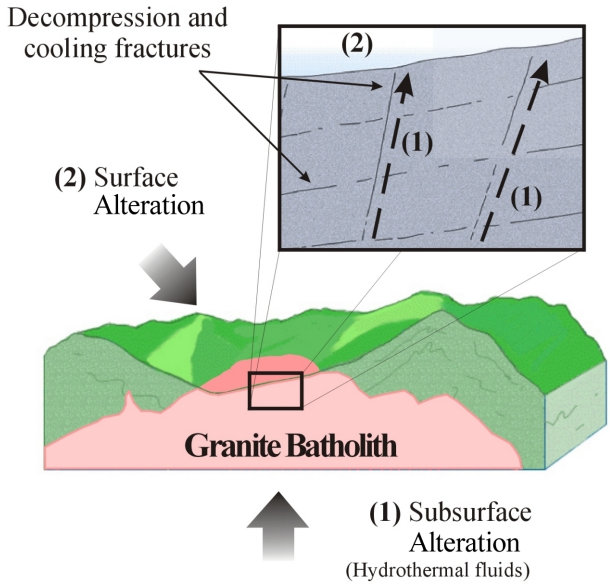

Figure 1.1: The alteration of granite.

1.2 Previous work

The features of chemical elements and their isotopes stored in geological formations and subjected to alteration processes have been the subject of numerous experimental investigations with the aim to understand the physical and chemical mechanisms responsible for element mobility and migration (Recio et al., 1997; Kostitsyn and Kremenetskiy, 1995; Schaltegger, 1990; Simon, 1990; Farmer and Depaolo, 1987; Zielinski et al., 1981; Brooks, 1968).

Many works have addressed recent alteration processes of granite. White et al. (2001) show with petrographic observations combined with elemental balancing and $^{87}Sr/^{86}Sr$ ratios, that plagioclase is converted to kaolinite at depths > 6 m in the granitic bedrock. They also measured the propagation rates of alteration fronts, which, based on cosmogenic dating and the primary hydraulic conductivities (describing the rates of meteoric water penetration) are between 4 and 7 $m/10^6$ years. Harlavan and Erel (2002), Erel et al. (1994) investigated the release of Pb and rare earth elements (REE) during granitoid alteration through dissolution experiments. During the early stages of granitoid dissolution, Pb and REE were preferentially released from some of the accessory phases (i.e., allanite, sphene, and apatite). Using the isotopic ratios of Pb, major elemental compositions, and REE concentrations, they established the following order of the alteration of accessory phases: allanite → apatite → sphene. The observed systematic changes in the isotopic composition of lead with time demonstrates the potential of lead isotopes to assess the degree (or maturity) of chemical alteration in granitoids.

Ancient alteration processes have been investigated by Audétat at al. (2000) who studied the chemical evolution of silicate melts and aqueous fluids during the late magmatic to the early hydrothermal transition. Komminou and Yardley (1996) proposed a thermodynamic model for hydrothermal alteration observed in deep drilling within the Rhine graben, providing information concerning hydrothermal alteration during rifting. The alteration of a volcanic deposit has been studied by Techer et al. (2001). The study, based on combining chemical, mineralogical and isotopic methods, shows that elements released by alteration of the basaltic glass, notably strontium, did not diffuse into the surrounding clay. This provides a natural analog for the deep geological disposal of nuclear waste, and highlights the importance of clay barriers.

1.3 Project description.

This study forms part of the project group “alteration processes” from the “Fluid-rock interaction” research program (Graduiertenkolleg 273, Einwirkung Fluider Phasen auf Locker- und Festgesteine) of the University of Heidelberg, funded by the Deutsche Forschungsgemeinschaft, DFG (German Research Council).

The project focuses on the alteration of rocks and minerals caused and controlled by fluids in the Rhine Graben area (chapter 2). Because of its well-constrained tectonic history, the Rhine Graben rift system provides a unique setting for this investigation. Due to uplift of the graben shoulders, various crustal levels are exposed at the surface today, where a wide spectrum of rock types can be sampled, reflecting a broad range of the Rhine graben history. This offers the opportunity to study rock and mineral alteration phenomena that occurred at different times of regional crustal evolution, under conditions resembling the present Earth's surface and at depth, in closely related materials and environments.

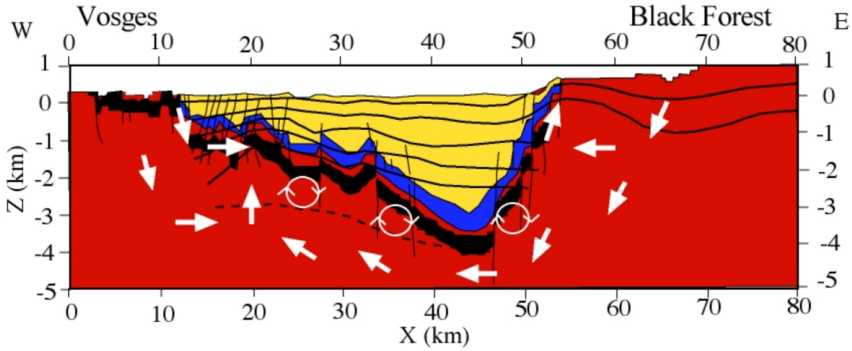

Figure 1.2: Rhine graben deep fluid circulation model. The cycled arrows indicated open fault. Notice the east-west circulation of the deep fluids. (Pribnow and Clauser, 1999).

The aim of this work is to investigate the isotope and element distributions and mobility across a faulted rhyolite-granite contact, situated along the eastern Rhine Graben shoulder, close to Heidelberg (SW-Germany). Rb/Sr -, U/Pb-isotopes and Th/U disequilibria are determined on the same samples to study the isotopic changes which occur during hydrothermal and recent alteration processes. The Schauenburg fault zone presents an excellent chance to investigate the alteration processes of felsic magmatic rocks and other associated fluid-rock-interaction processes along fault zones. The "Heidelberger Granite" and the overlaying Permian rhyolite are in faulted contact and thus provide two different geochemical and isotopic sources. This provides additional tools for a finer interpretation of the events which affected the history of the faulted granite. This work provides a source of data for further work on alteration processes and has implications for the investigation of the geothermal borehole of Soultz-sous-forêt (France), characterized by deep fluid circulation (fig. 1.2) similar to those of the graben shoulders before the uplift.

The studied granite experienced a complex alteration history of polyphase fluid/rock interaction in the course of Permian volcanic extrusion, late Jurassic hydrothermal activities, Tertiary formation of the Rhine Graben, and more recent Quaternary alteration. Based on previous work the, the following scenario of geological events are outlined (fig. 1.3).

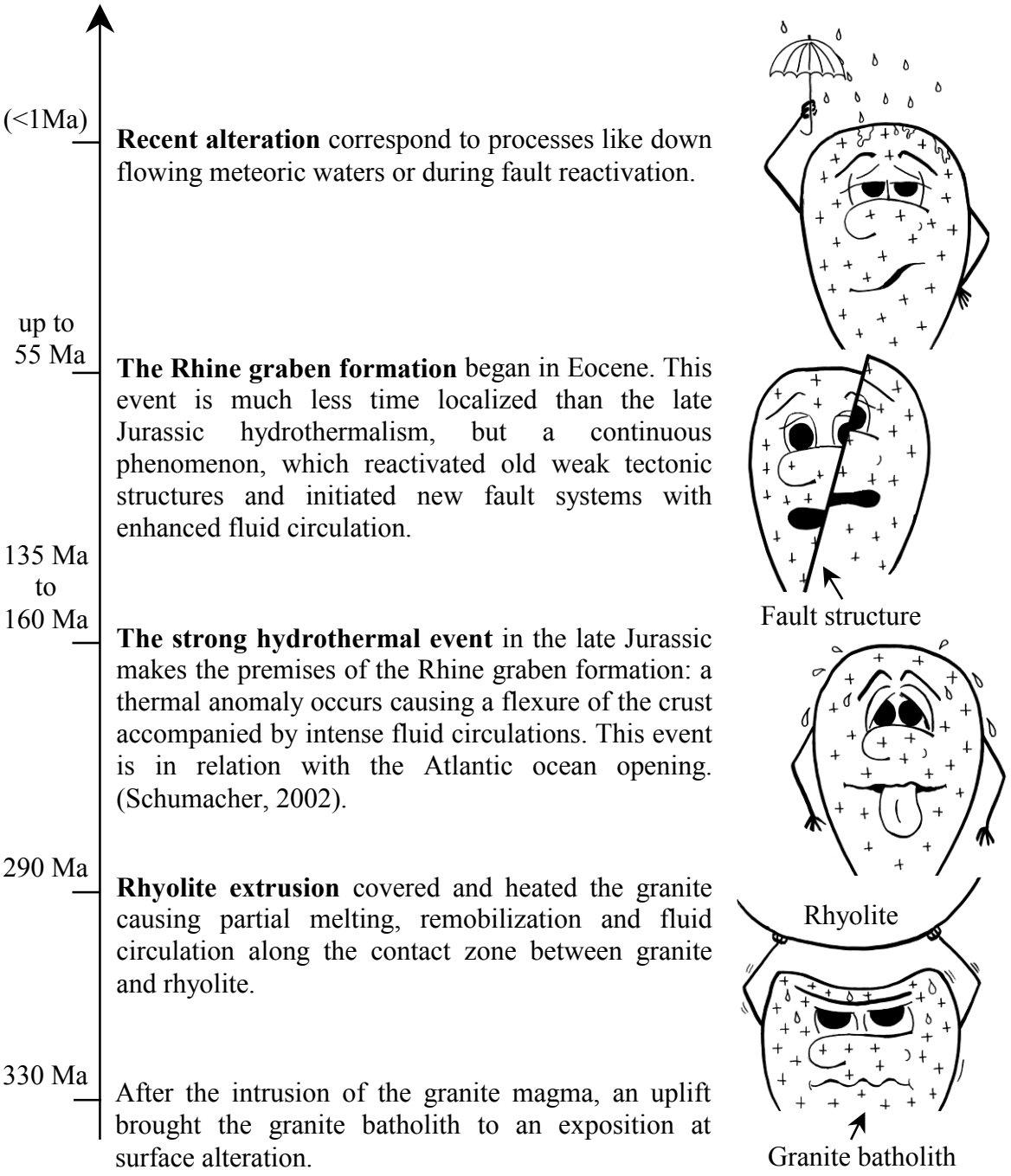

Figure 1.3: Geological scenario for the studied granite batholith.

There is the possibility that younger alteration overprint the signatures of older alteration phases. To address this problem, several isotopic systems are analyzed. Different alteration mechanisms (intense to weak) may then be traced by their geochemical and isotopical response.

The different alteration events are here studied with combining two complementary aspects:

- Major and trace element analyses to obtain quantitative information concerning the chemical changes induced by alteration,

- Isotopic analyses for qualitative and temporal information from U-Th-Pb and Rb-Sr isotope systems and Th/U disequilibria.

Application of the U-Th-Pb isotope systems, as well as the Rb-Sr system, is based on the fact that in a single rock individual minerals attain diagnostic isotope signatures in U/Pb, U/Th, Th/Pb and Rb/Sr ratios in the course of the mineral formation. The isotopic composition of the whole rock changes with the degree of alteration of each mineral phase and thus reflects the features of the alteration processes. Varying types and intensities of alteration (hydrothermal events, tectonic events) can be investigated with Rb/Sr and U/Pb-isotopes. The U-Th series radionuclides, because of their widely different geochemical behaviors allow through the U/Th disequilibria method to characterize weak and/or recent alteration processes (down flowing meteoric waters, fault reactivation, “cold” fluid circulation). The U-series nuclides provide a unique tool in this respect because disequilibrium in this series can potentially constrain both the extend and timing of elemental fractionation (Osmond and Ivanovich, 1992).

Chapter 2
Fluid/rock interaction history of the Rhine Graben

2.1 The Rhine graben: geodynamic settings and history

The Rhine graben rift, situated in western Europe, is one of the best geochemically and geophysically characterized continental rifts. Normal faults, trending parallel to the axis of extension, separate the graben from the adjacent Hercynian granitic massifs (fig. 2.1). A middle Eocene (40 Ma) unconformity separates pre-rift sedimentary units of up to 2 km in thickness from synrift sediments that can reach a thickness of more than 3 km (Sengör et al., 1978; Villemin et al., 1986). The Triassic (205 to 245 Ma) Buntsandstein, a red-bed sandstone, and the Triassic Muschelkalk, a dolomitic limestone with evaporites, constitute the lower part of the sedimentary sequence, overlying the Hercynian crystalline basement.

The Variscan orogeny (appendix D5) occurred due to the collision of the southern continent Gondwana with the northern "Old Red" continent Laurassia (Eurasia and Laurentia), as a result of which the super continent Pangea evolved. These Variscan mountain formations began in the Devonian (360 to 410 Ma), attained its main phase in the late Carboniferous (295 to 310 Ma), and ended in the early Permian (290 to 295 Ma ; Warr, 2000). The Hercynian granite basement constitutes the oldest rock in the working area and intruded 330 Ma ago (Hess and Lippolt, 1996) during the Variscan orogeny. The deep rocks reached the upper crust as magma and crystallized slowly. During Carboniferous times (295 to 360 Ma), parts of the Variscan basement were subject to exhumation and became exposed at the surface during Permo-Triassic times (205 to 295 Ma ; fig. 2.2 A). Variously thick, finely crystallized granitic dykes, originated during the main phase of the intrusion, intruded the granite batholith.

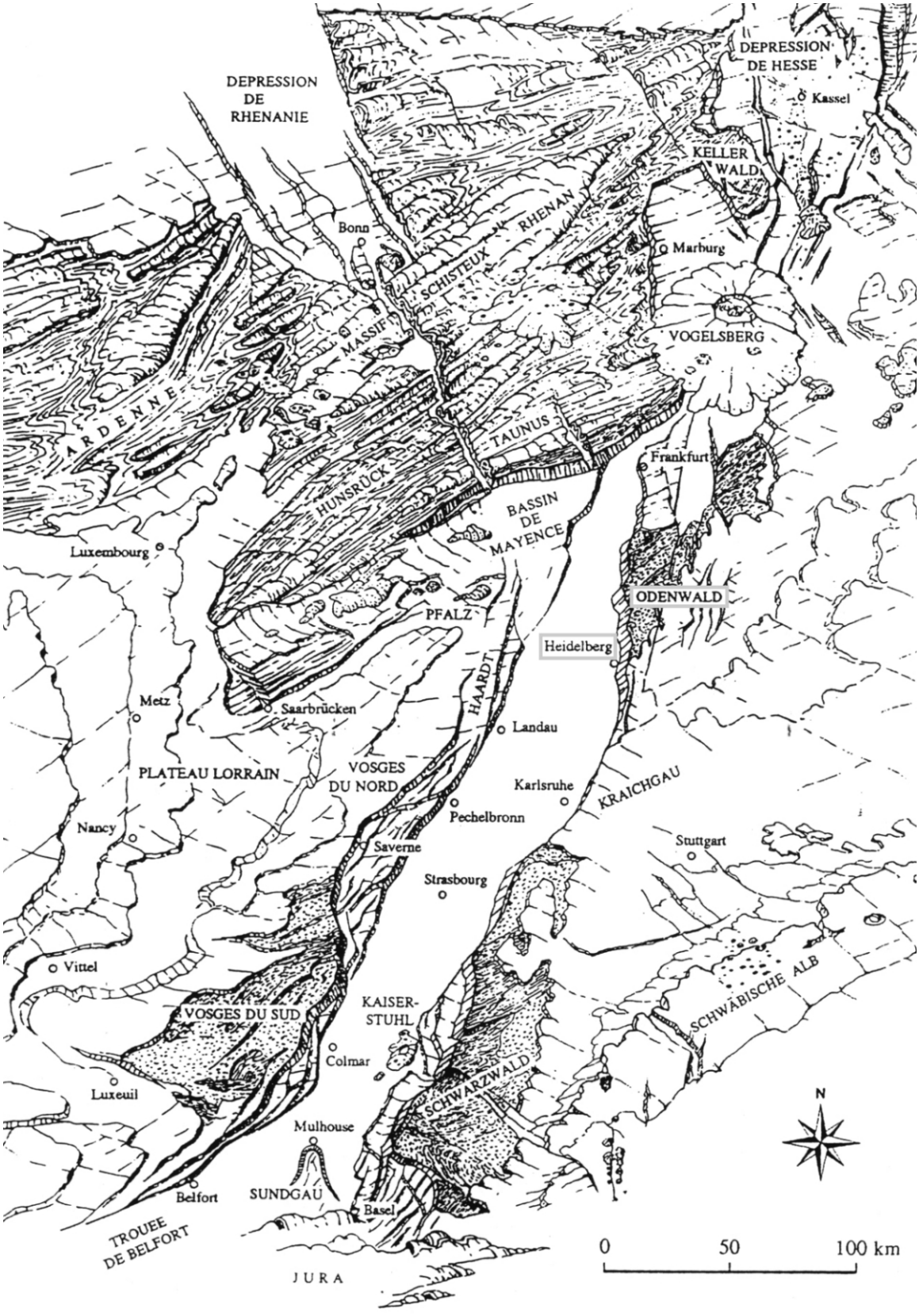

Figure 2.1: Structure of the middle Rhine graben. The crystalline basement without sedimentary covers is stippled (Sittler, 1992).

Toward the end of the Permian, central Europe underwent complex tectonic movements and faulting. A large amount of volcanic rhyolite was extruded through the faulted Variscan crust (Walter, 1992). 290 Ma ago (Hess and Lippolt, 1996), silica rich (acid) volcanoclastic lava in the form of hot tuff and ash clouds covered a large area (fig. 2.2 B). The large amounts of rhyolitic melt extruded from several chimneys, forming ignimbrite and tuff covers. The geographical distribution of the rhyolite was already controlled by N-S orientated faults long before the formation of the upper Rhine graben (Andrae and Osann, 1896).

Following volcanism, the area was subsequently covered by Mesozoic (65 to 265 Ma) sediments (fig. 2.2 C). During Jurassic (135 to 205 Ma) and Cretaceous (65 to 135 Ma) there was a continuous succession of transgression and regression events in the upper Rhine graben region (fig. 2.2 D). One of the thickest deposits was the Triassic Buntsandstein. Conditions at this time were continental and dry. The existing cross stratification, as well as the color of the rock reflect the fluviatil facies of sedimentation. Since the upper Cretaceous, the tectonic evolution of central Europe was controlled by the opening of northern Atlantic, the closing of the Tethys, and the Alpine orogeny.

The Rhine graben, with a length of approximately 300 km and an average width of 35-40 km, constitutes a fragment of a failed rift, running between the North Sea and the Mediterranean. According to Geyer and Gwinner (1991), the irruption of the upper Rhine graben began in the Eocene (34 to 55 Ma). The shoulders of the Rhine graben rose in the upper Pliocene (4,5 to 5,3 Ma), whereas the graben axis sank (fig. 2.2 E). At the beginning, the main fault zone was located in the south between the present Black Forest and the Vosges, and then later shifted during the middle Oligocene (30 Ma) into the northern part of the graben, between the Odenwald and the Palatinat forest. In many cases, the fault complex developed from reactivation of weak zones formed during the Variscan orogeny. Due to the tectonic stress, the granite became strongly fissured, allowing more intensive alteration processes to occur. The relative movement between the graben depth and the raised marginal shoulder is about 4500 m (Walter, 1992). Thermal waters penetrated along the graben margins and altered the rock composition through silicification and mineralization. Water also passed through the fissures and joints, inducing low temperature mineral reactions.

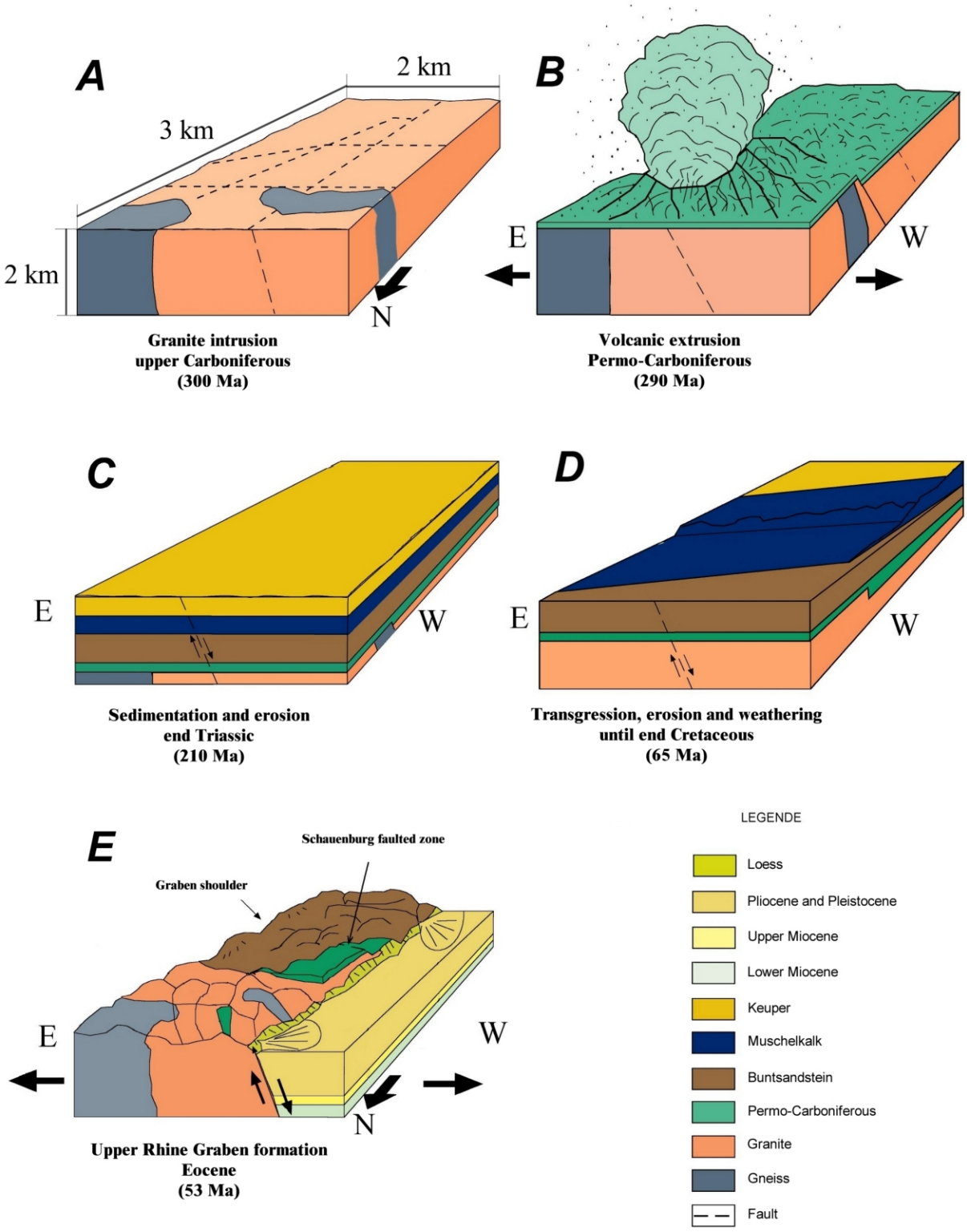

Figure 2.2: Schematic illustration of the geologic evolution of the southern Odenwald. (modified after Schweizer, 1996)

During the ice ages of the Quaternary (since 1,65 Ma), the Odenwald was ice free and experienced periglacial conditions. Fine loess from the plains was blown against the mountain edges to cover large areas in the western and north eastern Rhine Graben shoulder (fig. 2.2 E). These loess deposits (several meters thick) underwent a depletion of cations due to the dilution of the carbonate content, inducing the formation of clay minerals as residual product. The present-day topographic relief between the escarpment of the Rhine graben and the valley floor currently is at its highest since the formation of the graben, due to continuous graben subsidence and shoulder uplift over the past 40 Ma (Villemin et al., 1986). At the onset of the Tertiary Rhine Graben formation, the sedimentary cover was partly removed, and in the vicinity of the graben shoulders, basement rocks became exposed to present surface conditions (fig. 2.1). Today, the Rhine graben is an example of a passive NNE-SSW continental rift.

2.2 Working area

Together with the Black Forest, the Odenwald (appendix D4) forms the eastern shoulder of the northern upper Rhine Graben (fig. 2.3), with a downthrow of the eastern main normal fault of about 6 km. Starting in Eocene times (34 to 53 Ma) times, the uplift of the graben shoulder exposed the Variscan crystalline basement, consisting of metamorphic and plutonic rocks in the western part of the Odenwald (Okrusch et al., 2000).

The studied area is located at a faulted rhyolite-granite contact, the Schauenburg fault, in the southern part of the Odenwald. Amphibolites and paragneisses form relatively small, isolated patches within dominating granodiorite and granite intrusions. The granite within the working area belongs to the Heidelberg granite pluton.

The E-W Schauenburg fault (800 m long) is situated perpendicular to the main NNE-SSW Rhine graben fault, and runs through the Schauenburg castle trench (fig. 2.4). At this location, the rhyolite cover lies oblique to the granite ("oblique slip fault"). Assuming a rhyolite thickness of 120 m to the south of the faulted zone, the fault shift is considered to be at least 100 m. In the literature, a shift of approximately 150 m is reported (Andrae and Osann, 1896). Samples were taken of varying degree of alteration across the fault zone at intervals of a meter (fig. 2.4). The degree of alteration for each sample was estimated from macroscopical features. A total of 22 samples were collected (tab. 3.1). In order to distinguish local fault effects from other regional processes, reference samples (granite and rhyolite; tab. 3.2) were taken and analyzed from quarries situated around the study area.

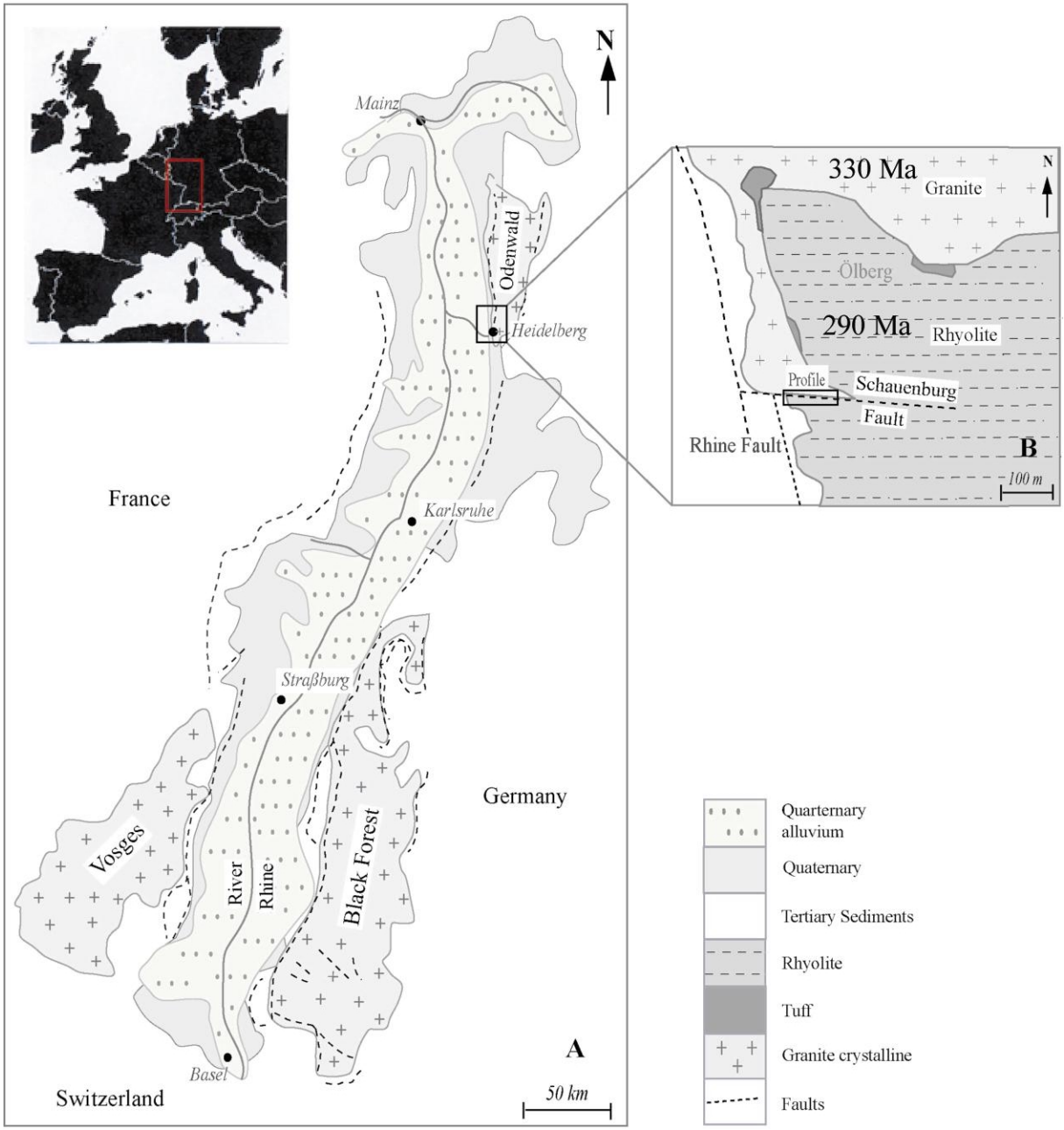

Figure 2.3: Working area location.

The Permian-Carboniferous Heidelberg granite is crossed by variously thick, mostly E-W-orientated granitic dykes. The primary minerals are quartz, plagioclase, K-feldspar and biotite. The younger volcanic rhyolite lies flat on the granite with a thickness between 40 and 150 m. The Heidelberg granite exposed in the working area has a high porosity and permeability. Fissures within the extrusive and magmatic bodies result mostly from cooling and contraction (Eisbacher, 1991; section 1.1) as well as post intrusional regional tectonic stress and extension based on a decompression in the cover layers. The formation of the Rhine graben was also associated with additional faulting. Fluids can penetrate more easily and in this way enlarge the fissures by fracturing and dissolution of the rock through physical and chemical breakdown (section 1.1). The mica and feldspar alteration within the granite is faster than that of the harder quartz. But large red K-feldspars still remain at the surface. The frequently scarlet to brown color of the granitic rocks is due to hematite formation (Fe_2O_3). Fe^{2+} oxidized to Fe^{3+}, and crystallizes as rins around the minerals. In the presence of water, the mineral goethite crystallizes by oxidation and hydrolysis of Fe^{2+}. The goethite minerals show a yellowish to fawn coloration. Dark-grey quartz, as well as greeny-black biotite give the rock a very dark appearance. With the presence of abundant whitish plagioclases, the granite appears bright orange to grey (Schleicher, 2001).

U-Pb dating on single zircons yielded concordant intrusional ages for the heidelberger granite of 342 and 332 Ma (Kirsch et al, 1988). Hess and Lippolt (1996) recorded well defined $^{40}Ar/^{39}Ar$ of 332 +/- 3 and 328 +/- 1 Ma, obtained on hornblendes and sericite-free plagioclase, confirming earlier K-Ar and Ar-Ar dates of around 335 Ma (Lippolt et al., 1990).

In the rhyolite, in contrast to the intense fracturing of the granite, the fissure density is lower and the rock therefore less permeable for fluids. Because of this reduced porosity and permeability, the degree of rhyolite alteration is significantly less than in the granite. Even in the altered state, the rock remains very hard. The rhyolite shows different alteration grades, with color variations ranging from orange brown to violet rock, containing millimeter large whitened phenocrystals (fig. 2.5 and 2.6). The alteration progresses mostly from the surface and intrudes into the rock interior along fissures.

For the rhyolite, $^{40}Ar/^{39}Ar$ age measurements that were carried out on minerals (sanidine, biotite, muscovite), indicate a Permo-Carboniferous age for the rhyolite (291 +/- 6 Ma 2σ errors ; Lippolt et al., 1990). Compared to the age data on plutonic rocks of the Odenwald, an age difference of about 45 to 55 Ma (Hess and Lippolt, 1996) exist between plutonism and the later rhyolitic volcanism.

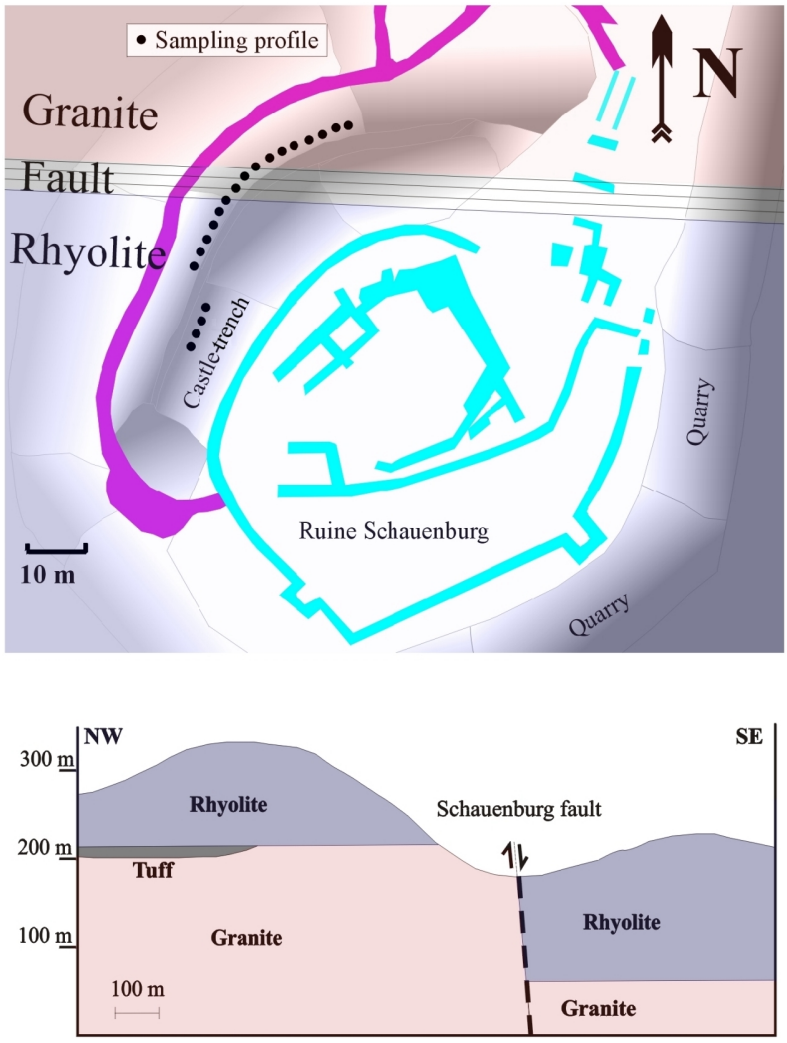

Figure 2.4: Sampling profile.

2.3 Petrography

As this project was based on the same samples as studied by Schleicher (2001) during her Master of Sciences work, mineralogical constraints were available. The co-operation permits to carry out standard laboratory techniques such as thin section microscopy, X-Ray Diffraction-analysis (XRD) and the Scanning Electron Microscopy (SEM) to characterize the samples and provide basic information about mineral composition. Schleicher (2001) described the formation and growth of clay minerals along the faulted zone, and their role in the development of these structures. The following petrographic data a largely taken from her work.

The sampling profile has been divided in 4 zones based on macroscopical observations:

- Rhyolite zone from sample 1/1 to 1/4: fine grained rhyolite,
- Altered zone I from samples G3 to G7: coarse grained, in part cataclastic, rhyolitic rock,
- Altered zone II from samples G8 to G11: strongly altered rock from the fault zone, mostly granitic and cataclastic,
- Granite zone from samples G12 to G18: altered granitic rocks with large alkali-feldspars, quartz and biotite.

2.3.1 Rhyolite

On the studied fault is the rhyolite (fig. 2.5) very fine grained, dark-purple to red. Irregularly distributed, up to 5 mm large quartz (dark-grey to orange) phenocrysts as well as K-feldspar and mica can be recognized. However, they are macroscopic difficult to distinguish and frequently not as crystals recognizable. White, up to 2 mm large kaolinite aggregates are roundish to squared shaped. The largest phenocrysts (up to 20 mm) are formed by grey and bright-green, very soft and altered material and contain sometimes small quartz.

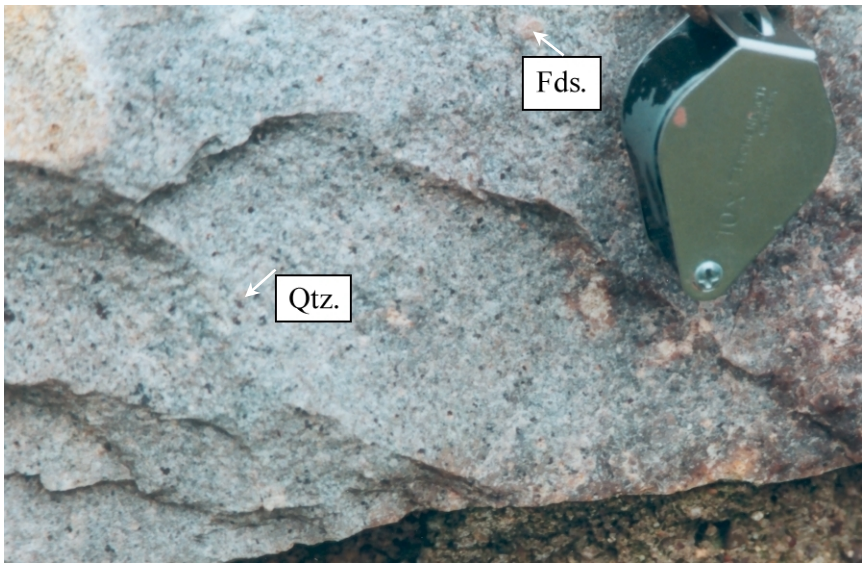

Figure 2.5: Fine grained rhyolite sample with quartz (Qtz.) and feldspar crystals (Fds.). (Schleicher, 2001)

2.3.2 Altered zone I

The examined rhyolite samples (G3 to G7) are rather uncharacteristic. They contain variously altered phenocrysts (mm up to cm) in various colors that are randomly distributed over the rock and its matrix (fig. 2.6). Microscopical description of the rhyolitic samples shows the main rock-forming mineral to be quartz, K-feldspar and biotite. Accessory components are sericite, muscovite, plagioclase, zircons and opaque phases. For a detailed description the representative thin section (sample G4) was selected. The rock is coarse-grained and strongly altered. 30 - 35 % of the minerals are large quartz grains with corroded edges and crossed by fracture planes. The K-feldspars constitute 20 - 25 % of the sample and the plagioclase are very strong sericitised and show a weak perthitic textures in albite. Altered biotites with a rock proportion of 10-15 % occur with Fe-rich opaque phases (SEM analysis). Some minerals are only recognized by outlines of opaque minerals, which are filled with recrystallized quartz. Zircons are accessory in nature.

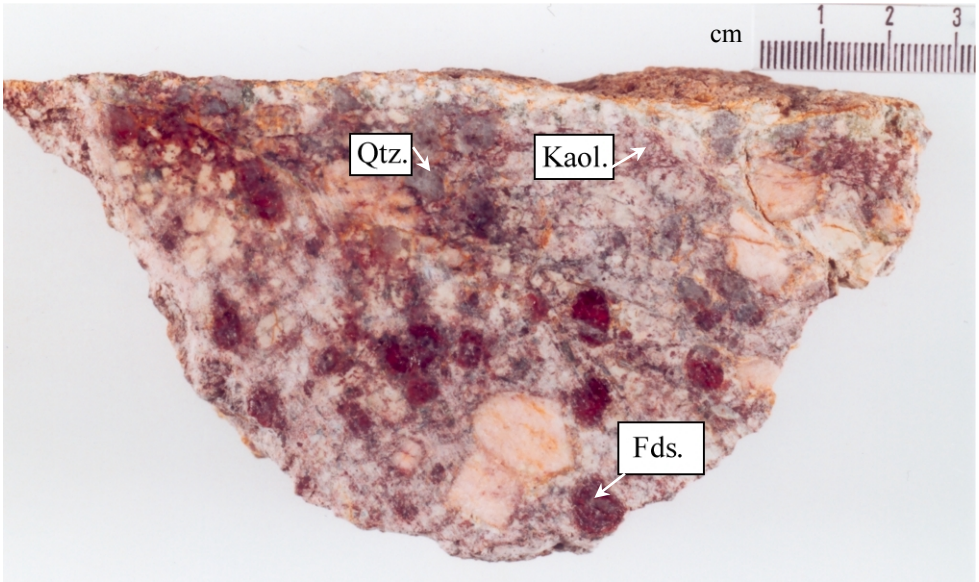

Figure 2.6: Altered rhyolite with quartz (Qtz.), clays (Kaol.) and large, bright, red feldspars (Fds.).
(Schleicher, 2001)

2.3.3 Altered zone II (cataclase)

The transition from rhyolitic to granitic rock lies between samples G8 and G11. The samples are extremely altered and clay-rich. Clay minerals are also visible as pore fillings. The microscopical description of the cataclastic samples G8 (fig. 2.7) sampled from the strong altered zone shows the rock building minerals quartz and K-feldspar, with accessory opaques, sericite and biotite. The rock is strongly altered with the quartz are predominantly sericitised feldspars. The large K-feldspars (30–40 %), quartz grains and quartz aggregates (40–45 %) are crossed by numerous fractures, which are filled with brown altered material. Relic of a perthitic texture and microcline structure in the feldspars still to be distinguished. Fragments of feldspar and quartz reside in a fine grained, recrystallized and strong altered matrix. There are many fractures and broken grains, giving the rock the appearance of a breccia.

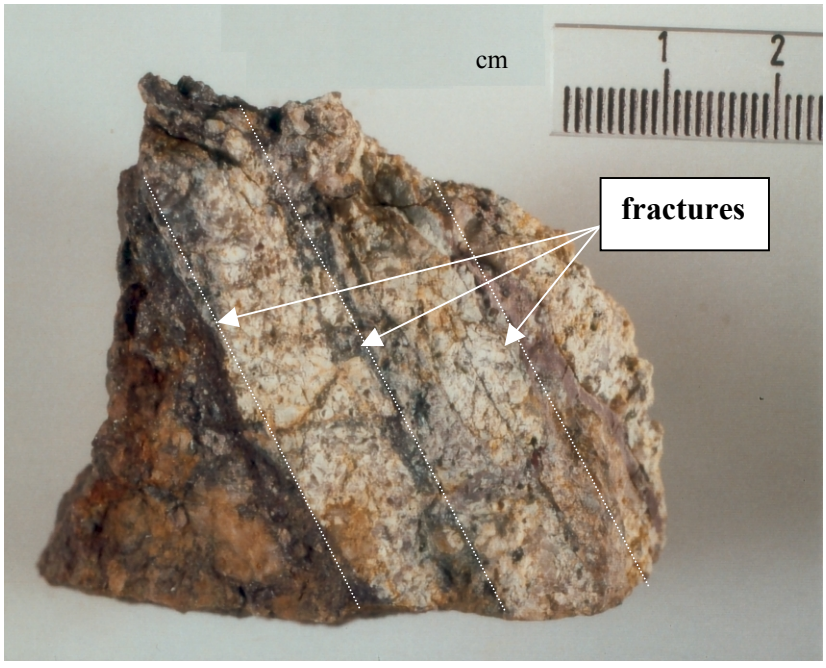

Figure 2.7: Cataclastic sample (G8b) with strong fracturing and alteration.
(Schleicher, 2001)

2.3.4 Granite

The granitic segment of the sampled profile (samples G12 to G18) shows the characteristic features of coarse grained granite. The granite sample G14 is representative and is composed of quartz, K-feldspar, plagioclase, biotite, sericite and opaque accessory phases. These coarse-grained rocks are less altered. Other samples are so strongly altered that the original protolith is not recognizable. Large quartz grains (40 % in the thin section) and feldspars are crossed by fractures. The feldspars make up 20 – 25 % of the rock thin section. The plagioclase with clear albite twinning and the K-feldspars with microcline structure and Karlsbad twinning are sericitised. Next to the biotite occur opaque phases. Some minerals are completely replaced by quartz.

2.3.5 Summary

	Sample	Quartz [%]		K-feldspar [%]		Plagioclase [%]	001-illite [%]	001-Kaolinite [%]
Altered zone I	G3	9	mean: 19	77	mean: 68	0	5	10
	G4	22		62		0	5	11
	G5	9		76		0	5	9
	G6	23		65		0	4	9
	G7	34		60		0	3	3
Altered zone II	G8	36	mean: 23	33	mean: 50	0	2	29
	G9	27		50		0	4	18
	G10	7		75		0	3	15
	G11	21		43		0	5	31
Granite	G12	8	mean: 11	35	mean: 40	36	2	3
	G13	13		30		32	4	7
	G14	11		57		29	0	3
	G15	8		37		43	6	6
	G18	16		41		39	0	3

Table 2.1: Main mineral contents in sample G3 to G18 (modified after Schleicher, 2001).

The principle minerals of the rhyolite and granite are quartz, alkali-feldspars, plagioclase, illite, kaolinite (tab. 2.1). Further alteration products within the faulted zone are metal oxides (hematite) which indicate oxidizing conditions. The plagioclase is exclusively found in the granite material. All other minerals are found over the whole sampled profile. The rock alteration is marked by the formation of significant quantities of kaolinite and illite, which have formed both as replacement reactions and as neocrystallized pore-filling minerals. SEM observations on whole-rock chips provided evidence for growth of platy and fibrous illite phases in the free pores. These alteration products are the dominant alteration products in the whole profile and in the clay fraction. In the granitic or rhyolitic range of the faulted zone is no any clear mainstream of the different mineral to identify, what on different growth phases or different growth processes of both clay mineral result. The exception lies within the cataclastic range of the faulted zone where an increased kaolinite content shows an intensified alteration of the minerals whereas the illite content remains nearly constant over the sampled area (fig. 2.8).

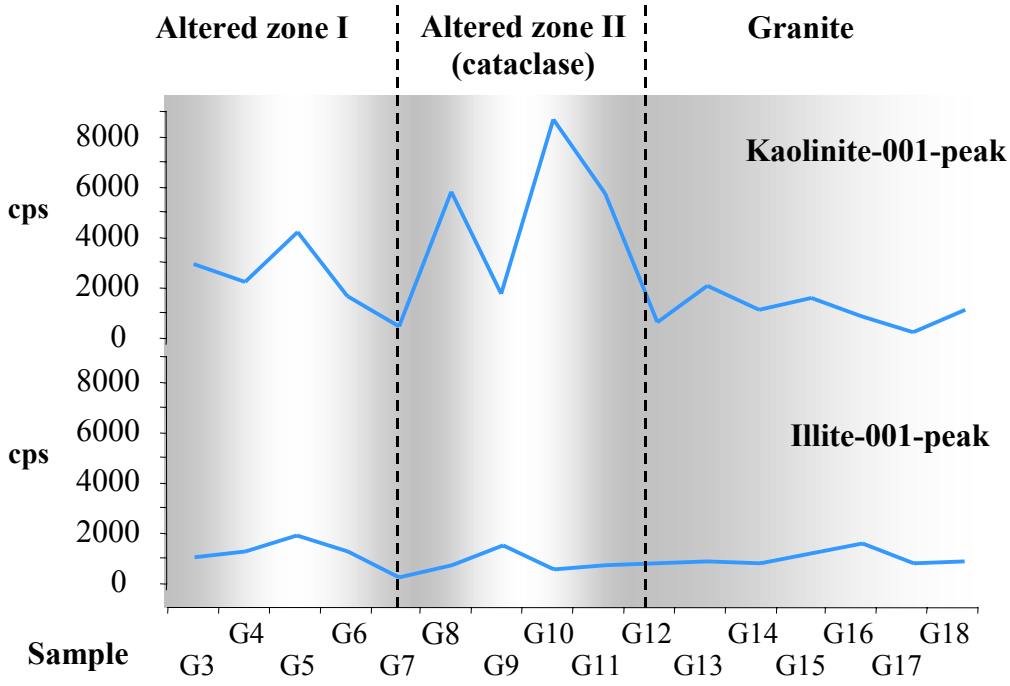

Figure 2.8: Kaolinite and illite content of the faulted zone based on XRD analyses
cps = counts per second
(modified after Schleicher, 2001).

Fluid movement within rock is function of permeability, fluid pressure and fluid composition (Han-Kechong & Wang-Xueming, 1983). Observations show that sufficient porosity and permeability is available along the Schauenburg fault for fluid movement and that fluids have circulated. Around the region of the study area, evidence for fluid circulation occur with several ore mineralizations along faults and fissures in Schriesheim and the surrounding area. Hydrothermal fluid movements also give rise to mineralizations within the faulted zone rock, which can be recognized by SEM analysis and thin section investigations, as well as the strong hematite growth. Very fine, recrystallized quartz which fill mineral cavities and also grain boundaries, point to late stage crystallization. Both the granite and rhyolite, but at most the medial range area of the profile (altered zone II) show cataclasis resulting in heavily fracturing and breakage of quartz and feldspars minerals in a fine grained matrix. Biotite and muscovite appear deformed and form kink bands. All these clues indicate temperatures not greater than 250 - 300 ° C and represent diagenetic up to low grade metamorphic conditions. Evaluation of the SEM images indicates several generations of kaolinite and illite with varying crystallographic properties. The formation of illite and kaolinite depends on different processes within the rock: illite/smectite occurs preferentially by alteration processes in deeper field under conditions up to 300 °C. Kaolinite formation is due to hydrothermal alteration or under low temperature conditions as surface near alteration product of feldspar (Velde, 1992). The new mineral crystallization can result through exchange reactions (sericitization of feldspar) or through new crystallization and growth (pores fillings). The kaolinite from the faulted zone originated predominantly from hydrothermal alteration and grew together with illite. The minerals occur frequently together and are intergrown, but also occur as individuals in pore fillings. They are both alteration products of plagioclase and K-feldspar, what can be recognized in the SEM and XRD data by the kaolinite decrease during the emergence of the feldspar minerals.

Chapter 3
Geochemical signatures of the Schauenburg fault

It is widely recognized that minerals dissolve or react at different rates, depending on a variety of factors such as mineral composition and structure, temperature, and chemistry of alteration solutions (White et al., 2001). The different element mobilities are a result of the dissolution of primary silicate minerals and precipitation of secondary clays and oxides (Stille et al., 1999). In a multi-mineralic system, like granite and rhyolite, these differential alteration rates should result in progressive changes in mineral proportions and net solute load with time and flowpath length. Thus major and trace elements like Rare Earth Elements (REE) can be used to quantify the changes induced by fluid-rock interaction.

In this section, major element and trace element data (appendix C2) from the whole rock samples are presented, taken from the fault zone and the reference quarries. Data are shown as major element oxide weight percentages and trace element concentrations (ppm). The whole rock analyses have been performed using ICP-MS, ICP-AES and TIMS. The samples were crushed and only chips from interiors were powdered in agate ball mill to prevent mixing with the altered crust. The powders were dissolved with suprapur and concentrated $HF/HNO_3/HCl$ mixture (1, 3, and 1 ml). The dissolution was carried out in closed, pressurized teflon bombs, in a microwave assistance oven (MLS Ethos with terminal M240, appendix A1).

3.1 Major elements

Table 3.1 and 3.2 give a description of the 22 faulted zone samples and of the reference samples respectively. To estimate the alteration degree of each sample from the faulted zone, several alteration indicator factors are shown (tab. 3.1).

	Name	Description	Distance [m]	A	CIA		A/CNK	
Rhyolite	1/1	fine grained	0	1	0,55	mean: 0,54	1,18	mean: 1,15
	1/2		1	1	0,54		1,15	
	1/3		2	2	0,54		1,14	
	1/4		3	2	0,54		1,15	
Altered zone I	G3	coarse grained, in part cataclastic, rhyolitic rock	4	4	0,57	mean: 0,57	1,31	mean: 1,32
	G4		5	4	0,57		1,29	
	G4b		6	4	0,56		1,25	
	G5		7	3	0,58		1,36	
	G6		8	3	0,57		1,30	
	G7		9	3	0,58		1,38	
Altered zone II (cataclase)	G8b	strongly altered rock, rather granitic, in part cataclastic	10	3	0,60	mean: 0,60	1,50	mean: 1,50
	G8c		11	3	0,59		1,42	
	G9		12	2	0,57		1,34	
	G10		13	4	0,63		1,66	
	G11		14	2	0,61		1,58	
Granite	G12	altered, granitic rock with large alkali-feldspars, quartz and partially many biotite	15	1	0,59	mean: 0,58	1,15	mean: 1,11
	G13		16	2	0,57		1,14	
	G14		17	3	0,53		1,04	
	G15		18	3	0,58		1,12	
	G16		19	4	0,61		1,14	
	G17		20	4	0,57		1,04	
	G18		21	4	0,59		1,14	

Table 3.1: Description of the fault zone, see following text for definition of terms.

- Macroscopical degree of alteration **A**:
  1 = fresh (<10%);
  2 = weakly altered (10-30%);
  3 = medium altered (30-70%);
  4 = strongly altered (70-100%)

- Chemical Index of Alteration **CIA**

  CIA = $Al_2O_3/(Al_2O_3+(CaO*(-3,33*P_2O_5))+Na_2O+K_2O)$
  (all oxides being in mol percent)
  CIA range in figure 3.1

  (Nesbitt and Young, 1982)

- **A/CNK** = $Al_2O_3/(CaO+Na_2O+K_2O)$

  (Irber, 1999)

The alteration indicators (CIA and A/CNK) can be used to monitor the mobility of the major elements (Al, Ca, Na, K, P). The order of chemical mobility of elements in alteration is Ca (highest mobility), Na, Mg, K and Sr (Faure, 1991; Chesworth, 1992). Aluminium, titanium, thorium, and iron are relatively immobile (Osmond and Ivanovich, 1992; Chesworth, 1992). Thus, the greater the volume of migrating fluids, the higher the Al concentration and the lower the concentrations of Ca, Na, Mg, and other mobile cations in the rock (Gu et al., 1997).

The A/CNK index shows a stronger loss of mobile cations in sample G3 to G11 (altered zones with A/CNK> 1,25) with high loss between G8b and G11 (altered zone II, tab. 3.1). The granite samples and the rhyolite also underwent a leaching of cations but weaker than in the altered zones. The CIA index is constructed in the same way than the A/CNK index and thus reflects the same processes. But in addition to the loss in cations, the CIA index permit to compare this loss with the change in the mineralogy using the reference data in figure 3.1 (Nesbitt and Young, 1982). The measured CIA indices (between 0,54 and 0,63) indicated a pronounced alteration (tab. 3.1). All the samples lost their primary signature of crystalline rocks and are now closer to the loess CIA signature (fig. 3.1). This shift in the

CIA signature can be explained by dissolution of primary minerals like feldspar with lower CIA, and an increase in alteration products like clay minerals, with higher CIA signature (fig. 3.1). The highest shift can be seen in the altered zone I and especially in altered zone II in agreement with the ANC/K and clay data, which shows an increasing kaolinite content (section 2.3.5). The granite also has a high signature, but lower compared to the next altered zone II. The granite signature can be explained by a higher permeability (section 2.2.3) than rhyolite allowing for enhanced alteration. This alteration can be qualified as a "normal" altered level in contrast to the altered zone samples where other processes are needed to explain the data. Most of the granite samples have the appearance of granitic arkose. The rhyolite samples have the lowest CIA values, close to the unaltered level of about 0,5 (fig. 3.1).

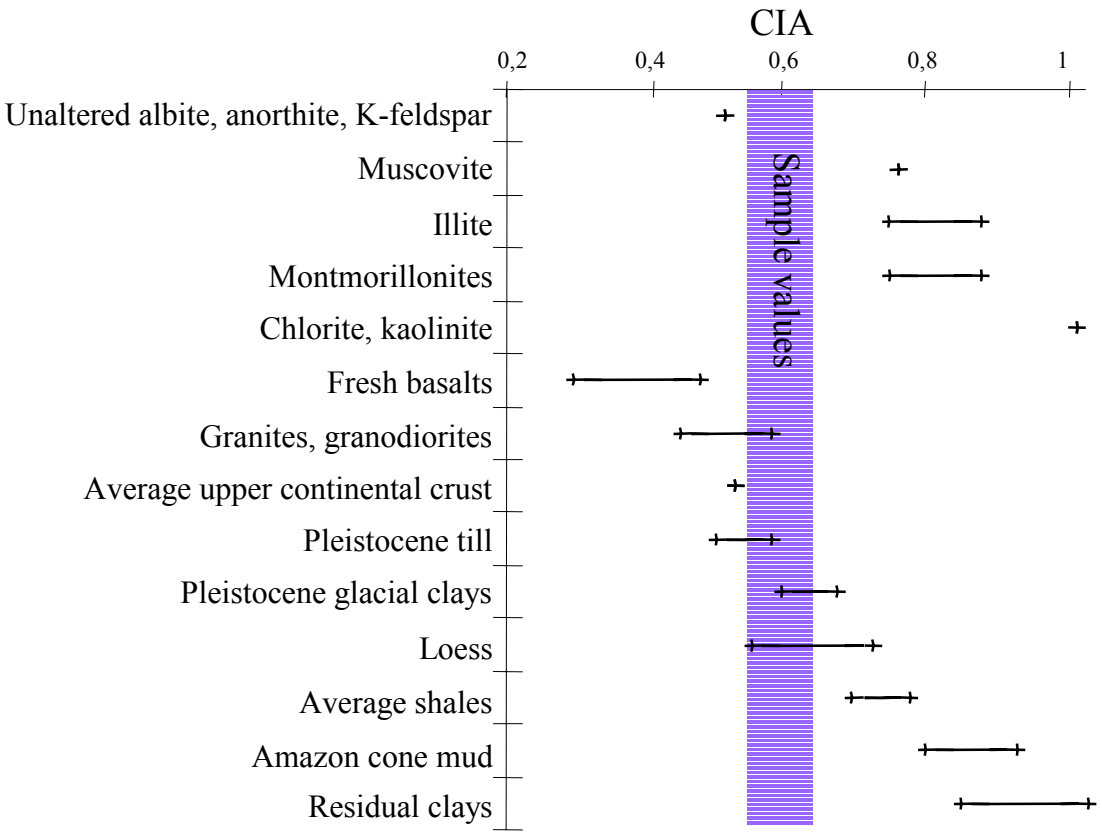

Figure 3.1: CIA alteration index (Nesbitt and Young, 1982). The samples values have lost their crystalline rocks signature.

Name	Description		Location
GB	Granite fresh	Coarse grained	Schriesheim - Branich
G1F2	Granite fresh	Coarse grained	Ziegelhausen - Stift Neuburg
G1W2	Granite altered	Coarse grained	Ziegelhausen - Stift Neuburg
G1F1	Granite dyke	Fine grained	Ziegelhausen - Stift Neuburg
G1W1	Granite altered	Coarse grained	Ziegelhausen - Stift Neuburg
G3W	Granite altered	Coarse grained	Dossenheim - Branichstrasse
QV	Rhyolite	Fine grained	Dossenheim - Quarry Vatter
QS	Rhyolite	Fine grained	Dossenheim - Faulted zone quarry
Po1F	Rhyolite fresh	Fine grained	Dossenheim - Quarry Vatter,
Po1W	Rhyolite (alteration crust)	Fine grained	Dossenheim - Quarry Vatter,

Table 3.2: Reference sample description.

Examining the major elements in detail reveals different compositions for each zone of the profile (fig. 3.2, appendix C2). Depending on the element, the altered zones have a composition close to the granite or to the rhyolite parent rock. For example, Ca and Na are mostly carried in plagioclase. The granite samples G12 to G18 with the highest Ca and Na concentrations are those with plagioclase content (tab. 3.1). The Mg composition is different for each zone. The altered zones have an intermediate composition between the low content of the rhyolite and the higher content of the granite. The Mg concentrations of the altered zones could reflect the presence of a Mg rich mineral like biotite. There is no clear tendency towards a geochemical distribution for the whole elements between the altered zone segments and the fresher granite and rhyolite segments. However, irregularities within the altered zones I and II are noticeable for the profiles of the immobile elements Si and Al (fig. 3.3). Samples G3 to G5 have compositions close to the granite composition. Samples G7 to G8c have typical rhyolitic compositions. The sample G6, between anomalies, has a transitional composition in Si and Al. These changes in Si and Al can hardly be explained by a geochemical shift caused by fluid circulation without affecting more mobile elements. The anomalies can be explained with partial remobilization and mixing processes at the granite surface during the Permian rhyolite extrusion. Mechanical mixing during faulting could also explain the mixtures of granite and rhyolite compositions in the altered zone. The isotopic investigation on feldspars of each anomaly from the altered zones is discussed in chapter 4.

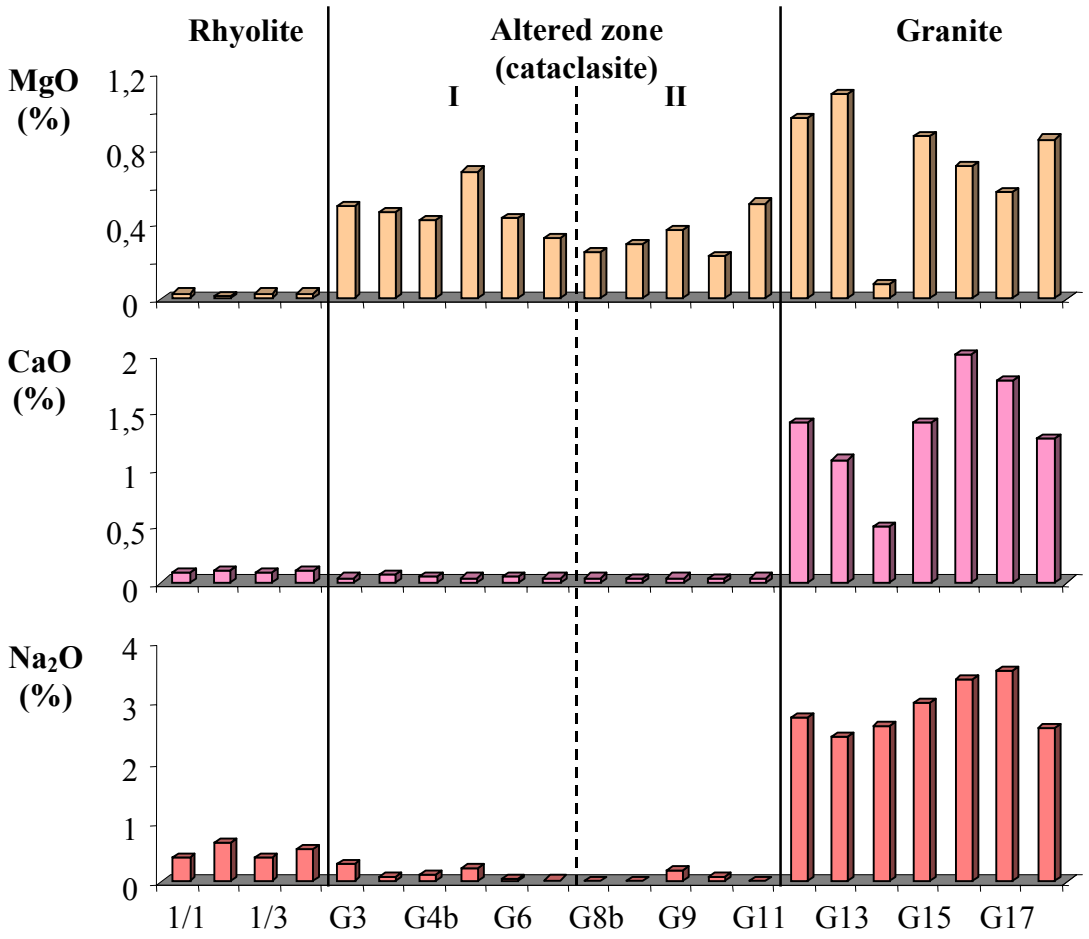

Figure 3.2: MgO, CaO and Na_2O concentrations profile. Each segment shows a different composition, especially for MgO.

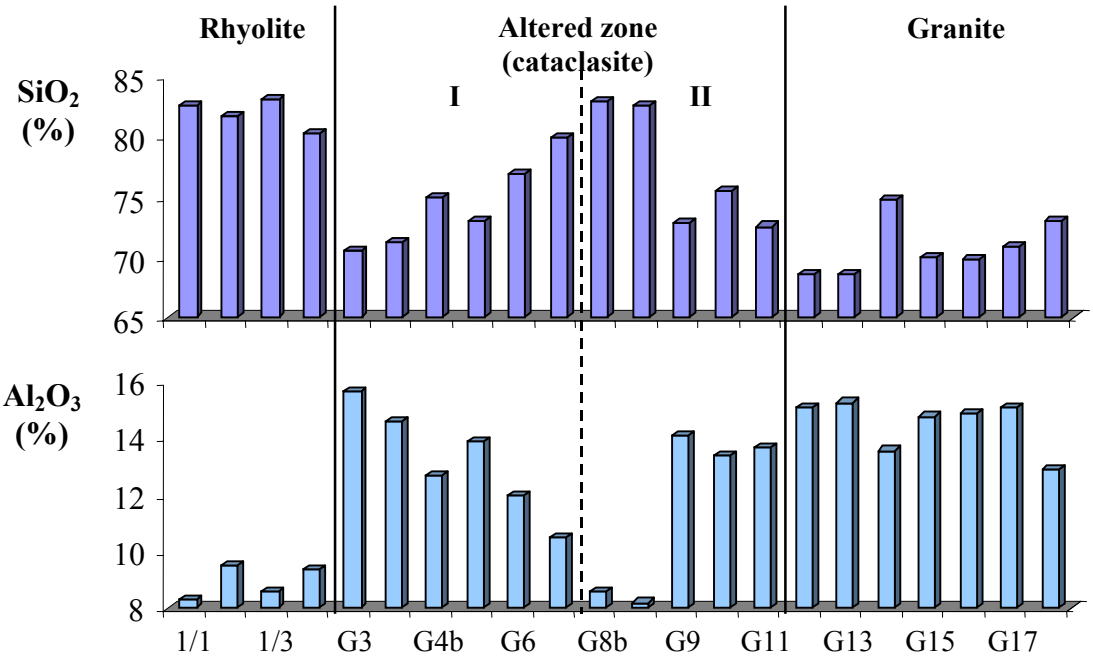

Figure 3.3: SiO_2 and Al_2O_3 concentrations profile. In the altered zones, the immobile elements show a mixing between granite and rhyolite.

3.2 Trace elements

The concentrations of the trace elements across the fault zone, as for the major elements, do not show any distinct trends. Some profiles (fig. 3.4) display different signatures for each zone of the sampling profile. The Sr concentration, because of its similar behavior with Ca, during mineral fractionation, displays the apparition of the plagioclase minerals in the granite zone (fig. 3.4). In the altered zones, some elements (Sb, Cu, Pb) are highly enriched in comparison with rhyolite and granite (fig. 3.5), evidence for a transport and deposition of the elements by hydrothermal fluids. Th is depleted in the altered zones. This depletion is hardly to explain because Th is known to be a highly insoluble element (Chesworth, 1992). The same irregularities, displayed in figure 3.3 with the major elements Si and Al, can be found in the distribution of Hf and Zr (fig. 3.6) which are immobile elements. Mostly immobile elements display these irregularities. The anomalies can be explained by mixing processes which occurred during the rhyolite extrusion on the granite surface or during fault formation. The more mobile elements show a different composition within the altered zones in respect to the granite and the rhyolite. The redistribution of the mobile elements can only has taken place after the mixing event inducing the immobile element anomalies. If not, the anomalies should be present in all element profiles and would not display own signatures for the mobile elements.

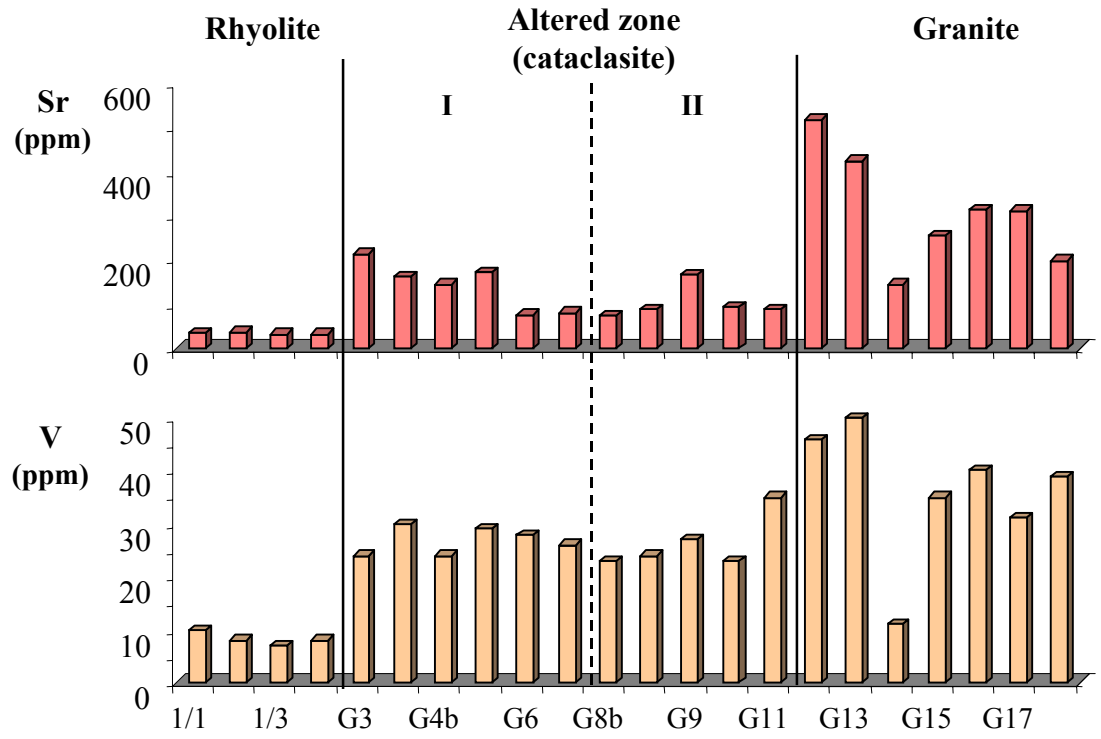

Figure 3.4: The strontium and vanadium, like the major cations reveal a different composition for each zone of the profile.

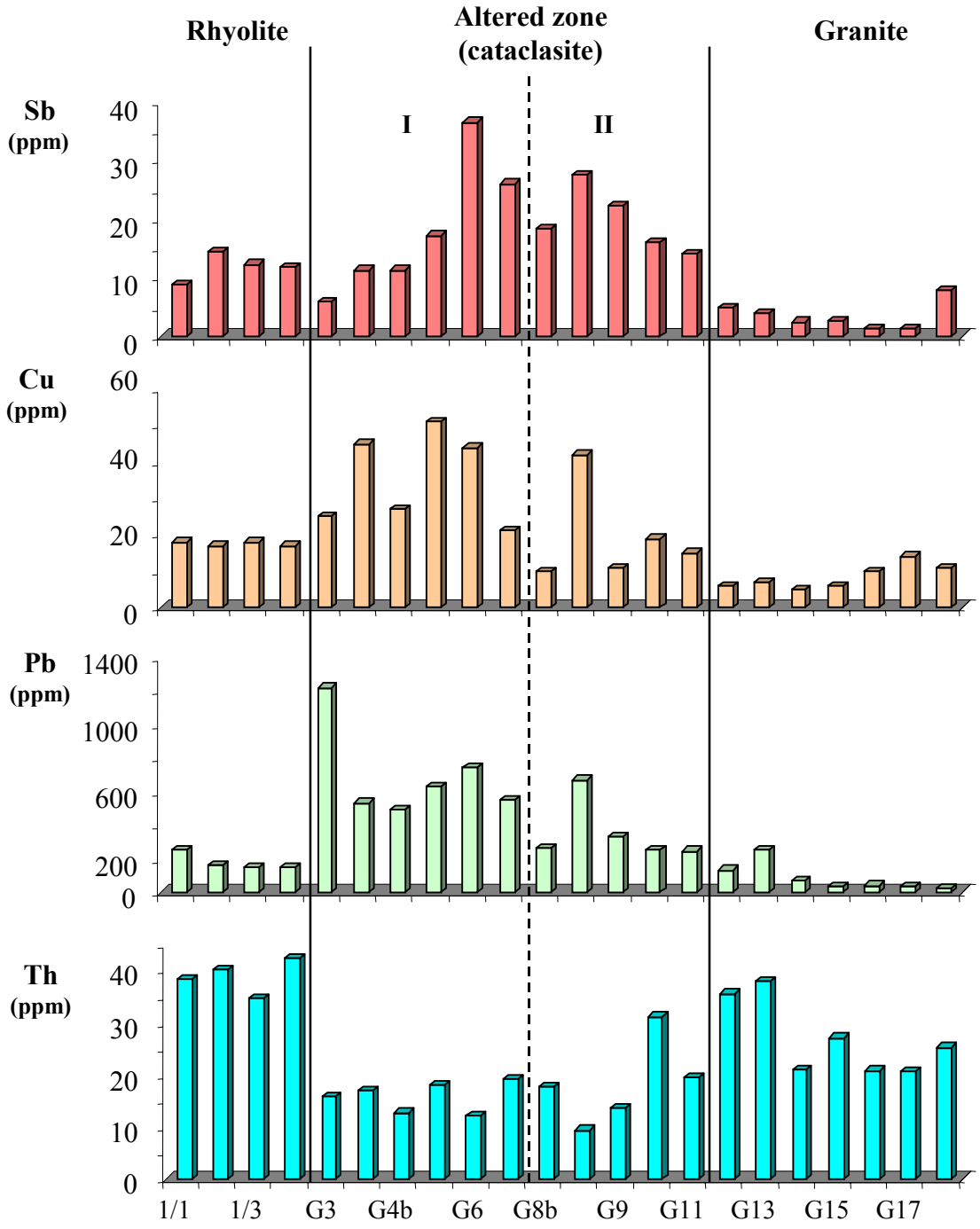

Figure 3.5: Sb, Cu, Pb and Th concentrations profile. Evidences for a transport through hydrothermal fluids in the altered zones.

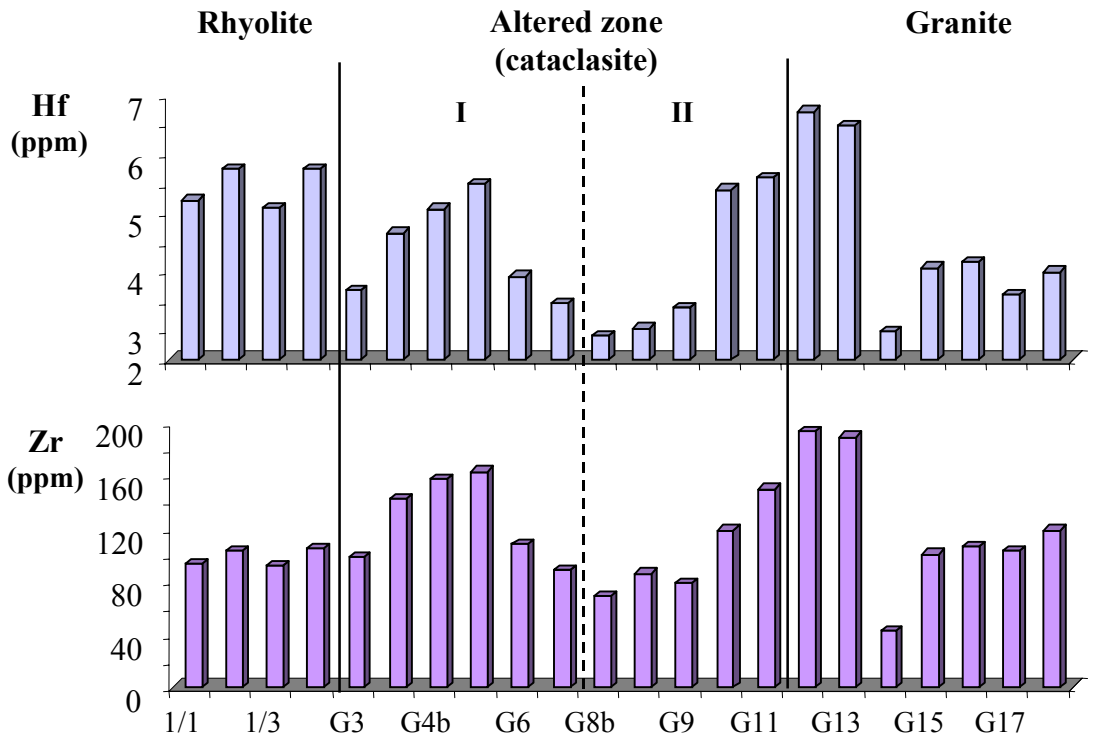

Figure 3.6: The Hf and Zr concentrations profile, like for Si and Al, shows a mixing between granite and rhyolite.

More information can be obtained using the Sr/Eu pair (fig 3.7). Strontium and europium have similar behaviors, although europium is known to be sensitive in ionic size, to oxygen fugacity and temperature (Bau, 1996). It provides information on the redox conditions and bears information relevant to trace element behavior in general. Under reducing conditions europium can exist in the divalent state, which results in larger ionic radii and enables Eu^{2+} to freely substitute for Sr^{2+} in feldspars (McKay, 1989). Increased oxidization will induce Sr/Eu increase and vice versa.

The Sr/Eu ratios in this study range from 111 to 476. The rhyolite and granite zones have a mean Sr/Eu value of 266 and 201, respectively. The altered zones display contrasting behaviors: zone I has a Sr/Eu mean value of 351 and the zone II a very low mean of 157 close to the Sr/Eu Chondritic value of 139 (Anders and Grevesse, 1989). The greater value in zone I is caused by oxidizing conditions. In zone II, the large decrease of the Sr/Eu ratio indicates highly reducing conditions. Two independent events can explain the differences at the boundary between altered zones I and II. However, it is difficult to find out the sequence of the redox events which affected the fault. Indications are given by the

alteration index A/CNK (fig. 3.7), displaying more enhanced alteration in zone II than in comparison to zone I. Thus zone II underwent a hydrothermal event which induced a high transport of the elements with reducing conditions. The oxidizing conditions in zone I can be associated to the hydrothermal event of zone II because the high transport of elements is evident for the two zones. An initial fluid circulation may have produced the reducing conditions in both altered zones. Later oxidizing conditions occurred, but only in zone I, implying a weak process or an element distribution due to adjacent sealing of the fault.

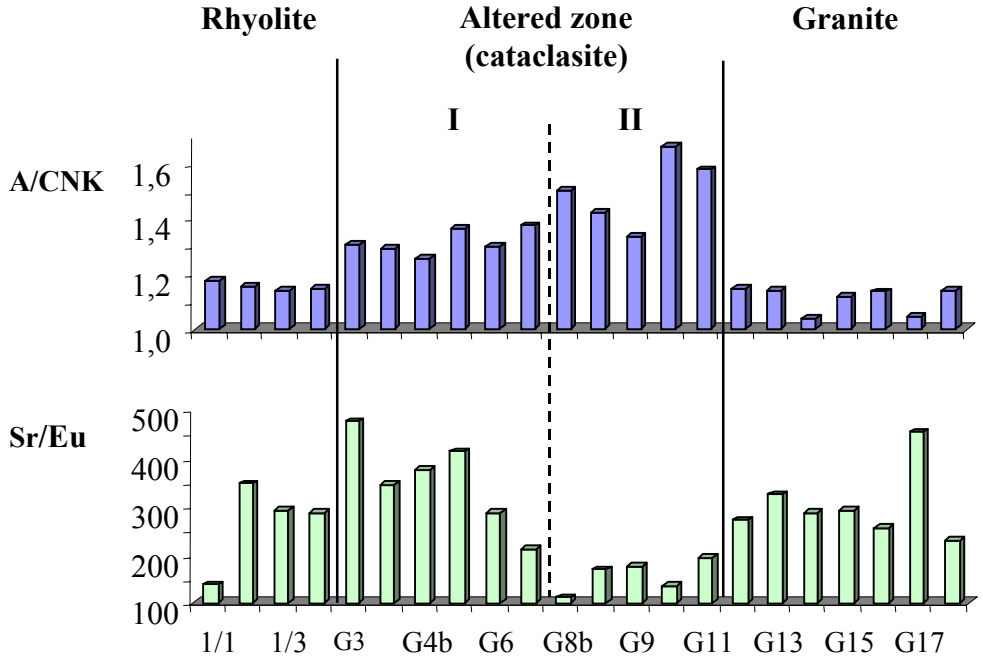

Figure 3.7: Comparison between A/CNK index and Sr/Eu ratio. The high loss in cations in altered zone II correspond to high reduced zone through hydrothermal activity.

3.3 Rare Earth Elements (REE)

Rare earth elements (REE or lanthanide) are widely used in studies of provenance analyses, petrogenesis, and chemical evolution of the earth (Taylor and McLennan, 1985). In nature, the REE occurs as valency $^{3+}$, except cerium which can be $^{4+}$ in oxidizing milieu and europium, $^{2+}$ in reducing milieu. These distributions are useful indicators of physico-chemical changes, and are efficient tracers of fluid-rock interactions and subsequent relationships between the fluids and the authigenic mineral growth (e.g. hydrothermal input, trace exchange and corrosion processes; Zwingmann et al., 1999). The REE form

also a coherent group of trace elements whose chemical properties change systematically across the series (lanthanum to lutetium). The main particularity of the lanthanide is the regular diminution of the ionic radii form lanthanum to lutetium, thus of the incompatibly degree what provides a good tool for quantitative information of processes (Vidal, 1998). The REE are divided in three groups, the light REE (LREE) from lanthanum (La) to neodymium, the middle REE (MREE) from samarium (Sm) to gadolinium (Gd), and the heavy REE (HREE) from dysprosium (Dy) to lutetium (Lu). Most of the REE in the rock are incorporated in accessory phases such as sphene, allanite, epidote and apatite (Gromet and Silver, 1983; Sawka and Chappell, 1988).

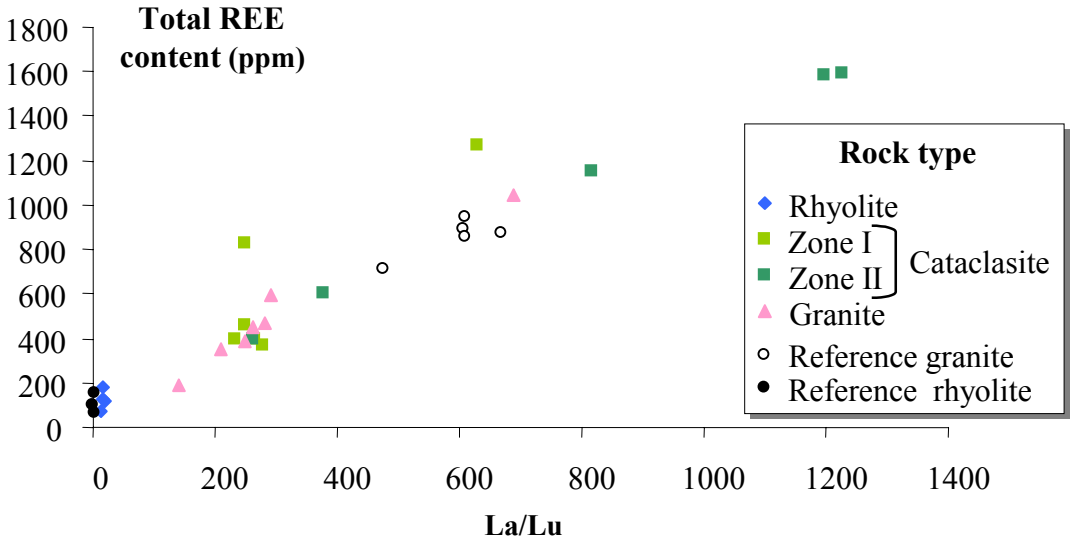

Figure 3.8: Total REE content vs. La/Lu. The enrichment in REE is proportional to the enrichment in LREE.

The total REE contents range from 74 to 1593 ppm (tab. 3.3, appendix C2.4). The rhyolite samples have the lowest content, the altered samples the highest. The enrichment of the LREE in respect to the HREE can be studied with the La/Lu ratios ranging from 12 to 1225 in the profile. The linear trend between La/Lu and the total REE (fig. 3.8) shows that the enrichment in LREE (depletion in HREE) is proportional to REE concentrations. The highest REE content can be seen in the altered zones. (tab. 3.3). In these samples HREE and LREE are fractionated, especially in altered zone II. The LREE are enriched, the HREE depleted. Depletion of HREE is explained by the preferential complexation and mobilization of the HREE by alteration solutions (Stille et al., 1999). This result is in good

agreement with the alteration index (tab. 3.1) and displays strong alteration in zone I and especially in zone II.

	Name	La/Lu	Total REE content [ppm]	Eu/Eu*	Ce/Ce*
Rhyolite	**1/1**	16	182	0,08	0,95
	1/2	18	129	0,06	0,84
	1/3	12	74	0,11	0,81
	1/4	18	121	0,08	0,79
Altered zone I	**G 3**	248	458	0,23	0,68
	G 4	629	1266	0,15	0,59
	G4b	248	826	0,14	0,66
	G5	232	393	0,29	0,74
	G6	278	366	0,32	0,59
	G7	265	392	0,34	0,60
Altered zone II (cataclase)	**G8b**	815	1155	0,36	0,43
	G8c	1225	1593	0,31	0,45
	G9	1196	1580	0,47	0,42
	G10	377	603	0,51	0,53
	G11	264	399	0,55	0,68
Granite	**G12**	689	1044	1,06	0,90
	G13	293	591	0,88	1,62
	G14	143	192	1,67	0,94
	G15	262	454	0,99	0,87
	G16	281	465	1,04	0,81
	G17	248	383	0,93	0,90
	G18	211	355	0,88	0,90

Table 3.3: REE data with the "granite" normalized profile (plotted in figure 11).

More insights into the REE association and fractionation may be obtained by normalizing the concentration data to a reference material. Thus “granite” (average of granite zone samples) and “rhyolite” (average of the rhyolite zone sample) normalized rare earth element abundances for the samples from this study have been made. Using the two rocks to normalize the REE allows to estimate the influence of these rocks in the composition and the evolution of the altered zones.

The cerium (Ce) and europium (Eu) anomalies are defined by (Stille and Shields, 1997):

$$Ce/Ce^* = Ce_N / (La_N^{2/3} \times Nd_N^{1/3})$$

$$Eu/Eu^* = Eu_N / (Sm_N \times Gd_N)^{1/2}$$

where Ce* and Eu* are the expected cerium and europium values from the linear smooth trend across the lanthanide series and the subscript N represents the REE normalized to that of the "granite" or "rhyolite" value. Negative or positive anomalies are defined as Ce/Ce* (and Eu/Eu*) smaller or greater than 1, respectively (tab. 3.3).

The normalized REE compositions show that the 4 recognized zones of the sampling profile have significantly different compositions (tab. 3.3). To estimate the influence of the fresher granite and the rhyolite in the altered zones, the "rhyolite" and "granite" normalization have been made for the two altered zones and plotted in figure 9 and 10 respectively.

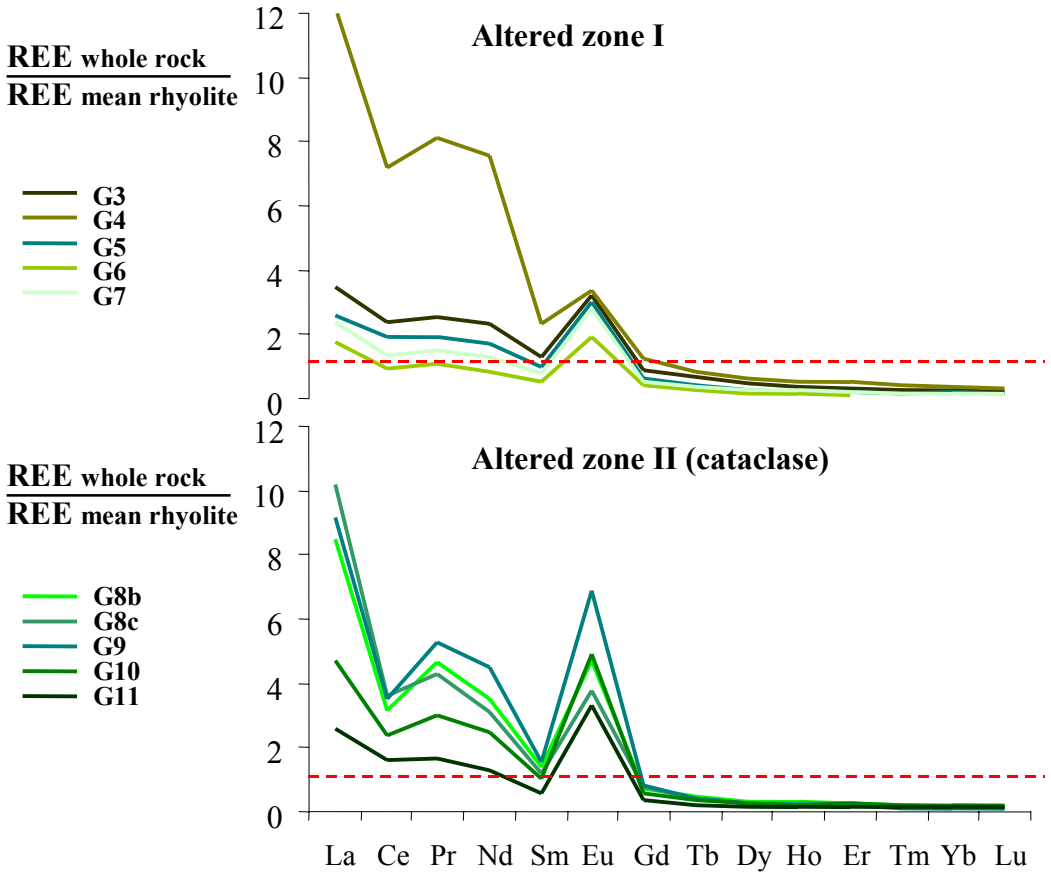

Figure 3.9: Rare Earth Element "rhyolite" normalized. The Eu peak indicates an enhanced influence in zone II. Both zones show a depletion in HREE and an enrichment in LREE.

The “rhyolite” normalized altered zones show an increase of the Eu peak from zone I to zone II (fig. 9). This transition indicates that zone II is more influenced by a granitic composition. The Eu peak is typical for granite, due to the feldspar content (Stille and Shields, 1997). Also to be seen, especially in zone II, is an enrichment in LREE and a loss in HREE. This result is in good agreement with the results plotted in figure 3.8 which showed a depletion in HREE and an enrichment in LREE with the increase of the total REE content. The rhyolite samples have the lowest total REE content and the altered zones, particularly zone II have the highest total REE content. Using “rhyolite” to normalize the altered zones, allows to shows the depletion in HREE and enrichment in LREE of the altered zones. In zone I, the sample G4 has a REE spectrum similar to those of zone II. Using the “granite” reference to normalize the altered zones (fig. 3.10) indicates differences but less significant than with the “rhyolite” normalization (the vertical scale is two times smaller). The “granite” normalized REE spectrum is closer to the granite value of 1 indicated by the red line. Differences still exist notably for Eu which is depleted. The HREE are enriched in zone I, the LREE are enriched in zone II.

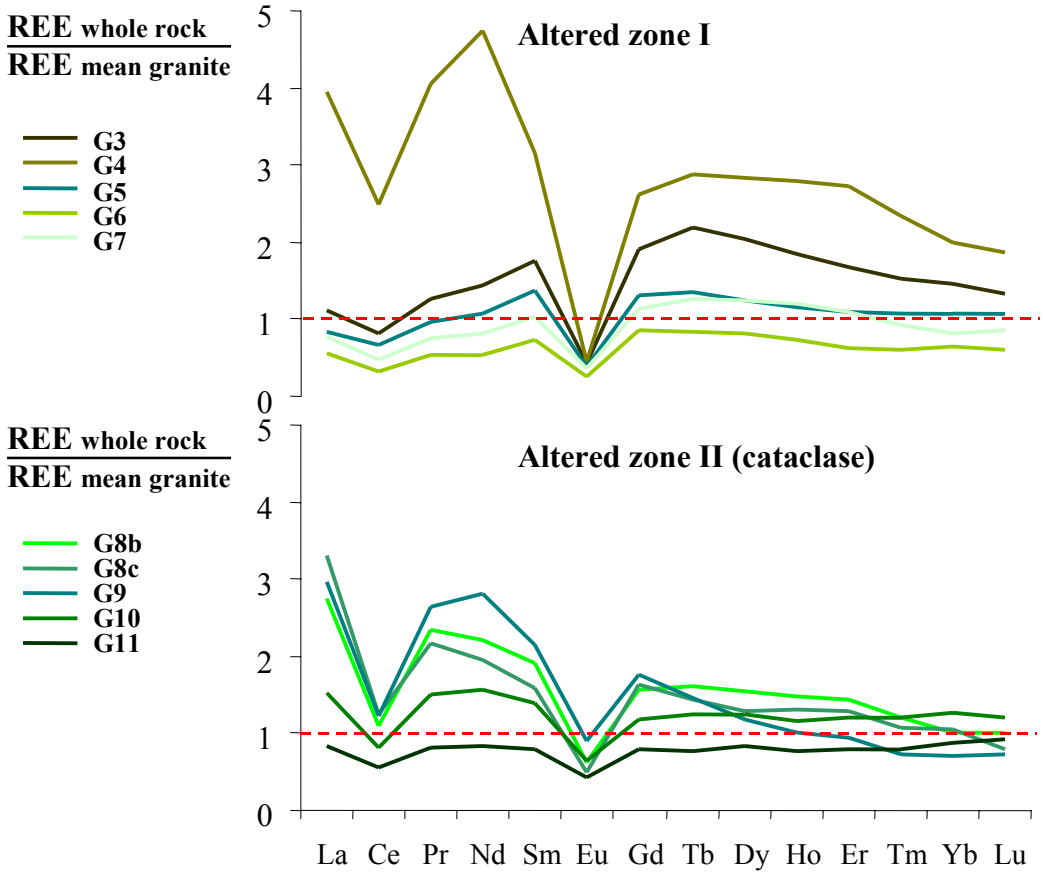

Figure 3.10: Rare Earth Element "granite" normalized. More similar to granite with depletion in Eu and HREE enrichment in zone I, LREE enrichment in zone II.

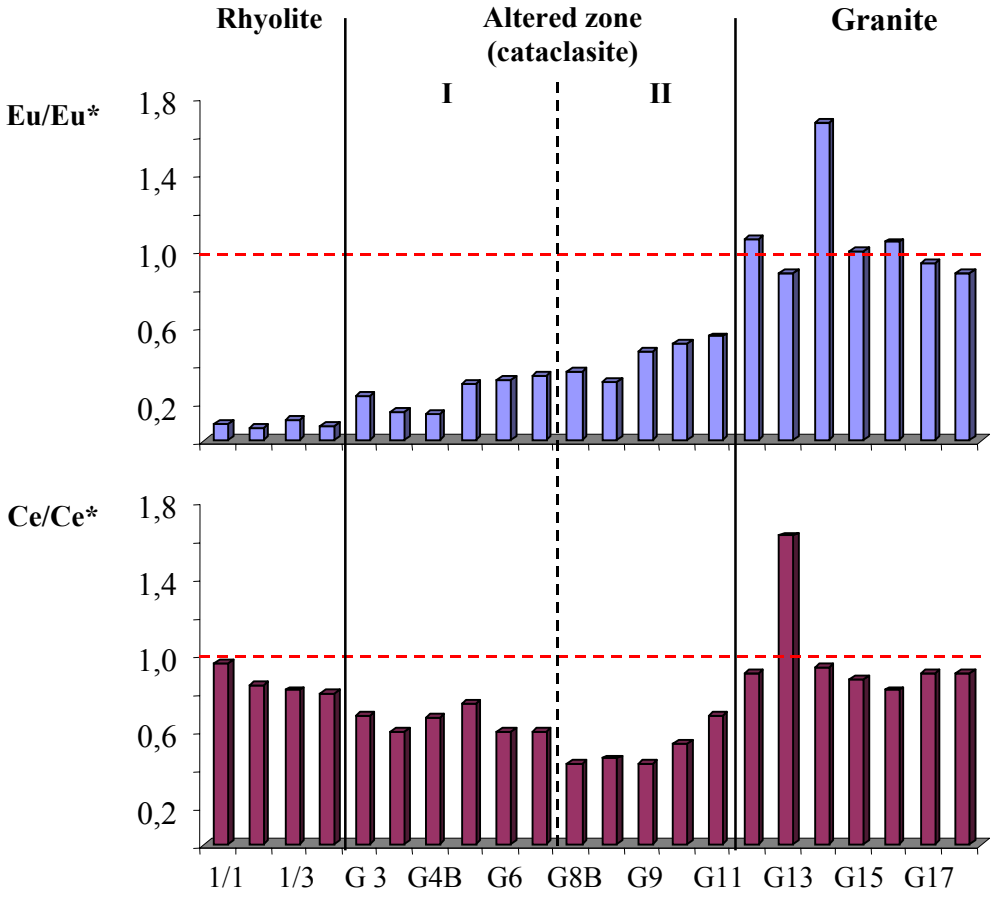

Figure 3.11: Eu and Ce anomalies, "granite" normalization. Eu anomaly shows a transition between granite and rhyolite. Ce anomaly indicates a Ce leaching in the altered zones under reducing conditions.

The normalized Ce values (fig. 3.11) are around 1 in the rhyolite and in the granite. The altered zones all show negative Ce anomalies. The altered zone II is depleted in cerium in respect to zone I. The depletion is very high compared to the granite and rhyolite. The reason for this is that cerium can exist in two valency states in nature, $^{3+}$ and $^{4+}$ in oxidizing conditions. In its oxidized form, cerium is preferentially complexed with Fe and Mn oxyhydroxides phases (Stille and Shields, 1997). Ce is mobile in reducing conditions. All other REE occur normally as $^{3+}$ ions except for europium, which can also exist as $^{2+}$ ions under extremely reducing conditions and at high temperatures. In this way, the cerium anomaly in the altered zones, especially in zone II, gives clues for a hydrothermal REE output in reducing conditions, which is in good agreement with the Sr/Eu data (fig. 3.7).

The europium anomaly (fig. 3.11) decreases from high negative values in the rhyolite to values around 1 on the granite side (the REE are "granite" normalized). The transition within the altered zones is regular and displays no abrupt changes. The europium anomaly can in part be explained by the difference of mineralogy between rhyolite and granite. The europium anomaly in zone II is higher than in zone I. The influence of the Eu/Eu* of the granite zone can explain the regular decrease across the altered zones from light negative anomalies close to the granite to negative anomalies close to rhyolite values. The REE patterns of the granite samples with the pronounced europium anomaly are typical for feldspar in granite (Stille and Shields, 1997). The progressive changes in europium anomaly across the profile can hardly be explained by the redox conditions found with the other redox tracers. The processes have not been reducing as to affect the europium content significantly. It can only be recognized that there is a smooth transition from granite to rhyolite due to a europium diffusion or to a rock mixing.

3.4 Summary

Four distinct zones can be recognized in the sampling profile, which can be identified with geochemical methods. The major and trace elements as well as the REE compositions indicate that the 4 zones have a significantly different composition. Differences are partly petrographic because the profile crosses the granite-rhyolite contact, but they are also due to different alteration levels induced by fluid circulation along the fault system that has structured and drained the alteration processes. The granite-rhyolite contact constitutes the primary structure on which the fault system was superposed. Only the most incompatible elements (Si, Al, Zr, Hf) retain their original signatures and reflect a mixing between typical granite and rhyolite lithologies across the altered zones (fig. 3.3, 3.6). This mixing can be explained by the partial remobilization of the granite by the lava flow during the Permian rhyolite extrusion on the granite surface or by physical mixing by mechanical processes during faulting.

The altered zones I and II are distinctly different from the granite and rhyolite situated on each side of the fault zone (fig. 3.2, 3.4, 3.5). This difference is due to fluid-rock interaction that will be characterized by their isotopic signatures in chapter 4. The geochemical tracers suggest at least one strong hydrothermal event with reducing conditions (fig. 3.9, 3.10, 3.11). Altered zone II underwent more complex and strong alteration events. Zone I seems to have recorded a weak oxidizing event (fig. 3.7). The

altered zones could have recorded the evolution of a hydrothermal event, which shifted from an initial reducing endmember to a more oxidizing endmember toward the end hydrothermal activity. The final oxidizing process was weaker or, due to fault sealing, only effective in zone II. These results are in agreement with the clay results (Schleicher, 2001) which shows an increase of kaolinite in altered zone II, evidence for a stronger alteration in this segment. The altered zones acquired their own geochemical patterns for the mobile elements and have lost the initial one.

Chapter 4
Isotopical investigations of the Schauenburg fault

The Rb-Sr and Pb isotopic data were collected on a Finnigan MAT 261 solid source mass spectrometer (appendix B2). Rb-Sr and Pb were separated with HCl using cation exchange columns (appendix A5). The separation and purification of thorium and uranium were made using anion exchange procedures with HNO_3 and HBr as eluants (appendix A7). U-Th isotopic measurements were performed on a Finigan MAT 262 thermal mass spectrometer (appendix B3). The analyses have been performed on whole rock samples because mineral separation methods may influence the uranium concentration. Whole rock analyses also allow a quick overview of the sampling profile and to pick out the most interesting samples for more precise investigations including mineral separation analyses. In this study some samples were selected whereby the potassium-feldspar, apatite, and biotite were separated from the whole rocks using heavy liquid and magnetic separation techniques. The porosity of some samples has been measured by mercury injection porosimetry at the Centre de Géochimie de la Surface in Strasbourg using the methodology of Surma and Geraud (2003). The isotopic data are shown in appendix C1.

4.1 Rubidium (Rb) - Strontium (Sr)

4.1.1 Rb-Sr whole rock analysis

The main phase of hydrothermal activity in the SW German area occurred during the Late Jurassic (135-160 Ma) in relation with the opening of the Atlantic ocean. The dates of established hydrothermal activity are 145-150 Ma for the Clara mine (Central Schwarzwald), 160 Ma and 134-140 Ma for the Käfersteige mine (N Schwarzwald), 140 Ma for the mineralizations of the NW Odenwald (Mertz, 1987; Kirsch, 1989). The collective hydrothermal activity was most probably related to rifting and extensional tectonic movements (Gaupp et al, 1993), further supported by several documented studies on illite-type minerals from several places of the western European craton (Clauer et al., 1996). These tectonic activities are often accompanied by hydrothermal activities (Zwingmann et al., 1999).

The granite segment of the sampling profile has undergone a fluid-rock interaction event which set up a new Rb-Sr isotopic composition and reset the original age of 330 Ma given for the Heidelberger Granite (Hess and Lippolt, 1996). The Rb-Sr data of the granite samples produce a whole rock isochron (fig. 4.1) of 152 ± 5,7 Ma (2σ error) in good agreement with the well-known late Jurassic hydrothermal event that induced widespread sericitization and formation of illite in the regional basement (Clauer et al., 1996).

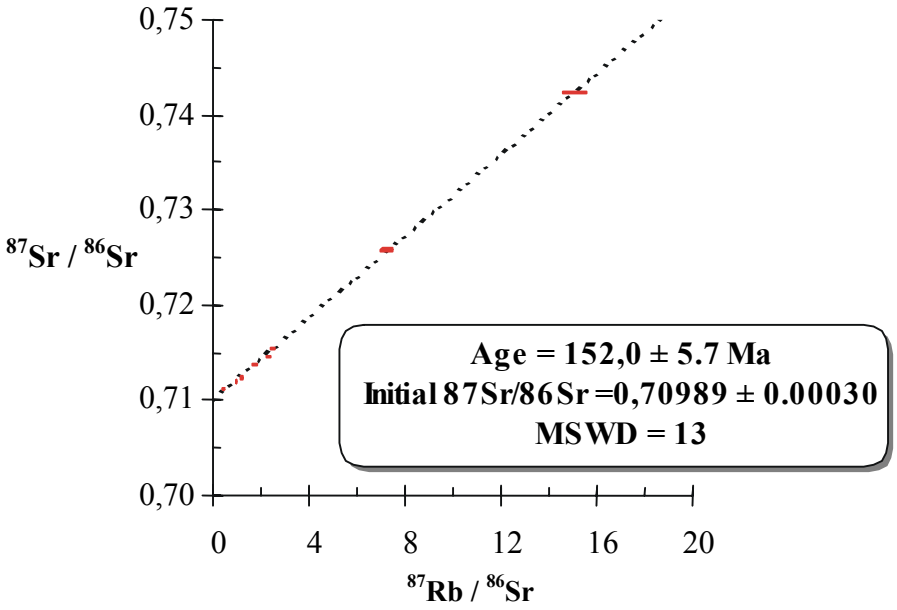

Figure 4.1: The granite whole rock isochron is in good agreement with the well-known late Jurassic hydrothermal event (135-160 Ma).

For the altered zones of the sampling profile, the calculations give incoherent ages. In altered zone II, the Rb-Sr signal is heavily perturbed and the samples do not fit to any isochron. The calculated age for altered zone I, with a high error range (232 ± 55 Ma, 2σ error), is younger than the Permian rhyolite $^{40}Ar/^{39}Ar$ age of around 290 Ma presented by (Lippolt et al., 1990). The rhyolite segment of the profile does not contain enough samples to determine an useful isochron. The trend of the Rb-Sr data within this segment is around 300 Ma, which is in agreement with previous work (Hess and Lippolt, 1996).

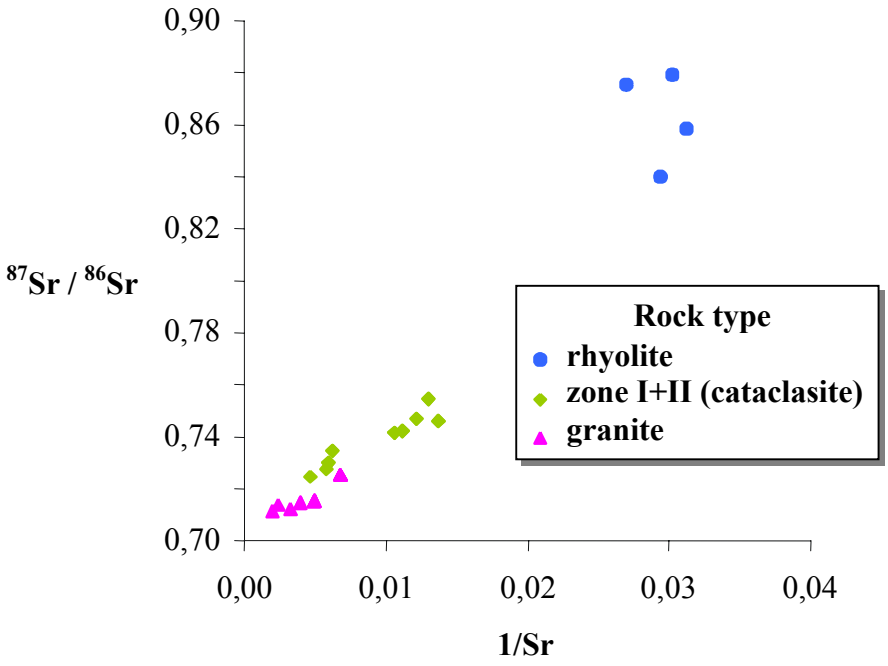

Figure 4.2: The strontium mixing diagram reveals that the altered zone samples are situated between "granite" and a "rhyolite" endmembers.

The segments of the sampling profile show, for the Rb-Sr data, a transition ranging from a highly perturbed granite zone with a new isotopic composition, in agreement with the late Jurassic hydrothermal event, to an unperturbed rhyolite zone. The altered zones between these two segments are also perturbed, notably zone II which is the closer to the granite zone. Plotting the data on a $^{87}Sr/^{86}Sr$ vs. 1/Sr diagram (fig. 4.2) reveals that the cataclase samples are between the "granite" and "rhyolite" endmembers. Altered zone II has the highest clay content, notably kaolinite (Schleicher, 2001) which reduce the permeability and indicate a high fluid-rock interaction. This cataclastic zone seems to have played a barrier role during the late Jurassic hydrothermal event. This event can be well identified

on the granite side but in altered zone I the measured age is perturbed and not overprinted as in the granite. The altered zone II seems to have slowed down (reduced permeability) the diffusion acting within the granite segment, which also explain that the altered zones are closer to the granite in the mixing diagram (fig. 4.2). This result highlights the importance of clay barriers. The role of the clay as barrier for fluid circulation has been shown in a previous study (Techer et al., 2001). The granite is the underlying rock and thus more altered by deep fluid circulation. The boundary between the granite and the overlying rhyolite can also slow down the flowpath and drain the hydrothermal fluids.

4.1.2 Rb-Sr mineral analysis

The geochemical results of immobile elements (chapter 3) indicate a mixing of granitic and rhyolitic rock within the altered zones. The K-feldspars of sample (G4) from the altered zones has been compared to samples from the granite zone (G12 and G13) and to fresh and altered reference samples in order to assess differences or similarities in the Rb-Sr composition (tab. 4.1). G4 is a rhyolitic sample. However, this sample contains K-feldspars and belongs to the sample of the altered zones with a granitic signature in the immobile elements.

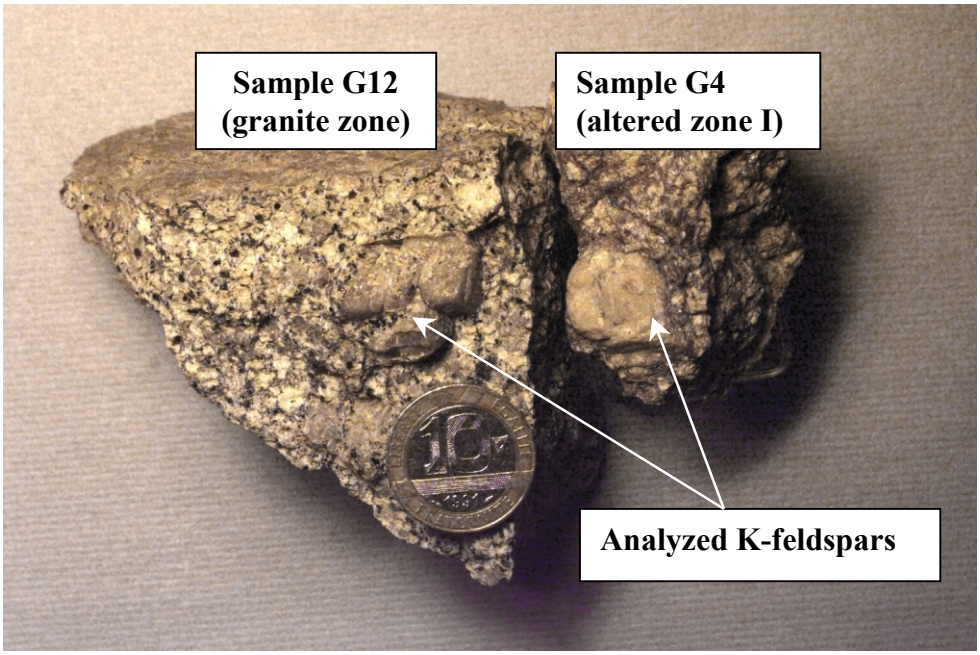

Figure 4.3: Samples of granite (G12) an drhyolite (G4) from which K-feldpars were extracted. G4 is a rhyolitic sample. However, this sample contains K-feldspars and belongs to the sample of the altered zones with a granitic signature in the immobile elements.

Description	$^{87}Rb/^{86}Sr$		$^{87}Sr/^{86}Sr$		Sr	Rb
		2σ abs		2σ abs	[ppm]	[ppm]
Reference sample: granite fresh (Stift Neuburg)	0,91	3E-02	0,7112	9E-05	934	294
Reference sample: granite altered (Stift Neuburg)	0,90	3,E-02	0,7117	8,E-05	1066	334
G4 (altered zone I)	2,32	7E-02	0,7161	9E-05	450	362
G12 (granite zone)	0,47	1E-02	0,7088	9E-05	1418	230
G13 (granite zone)	3,06	9E-02	0,7207	2E-04	348	369

Table 4.1: Rb-Sr composition of K-feldspars from the Schauenburg fault and reference samples.

Plotting the data on a $^{87}Sr/^{86}Sr$ vs. 1/Sr diagram (fig. 4.4) shows that the samples of the Schauenburg fault are not in concordance with the reference granite samples. The whole rock Rb-Sr results have shown that the granite samples of the sampling profile have been perturbed by the late Jurassic event. Thus it is difficult to compare the Rb-Sr data of sample G4 with other samples of the fault. However, G4 is situated in the "granitic" range compared to the rhyolite whole rock results, which have much higher $^{87}Sr/^{86}Sr$ ratios (appendix C1.2).

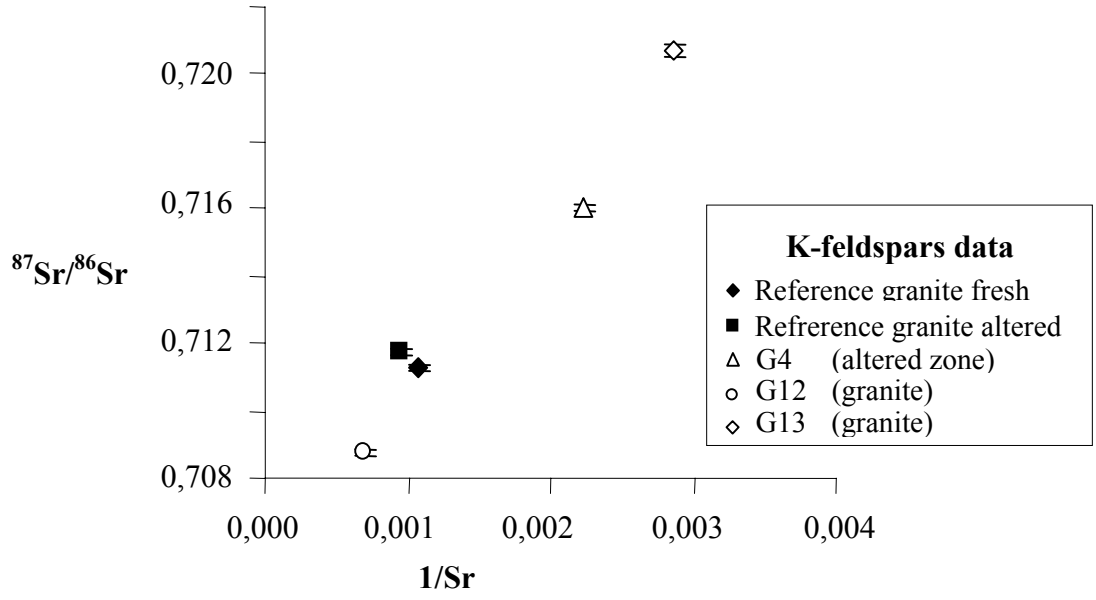

Figure 4.4: The 1/Sr vs. $^{87}Sr/^{86}Sr$ plot shows that the K-feldspars are perturbed against the reference samples, in agreement with the whole rock result of the fault zones, perturbed by the late Jurassic event.

4.2 Lead (Pb)

4.2.1 Schauenburg fault lead signature

The samples of the rhyolite zone have a high lead content, between 147 and 254 ppm, 10 times more than the maximal lead content of a "normal" extrusive rock (fig. 4.5). The altered zones I and II also have even higher lead contents. In zone II the lead concentrations are around 300 ppm and in zone I the contents are much higher, around 600 ppm, with one sample even reaching 1200 ppm (fig. 4.5). All these samples (rhyolite, altered zones I and II) with high lead contents also have unusual stable isotopic ratios. $^{206}Pb/^{204}Pb$ rhyolite ratios plotted along the profile are around 18,75 (fig. 4.5). The two first granite samples on the cataclase side also have high lead content with the same isotopic signatures as the rhyolite and the altered zone samples. The other granite samples show "normal" granite lead content (around 30 ppm) with $^{206}Pb/^{204}Pb$ ratios between 18,3 and 18,6.

Several features of the Pb-isotopic compositions for the rhyolite and altered zones samples need to be explained:

- the high lead content,
- the regularity of the isotopic data,
- the relation of the isotopic signatures between rhyolite, the altered zones and granite.

Analytical errors are considered an unlikely explanation for the high lead content and the linearity of the isotopic data (fig. 4.5). None of the chemicals used in the laboratory have isotopic ratios and high lead content that would provide suitable endmembers for the trends in figure 4.6 to be explained by a two-component mixing. Three samples were measured twice (new dissolution, other ion-exchange techniques) and the result corresponds to the first run. Lead contents from 7 samples have also been measured on TIMS and the produced results are in good agreement with the ICP-MS results (appendix B5). Geological sampling errors are also considered unlikely because of the similarity in behavior of isotopic compositions and lead contents from the different quarry rhyolite reference samples (fig. 4.5).

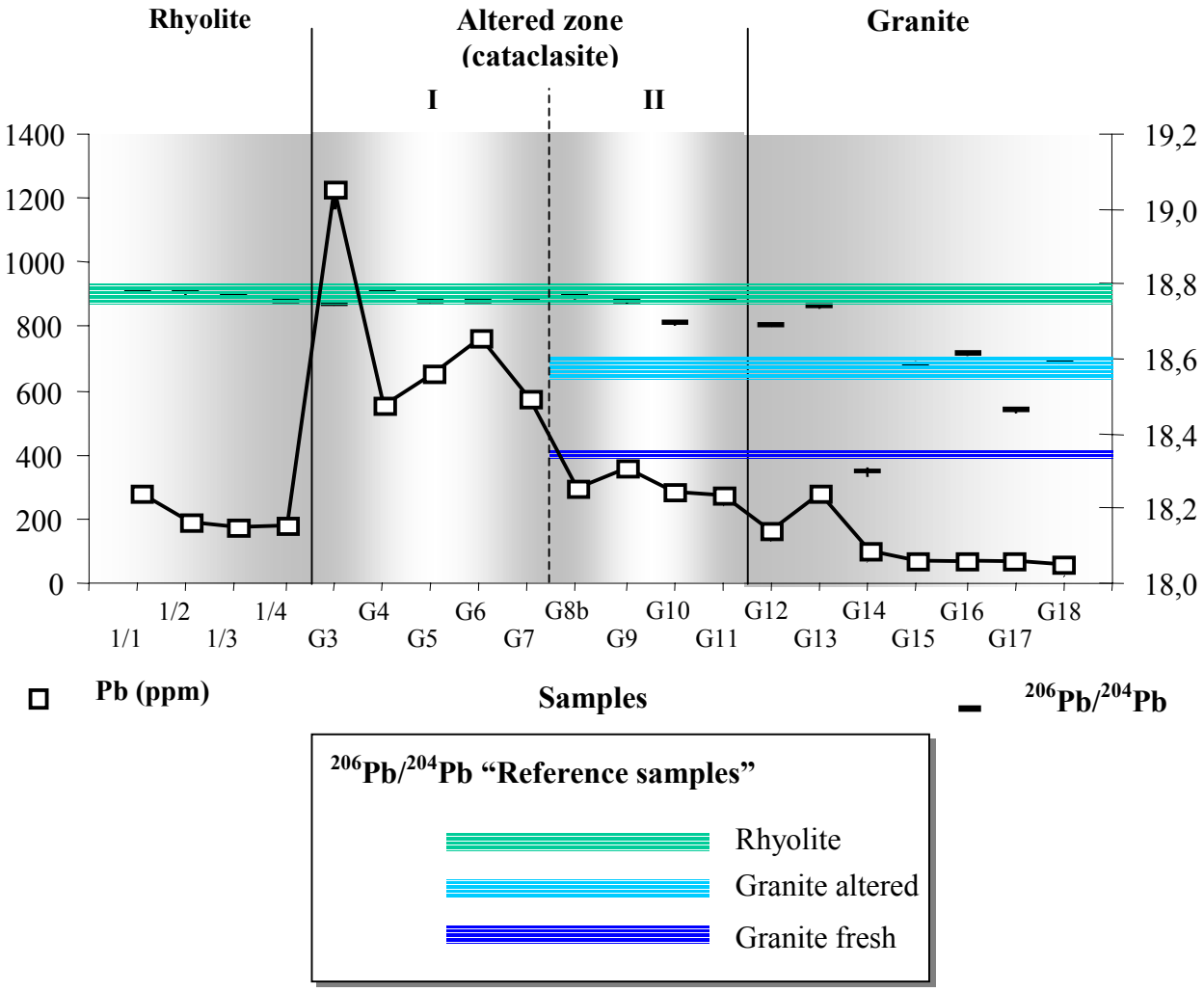

Figure 4.5: Lead content and ^{206}Pb / ^{204}Pb ratio. The rhyolite samples and especially the altered zones samples have high lead contents. These samples have the same isotopic ratios. The granite zone does not have a perturbed lead signature.

The altered zones have the same isotopic composition as the rhyolite sample, but show an additional enrichment in lead. The altered zones enriched in lead require a process that has affected the Pb-isotope systematics of the sample G3 to G11 without apparently affecting the granite samples farther away from the boundary. One possible explanation could be a local effect induced by the altered zones. The geochemical results (chapter 3) have shown that some elements have been enriched in the altered zones. A flowpath could have altered the rocks that lie within m-distance on both sides of the altered zones and enriched them in lead and set up a new lead isotopic composition. However, the rhyolite reference sample

analysis from neighboring quarries also produced high lead contents with the same isotopic composition (fig. 4.5). The uniformity of the high lead content with stable isotopic ratios in the rhyolite cover induces that this lead signature is probably the original composition of the Permian extrusion. Thus sources of the additional lead are not the altered zones but is most likely from the rhyolite body.

The granite samples (G14 to G18) have $^{206}Pb/^{204}Pb$ isotopic ratios between 18,3 and 18,6. The lowest value (18,3) corresponds to that of the "fresh" granite reference sample and 18,6 corresponds to the "altered" value of the granite reference sample.

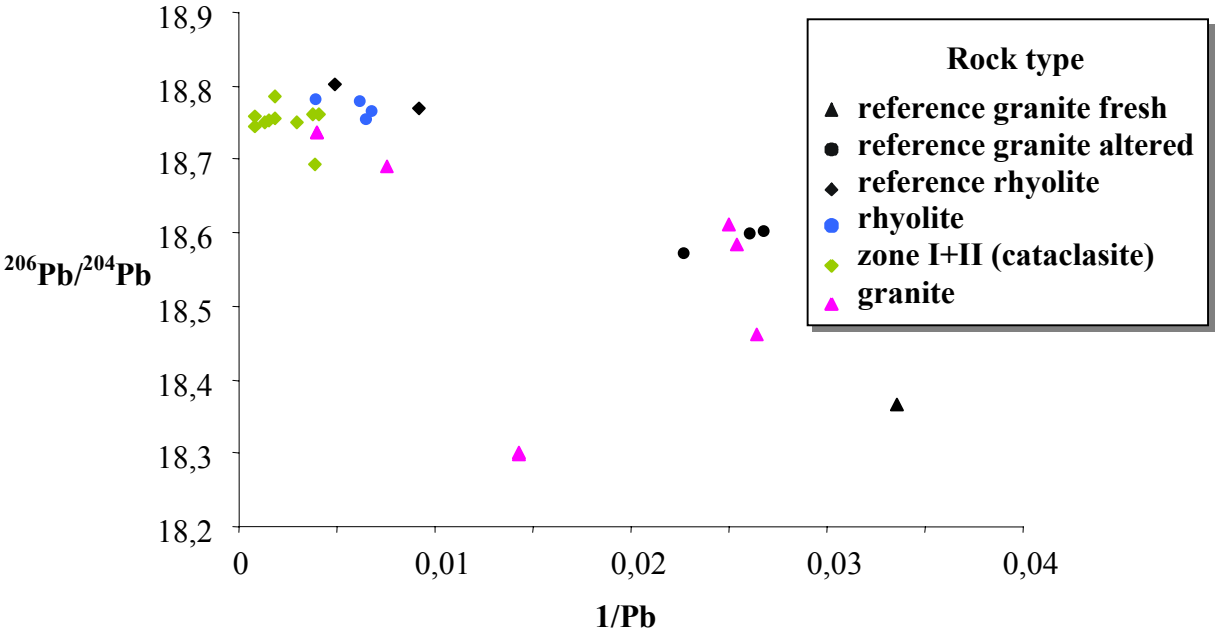

Figure 4.6: The lead mixing line shows that the lead signature of the altered zones is similar to the rhyolite samples.

4.2.2 The altered zones lead signature

For the altered zones, the lead enrichment could have been acquired during the Permian rhyolite extrusion (290 Ma), without affecting the underlying granite farther away from the boundary. This assumption explains the high lead content of the altered zones but not the regularity of the isotopic composition over the rhyolite zone and the altered zones. If the lead signature of the altered zones had been acquired during Permian times, the samples should have acquired a different isotopic composition with respect to the rhyolite. A more

recent enrichment process is needed to explain the stable isotopic composition in the zone with a high lead content, also in good agreement with the geochemical analysis presented in chapter 3. Some immobile elements display irregularities in their profiles providing evidence for a primary mixed granite-rhyolite composition in the altered zones. Several mobile elements (Al, Si, Zr, Hf) do not show these anomalies and provide clues of one or more younger events setting up a new composition.

The Pb-isotopic ratios do not enable any realistic age calculation. The regularity of the results induces that the plots do not show any trend and therefore suggest that these rocks contain an additional lead component that has been mixed with the original lead. The original lead is assumed to be negligible against the lead enrichment. A regression of the $^{206}Pb/^{204}Pb$ ratio of the rhyolite samples and the altered zones samples, using the equation:

$$\alpha_t = \alpha_M - \mu \times \left(e^{\lambda_{238} t} - 1\right) \qquad (1)$$

Where α_t is the $^{206}Pb/^{204}Pb$ ratio at time t, α_M is the measured $^{206}Pb/^{204}Pb$ ratio, μ the $^{238}U/^{204}Pb$ ratio and λ_{238} the ^{238}U decay constant.

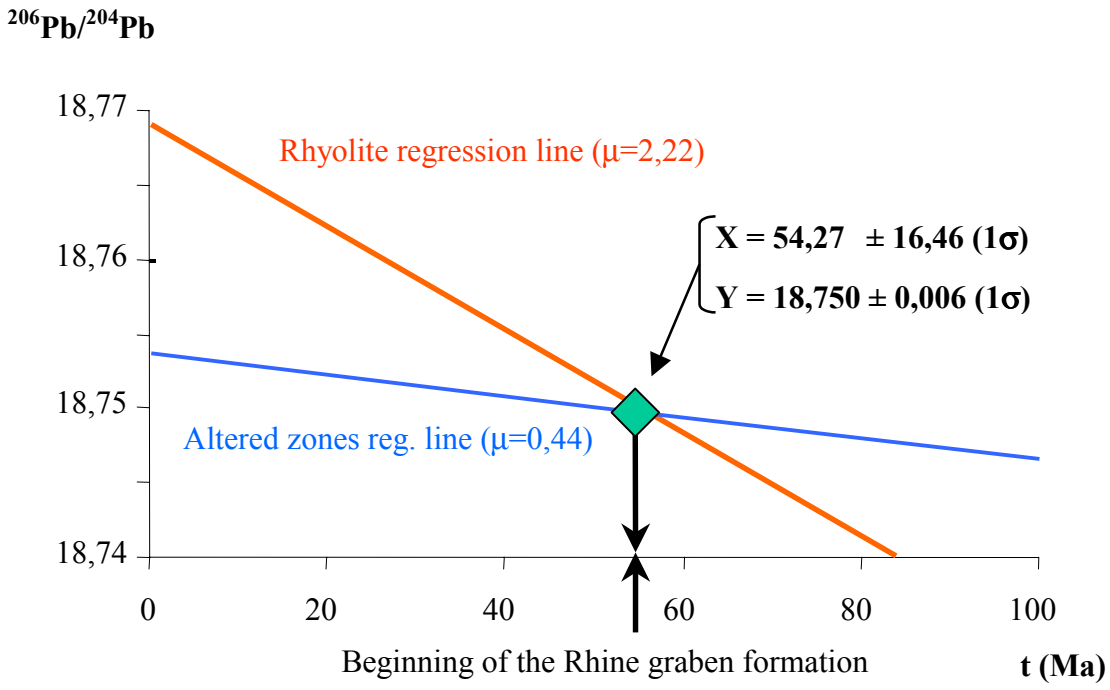

Figure 4.7: Estimated age of the Pb enrichment if the altered zones. The regression line of the altered zones samples suggests an event connected with the Rhine Graben formation explaining the similar lead isotopic ratios in both zones.

The regression of the $^{206}Pb/^{204}Pb$ ratio from the rhyolite samples and the altered zones samples has been calculated in order to find out a common point where the two zones had the same lead isotopic composition. Tertiary events, potentially connected with the development of the Rhine Graben have been established (fig 4.7). The regression lines are crossing each other at an age of 54 Ma ± 16 (1σ). The error is high but the covered range from 70 to 38 Ma corresponds to the first steps of the Rhine Graben formation (Geyer and Gwinner, 1991). This rifting event is much less time localized than the late Jurassic hydrothermalism (section 4.1), but a continuous phenomenon, which reactivated old weak tectonic structures and initiated new fault systems with enhanced fluid circulation. This could explain the wide error range.

4.2.3 Lead mineral analysis

Mineral analyses have been made on the same samples as studied by the Rb-Sr method (section 4.1.2) in order to determine the location of the additional lead (tab. 4.2).

In the reference samples, the whole rock lead content and isotopic composition can be explained by the lead content and the isotopic composition of the minerals analyzed. In sample G13, which is one of the granite samples with high lead content (191 ppm) next to the altered zones, the lead content is higher than any of the values measured for the different minerals (tab. 4.2). The lead enrichment can not be explained with the rock forming minerals content but requires another mineral phase to carry the high lead content. A vitriol sample from the mine “pit Anna Elisabeth” has also been measured and reveals a high lead content (847 ppm) and a high lead isotopic ratios (tab. 4.2). The hydrothermal formed gangue in the granitic body (“Branigsberger” silver- and vitriol mine of “pit Anna Elisabeth” in Schriesheim) probably occurred during the irruption of the upper Rhine graben in Eocene (Schleicher, 2001), thus at the same time as the lead enrichment event in the altered zones. New accessory mineral phases could have precipitated, like vitriol, and hosted the additional lead in the rock.

Like for the Rb-Sr measurements, the sample G4 of altered zone I can be compared to samples of the granite zone in order to evaluate if this sample belongs to granite or to rhyolite. The geochemical results of the immobile elements (chapter 3) indicates a mixing of granite and rhyolite rock within the altered zones. Although G4 is a rhyolitic sample, the immobile element composition better fit to the granitic sample suite. As for the Rb-Sr measurements, the Pb K-feldspar results do not show clearly the appartenance of sample

G4. The sample does not belong to the same source as the K-feldspars of the granite zone and the granite reference samples. In sample G4 the Pb isotopic signature is highly perturbed and is difficult to interprete.

Description		$^{206}Pb/^{204}Pb$	1σ abs	$^{207}Pb/^{204}Pb$	1σ abs	$^{208}Pb/^{204}Pb$	1σ abs	Pb [ppm]	μ
Ref. sample: granite fresh (Stift Neuburg)	Whole rock	18,306	2E-02	15,620	2E-02	38,376	5E-02	31	3,6
	K-feldspar	18,173	9E-03	15,613	7E-03	38,310	2E-02	107	
	Apatite	26,617	3E-01	15,924	2E-01	39,063	4E-01	14	202,9
	Biotite 100-200 μm	18,296	9E-02	15,397	7E-02	37,736	2E-01	13	9,9
	Biotite 200-315 μm	18,656	1E-01	15,492	1E-01	38,157	3E-01	15	8,0
Ref. sample: granite altered (Stift Neuburg)	Whole rock	18,598	3E-02	15,750	3E-02	38,998	7E-02	38	3,4
	K-feldspar	18,180	4E-03	15,600	4E-03	38,259	1E-02	63	0,2
	Apatite	24,122	1E-01	16,056	1E-01	39,906	2E-01	23	76,8
	Biotite 100-200 μm	19,145	3E-03	15,675	3E-03	39,089	1E-02	64	13,8
	Biotite 200-315 μm	19,263	8E-03	15,688	7E-03	39,138	2E-02	74	16,1
G4 (altered zone I)	Whole rock	18,786	0,001	15,665	1E-03	39,016	4E-03	533	0,6
	K-feldspar	18,371	6E-03	15,591	5E-03	38,324	1E-02	87	0,1
G12 (granite zone)	Whole rock	18,689	0,001	15,637	1E-03	38,859	5E-03	132	2,0
	K-feldspar	18,185	1E-02	15,570	9E-03	38,224	2E-02	57	0,2
G13 (granite zone)	Whole rock	18,737	1E-03	15,643	1E-03	38,914	3,E-03	191	1,0
	K-feldspar	18,243	3E-03	15,614	2E-03	38,214	6E-03	87	0,3
	Apatite	28,641	6E-02	16,223	3,E-02	42,663	9,E-02	20	93,6
	Biotite 100-200 μm	19,273	1E-02	15,655	1E-02	39,056	3E-02	16	14,2
	Biotite 200-315 μm	19,144	1E-02	15,653	9E-03	38,958	2E-02	13	11,3
Anna-Elisabeth	Vitriol	18,930	2E-03	15,713	2E-03	39,129	5E-03	847	

Table 4.2: Mineral analysis from reference material and from samples of the Schauenburg fault.

4.3 Thorium (Th) – Uranium (U) disequilibrium

4.3.1 Results

The $\delta^{234}U$ (([$^{234}U/^{238}U]_{a.r.}$ –1) x 1000)) and the concentration of ^{238}U are listed in Table 4.3 together with that of $^{230}Th_{exc}$ activity and porosity.

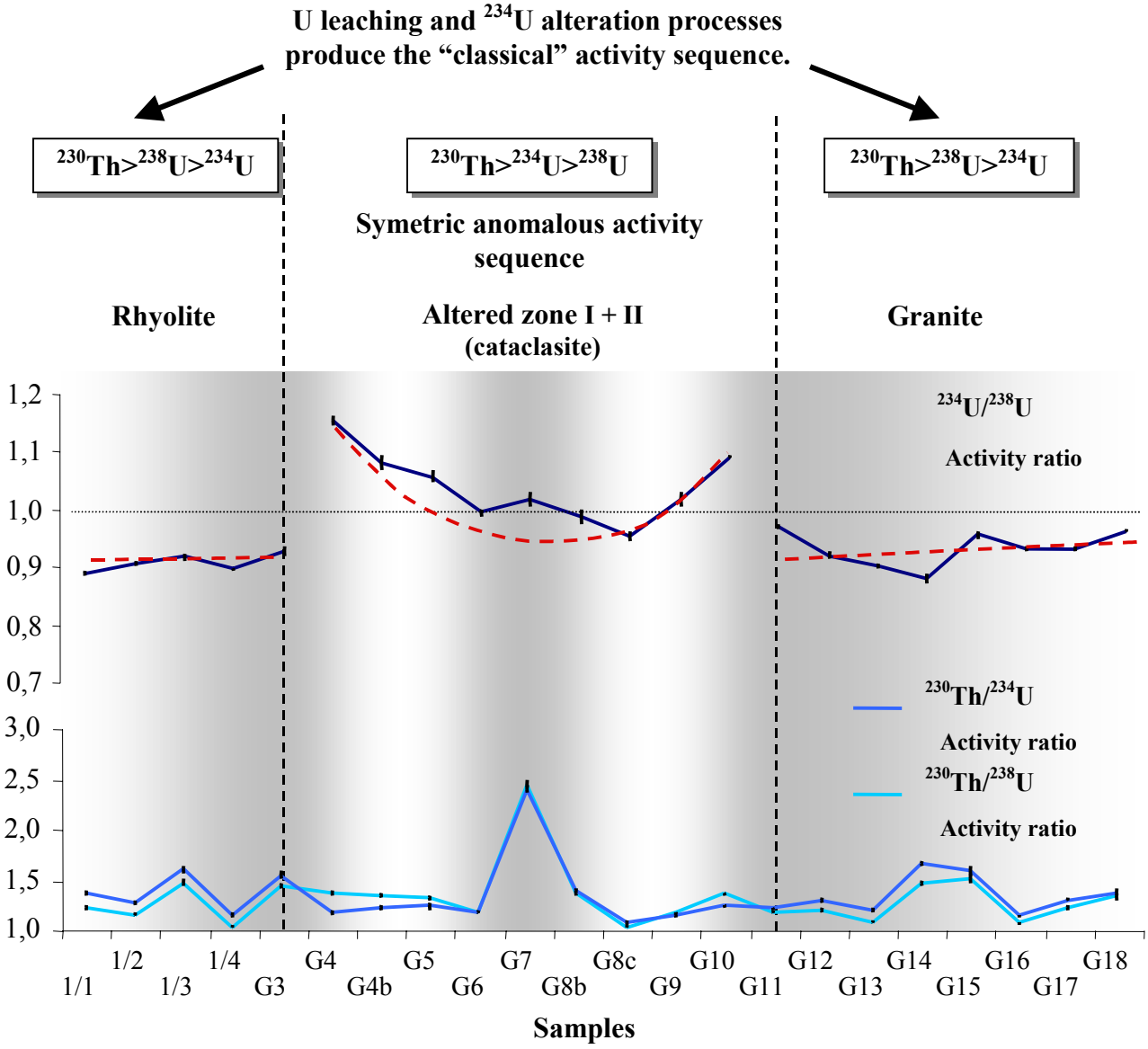

Figure 4.8: The disequilibrium profile reveals that all the samples display a Th excess. The samples of the altered zones show a symetric anomalous activity sequence due to an exchange with the aqueous phase.

	Name	Distance [m]	Run	$\delta^{234}U$ [o/oo]	error abs.	^{238}U [ppm]	error abs.	$^{230}Th_{exc}$ [dpm/g]	error abs.	Porosity [%]
Rhyolite	1/1	0	1	-106	4	7,188	0,019	1,91	0,14	
	1/2	1	1	-90	4	6,027	0,012	1,19	0,08	
	1/3	2	1	-79	7	5,094	0,010	2,18	0,17	
	1/4	3	2	-101	3	5,721	0,008	0,65	0,07	
Altered zone I	G3	4	2	-69	10	3,060	0,011	1,21	0,09	6,68
	G4	5	1	158	8	4,947	0,023	0,83	0,12	
	G4b	6	1	86	13	3,775	0,020	0,76	0,10	8,38
	G5	7	2	61	11	3,485	0,016	0,71	0,09	7,44
	G6	8	2	-2	6	4,625	0,014	0,70	0,06	7,23
	G7	9	1	21	13	2,933	0,011	3,18	0,10	
Altered zone II	G8b	10	1	-11	13	1,599	0,005	0,49	0,05	3,51
	G8c	11	1	-43	7	4,954	0,019	0,35	0,07	
	G9	12	3	20	13	1,999	0,012	0,26	0,03	6,84
	G10	13	3	95	3	2,064	0,003	0,44	0,03	13,43
	G11	14	3	-27	3	2,570	0,002	0,44	0,02	8,18
Granite	G12	15	2	-77	7	3,037	0,008	0,68	0,06	
	G13	16	2	-95	3	3,215	0,005	0,49	0,05	4,87
	G14	17	2	-115	8	1,754	0,004	0,79	0,05	3,6
	G15	18	1	-40	7	3,335	0,010	1,45	0,13	
	G16	19	3	-63	4	4,631	0,012	0,52	0,06	
	G17	20	1	-63	4	2,529	0,004	0,57	0,04	
	G18	21	1	-33	3	2,659	0,004	0,77	0,07	

Table 4.3: Isotopic compositions of Th and U across the fault zone. The uncertainties are ± 2σ

All the samples display a ^{230}Th excess (tab. 4.3) and thus have undergone a leaching of uranium, revealing that uranium and thorium redistribution processes have occurred within the last ~ 10^6 years. The granite and the rhyolite samples display an uranium activity ratio<1 with probably no exchange with the aqueous phase (fig. 4.8). Instead, the samples of the altered zones (G4 to G10), with $^{234}U/^{238}U$ >1, record a more complex history of uranium exchange with the aqueous phase (fig. 4.9). The uranium exchange is higher on the marginal samples of the altered zones closer to the fault boundaries and lower in samples situated in the middle of the fault. The ^{238}U-, ^{234}U-, ^{230}Th- concentrations (fig. 4.10) and the ^{230}Th excess (tab. 4.3) do not show any trend across the sampled profile, thus no correlation with $\delta^{234}U$. That suggests an exchange with the aqueous phase without loss or sorption of uranium. It has to be explained why the symmetric uranium exchange trend is localized only inside the altered zones (sample G4 to G10) with an abrupt transition along the boundary between the altered zones and the granite and rhyolite samples where only uranium loss is observed. The relationship between the porosity and the exchange of uranium could be a suitable explanation and will be investigate.

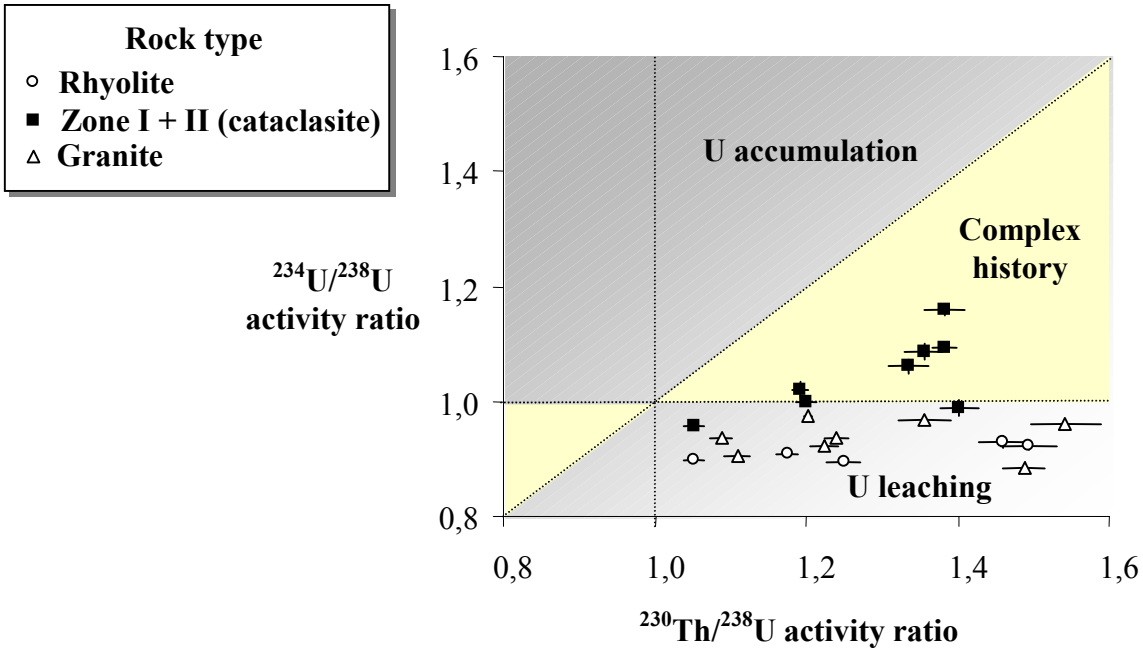

Figure 4.9: Interpretation of uranium disequilibria (after Thiel et al., 1983). Samples from the altered zones indicates a more complex history of uranium accumulation and leaching.

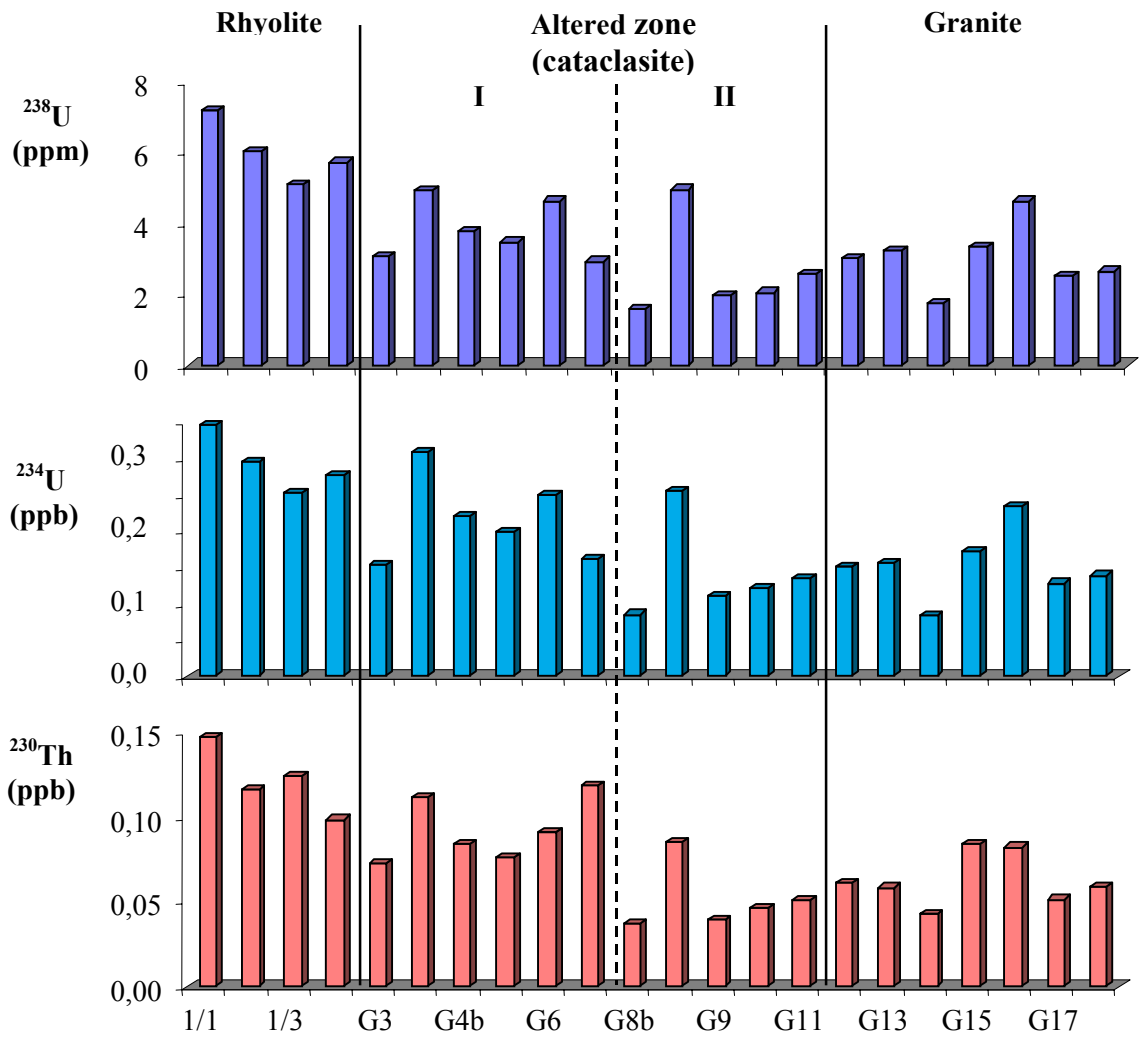

Figure 4.10: Concentrations of ^{238}U, ^{234}U and ^{230}Th across the Schauenburg profile.

4.3.2 Fault reactivation

Studies of tectonically active terrains have shown that fault displacements in the upper continental crust are largely accomplished by increments of seismic slip along pre-existing structures (Sibson, 1994). In the vicinity of faults that undergo intermittent rupturing, permeability and fluid flux is related to this earthquake cycle through a range of mechanisms, leading to complex interactions between stress cycling, the creation and destruction of permeability, and fluid flow (Sibson, 1994). Faults often act as impermeable

seals through the presence of clay-rich gouge and hydrothermal cementation (Smith, 1980; Hooper 1991). The intrinsic roughness of natural fault surfaces (Power et al., 1987) has the implication that freshly ruptured faults should become highly permeable channel-ways post-failure. Rupture zone permeability is, however, likely to be short-lived. Evidence from geothermal fields suggests that hydrothermal flow along fractures rapidly leads to hydrothermal precipitation and self-sealing (Batzle and Simmons 1977). Thus in fault zone, a continual competition can be expected between the creation and destruction of fracture permeability. It can be noted that the permeability is proportional to the porosity and can be calculated, for example, with equation 2 established by Katz and Thompson (1987):

$$K = C \times L^2 \times \phi^{1,5} \tag{2}$$

where C is a constant (1/226), L is the pore diameter at the mean porosity (in meter) and ϕ is the measured porosity (%). The U-Th data will be discussed against the porosity data of some samples.

The $^{234}U/^{238}U$ ratios along the profile, especially the symmetric anomaly of the altered zones, could reflect the change of porosity in relation to tectonic events in the Rhine Graben inducing fault reactivation. On both sides of the altered zones the fault mechanisms have increased the porosity that enable a higher w/r index (longer contact between water and rock). At this location, a higher exchange of uranium with the aqueous phase without any sorption occurs. Within the altered zones, the porosity is lower in the central area, similar to the porosity of the rhyolite and granite samples situated beside the altered zone. In these segments, low volumes of circulating fluid have restricted uranium exchange between the rock and the aqueous phase.

4.3.3 Exchange model

To relate the porosity data with the $\delta^{234}U$ value, a simple exchange model was here developed.

The equation describing the behavior of the $\delta^{234}U$ (R) in the rocks due to radioactive decay of excess ^{234}U and to the exchange with pore water uranium with the $\delta^{234}U$ of the rain water is:

$$\frac{dR}{dt} = -(\lambda_E + \lambda_{234})R + \lambda_E R_f \tag{3}$$

Where R_f is the $\delta^{234}U$ of the aqueous phase. In surface waters, the $\delta^{234}U$ varies from nearly 100 ‰ to about 200 ‰ (Osmond and Cowart, 1982). The range is relatively less than found in ground waters; this is because most surfaces waters are mixtures of runoff and diverse ground-water sources (Ivanovich and Harmon, 1992). In this study, the $\delta^{234}U$ of the aqueous phase (R_f = 160 ‰) has been fixed to explain the highest $\delta^{234}U$ measured and fitted to the range given for surface waters by Osmond and Cowart (1982). λ_E is the exchange coefficient of uranium incorporated in the rocks with uranium dissolved in pore water and λ_{234} is the decay constant of ^{234}U. Applying this equation, it is therefore assumed that for each porosity a certain amount of the uranium (with the $\delta^{234}U$ corresponding to the age of this layer) exchanges with pore water uranium and $\delta^{234}U$ of rain water. The solution for equation (3) is :

$$R(t) = \left(1 - \frac{R_f}{R_0} \times \frac{\lambda_E}{(\lambda_{E+}\lambda_{234})}\right) R_0 e^{-(\lambda_E + \lambda_{234})t} + \frac{\lambda_E R_f}{(\lambda_E + \lambda_{234})} \qquad (4)$$

Where R_0 is the $\delta^{234}U$ of the rocks with negligible exchange with the aqueous phase. The initial $\delta^{234}U$ of the altered zones samples (R(t = 0) = -78 ‰) have been evaluate from an average of the granite and rhyolite $\delta^{234}U$. The rate of exchange with pore water uranium controls both the steady state value (the second term of the equation) as well as the slope of the curve of the $\delta^{234}U$ (the exponent). The higher the rate of exchange, the flatter becomes the slope and the higher is the steady state value of the $\delta^{234}U$.

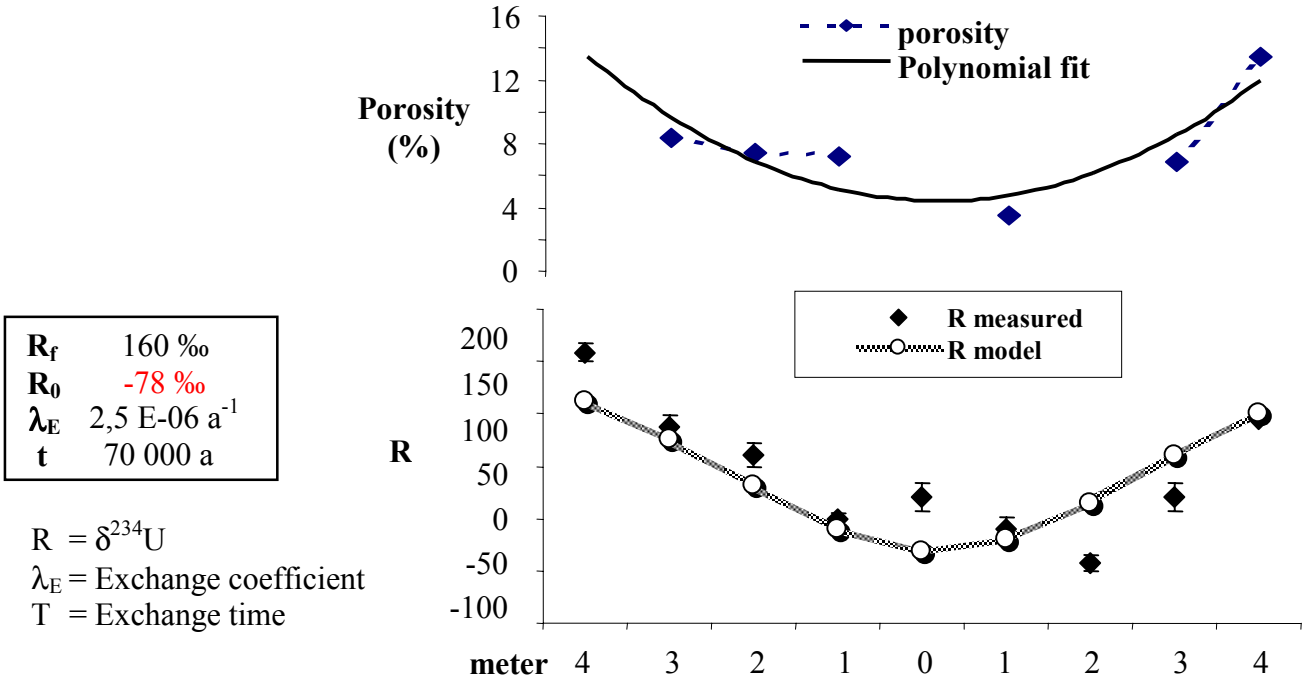

Figure 4.11: Best fit result of the exchange model applied on the altered zones.

The first step involves a polynomial fit of the porosity data across the altered zones (fig. 4.11). The obtained fit is then applied to the exchange coefficient of uranium λ_E. In doing so, the exchange of uranium is assumed proportional to the porosity. Thus a higher porosity originates a greater λ_E. The model calculates for a given λ_E, for the central sample, the λ_E for the whole altered zones. Using equation (4), the $\delta^{234}U$ for the altered zones can be calculated.

The best approximation to the data of the altered zones of the sampling profile is obtained assuming an exchange coefficient for uranium ranging from 2,5 E-06 [a^{-1}] in the middle of the altered zones to 2,5 E-05 [a^{-1}] on the sides of the altered zone (fig. 4.11). These values corresponds to a residence time of absorbed uranium of 400 000 ka to 40 000 ka respectively. The resulting exchange time for the approximation is 70 000 ka and can be considered to be the alteration age for the samples within the altered zones. The exchange is higher on the sides of the fault than in the middle, in relation with the porosity, thus the permeability (Katz and Thompson, 1987), across the altered zones. The symmetry of the permeability can be explain by the reactivation history of the fault inducing creation and destruction of fracture permeability (section 4.3.2).

Also shown is the sensibility of the calculated $\delta^{234}U$ when various exchange coefficients of 1,0 E-06 [a^{-1}] and 5,0 E-06 [a^{-1}] are used for the central sample (fig. 4.12). This shows that the range for suitable exchange coefficient is very small. A lower λ_E (1,0 E-06 [a^{-1}]) induce less exchange with the aqueous phase. A similar effect can be obtained by reducing the exchange time of the model to 35 000 ka (fig. 4.13). In this case, the sample does not have enough time to equilibrate with the aqueous phase. Using a higher λ_E (5,0 E-06 [a^{-1}]), shows a more rapid exchange with the aqueous phase. This, however, can also be reached by increasing the exchange time of the model to 140 000 ka (fig.4.13). Earlier results by Neff et al. (1999) give a value for the uranium exchange coefficient λ_E in the Mn-crusts from Pacific Ocean of 5,0 E-06. This similar result is in good agreement with our data. The light difference between the two studies can be explained by the differences in the chemical processes, mineralogy and porosity.

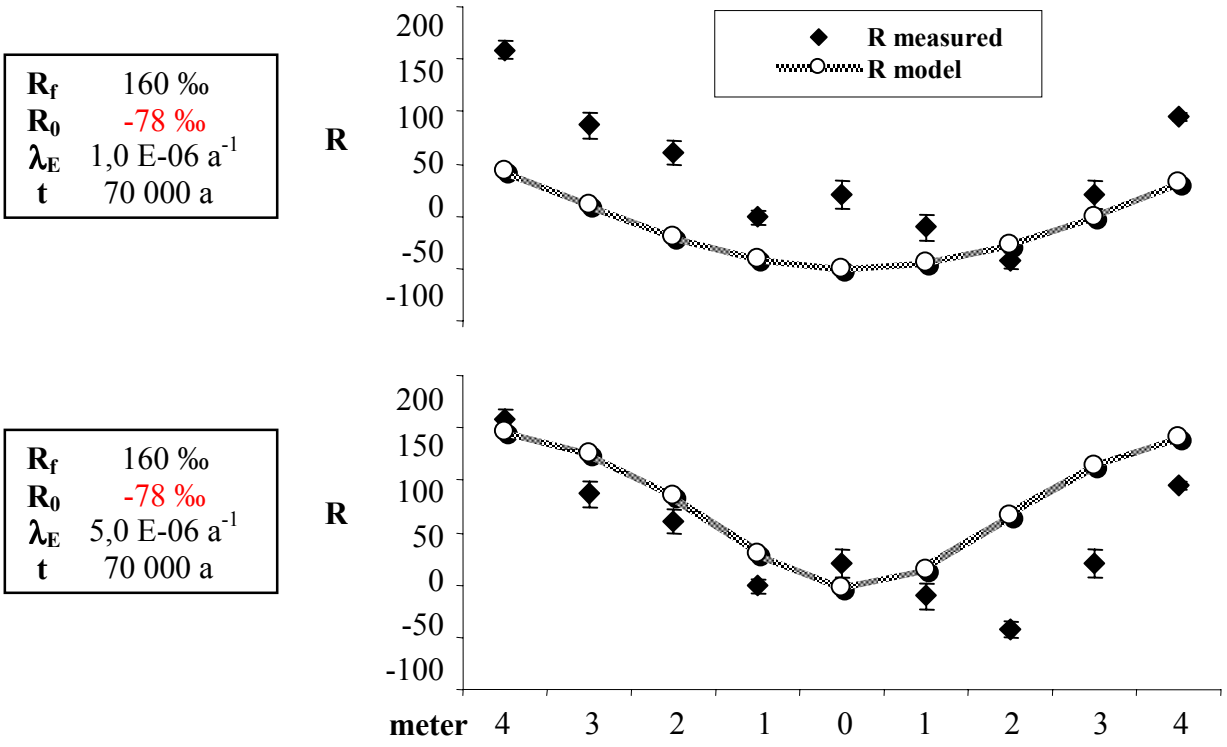

Figure 4.12: Influence of λ_E on the exchange model applied on the altered zones. The range for suitable exchange coefficient is very small.

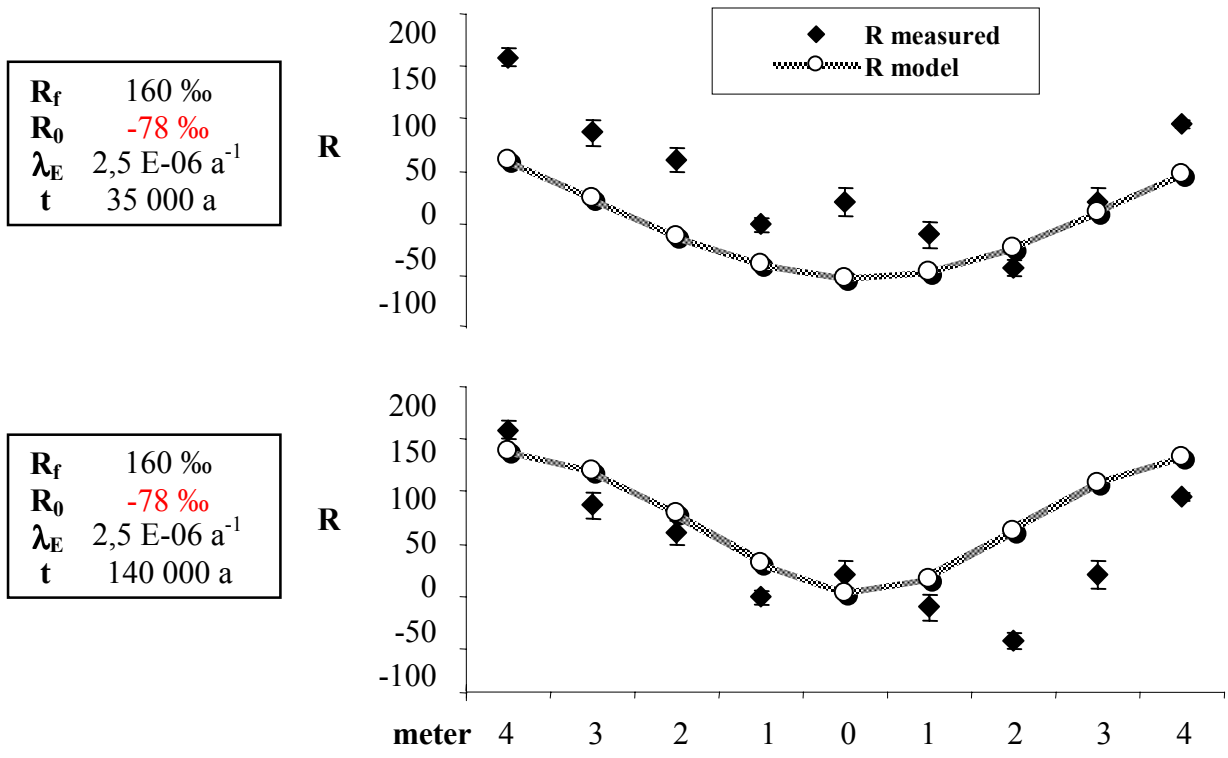

Figure 4.13: Influence of time on the exchange model applied on the altered zones. The effect are similar to those obtain by various exchange coefficient.

4.4 Summary

The isotopical investigations provide evidence for a complex fluid rock interaction history which affected the Schauenburg fault, particularly during the late Jurassic thermal activities, the Tertiary rifting with the Rhine Graben, and the recent (< 1 Ma) alteration processes:

- The granite zone of the sampling profile has undergone an event which set up a new Rb-Sr isotopic composition corresponding to an age much lower than the original age of 330 Ma given for the Heidelberger Granite (Hess and Lippolt, 1996). The Rb-Sr data of the granite samples produce a whole rock isochron (fig. 4.1) of 152 ± 5,7 Ma (2σ error) in good agreement with the well-known late Jurassic hydrothermal event that induced widespread sericitization and formation of illite in the regional basement. Altered zone II has the highest clay content, notably kaolinite (Schleicher, 2001). This cataclastic zone seems to have acted as a barrier during the late Jurassic hydrothermal event. This event can be well identified on the granite side but in altered zone I the measured age is perturbed and not reset like for the granite. The altered zone II seems to have slowed down the diffusion acting within the granite material. This result highlights the importance of clay barriers.

- The rhyolite and the altered zones have high lead contents with homogeneous stable Pb isotopic ratios. Tertiary events, potentially connected with the development of the Rhine Graben have influenced the Pb isotopic distribution (fig 4.7). The rhyolite seems to be the source for the lead enriched in the altered zones. The rocks evolution lines for Pb support a Tertiary hydrothermal event (54 Ma ± 16). This rifting event is much less localized in time than the late Jurassic hydrothermal activity (section 4.1), but a continuous phenomenon, which reactivated old weak tectonic structures and initiated new fault systems with enhanced fluid circulation. The events, connected with the Rhine Graben formation, are considered as have been responsible for the geochemical changes identified in the altered zones (chapter 3). The location of the additional lead has not been established. Accessory mineral phases, like oxides, which have precipitated during the lead enrichment event, could host the additional lead. The granite was not affected. Only the two first granite samples on the cataclase side have been disturbed. This shows again the barrier role of the fault structure and clay rich zone.

- The fault zone samples display a ^{230}Th excess (tab. 4.3) and thus have undergone a leaching of uranium, revealing that uranium and thorium redistribution processes have occurred within the last ~ 10^6 years. The granite and the rhyolite samples display an uranium activity ratio <1 with probably no exchange with the aqueous phase (fig. 4.8). Instead, the samples of the altered zones (G4 to G10), with $^{234}U/^{238}U$ >1, had a more complex history of uranium exchange with the aqueous phase (fig. 4.9). The result of this study is that the rate of exchange of absorbed uranium is related to porosity/permeability structure. Thus the variation of $\delta^{234}U$ can be explain by the variation of the permeability and can be explain by the reactivation history of the fault inducing creation and destruction of fracture permeability. The best approximation is reached for an exchange coefficient (λ_E) for uranium ranging from 2,5 E-06 [a^{-1}] in the middle of the altered zones to 2,5 E-05 [a^{-1}] at the margins (fig. 4.11). The various λ_E (fig. 4.12) show that the range for suitable exchange coefficient is very small because the changes in λ_E imply high shifts between the measured $\delta^{234}U$ and the model. Other materials have to be analyzed to study the range of the exchange coefficient of uranium, which is a useful tool for understanding the mobility of uranium and thus improve U/Th dating method on systems perturbed by uranium exchange.

Chapter 5
Conclusions: Fluid-rock interaction along the Schauenburg fault

The alteration history of the Schauenburg fault has been investigated with isotope and element distributions across the faulted rhyolite-granite contact. Major and trace element analyses allow to obtain quantitative information concerning the chemical changes induced by alteration. The isotopic analyses delivered qualitative and temporal information. The use of several isotopic systems, Rb/Sr -, U/Pb-isotopes and Th/U disequilibria, reveals a complex history of polyphase fluid/rock interaction following the Permian volcanic extrusion, showing notable disturbances during the late Jurassic hydrothermal activities, the Tertiary rifting of the Rhine Graben and more recent Quaternary alteration.

5.1 Primary signatures

Four distinct zones are recognizable across the sampling profile, each of which show characteristic geochemical signatures (fig. 5.1). The granite-rhyolite contact constitutes the primary structure. Only the most incompatible elements (Si, Al, Zr, Hf) retain their original signatures and reflect a mixing between typical granite and rhyolite lithologies across the altered zones (cataclasite). The immobile element signatures can hardly be induced by a geochemical shift caused by fluid circulation. Remobilization of components of the granite during the Permian rhyolite extrusion on the granite surface could explain the mixing but needs the assumption to be on the granite-rhyolite boundary. But the rhyolite cover has been displaced oblique to the granite by a fault shift considered to be at least 100 m (Schleicher, 2001). The original rhyolite-granite boundary can not be a suitable explanation. The mixtures of granite and rhyolite compositions in the altered zone can only

be explained by mechanical mixing during faulting. The primary signature has been reset for the most elements, and do not deliver enough information to reconstruct the fault structure.

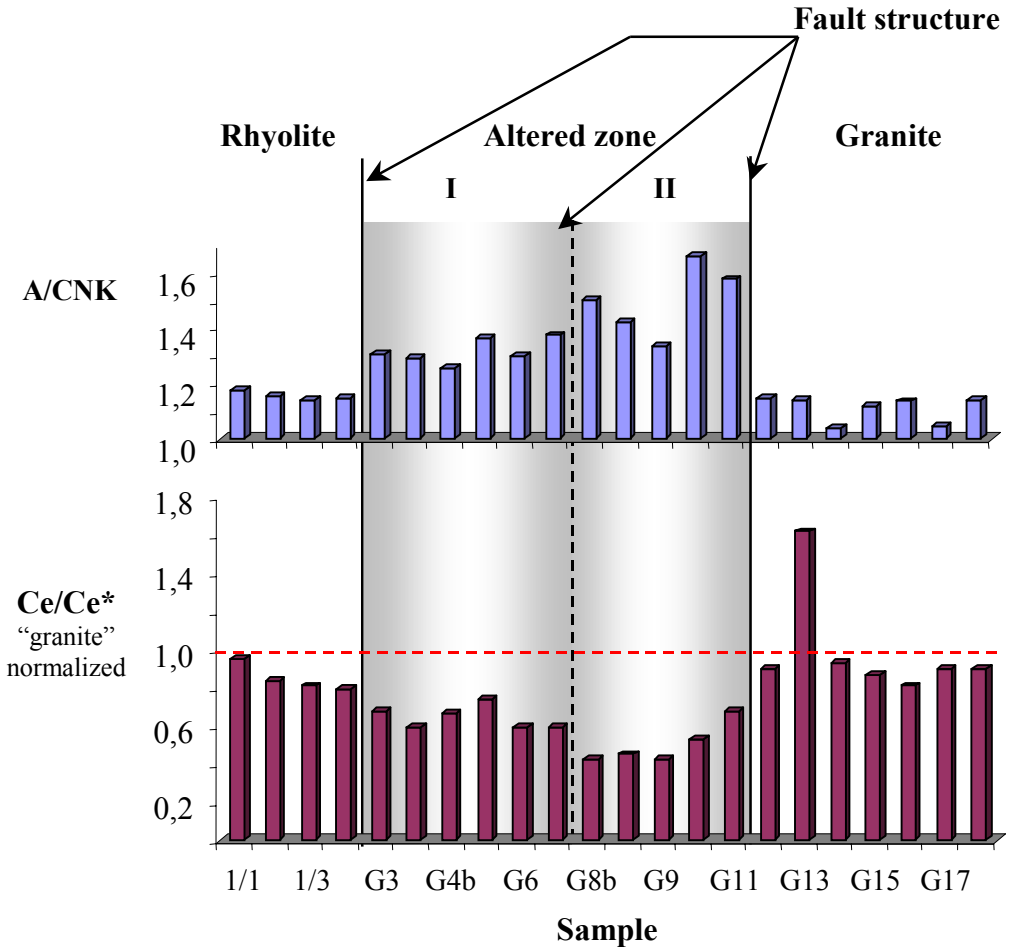

Figure 5.1: Geochenical tracers. The A/CNK index shows a higher alteration in the altered zones, especially in zone II. This alteration is characterized by the Ce/Ce* index which displays a strong reducing alteration event.

5.2 Secondary modifications during fluid-rock interaction

Differences are partly petrographic because the profile crosses the granite-rhyolite contact, but they are also due to different alteration levels induced by fluid circulation along the fault system which has drained the alteration processes. The more mobile elements show a different composition within the altered zones (cataclasite) notably a high leaching of

cations (fig. 5.1). The redistribution of the mobile elements can only have taken place after the mixing event inducing the immobile element anomalies. If not, the anomalies should be present in all element profiles and would not display own signatures for the mobile elements. The geochemical tracers suggest at least one strong hydrothermal event with reducing conditions in the altered zones (fig. 5.1). By integrating various isotope systems, we can demonstrate that chemical exchange or movement of materials has taken place in the fault as a result of water-rock exchange.

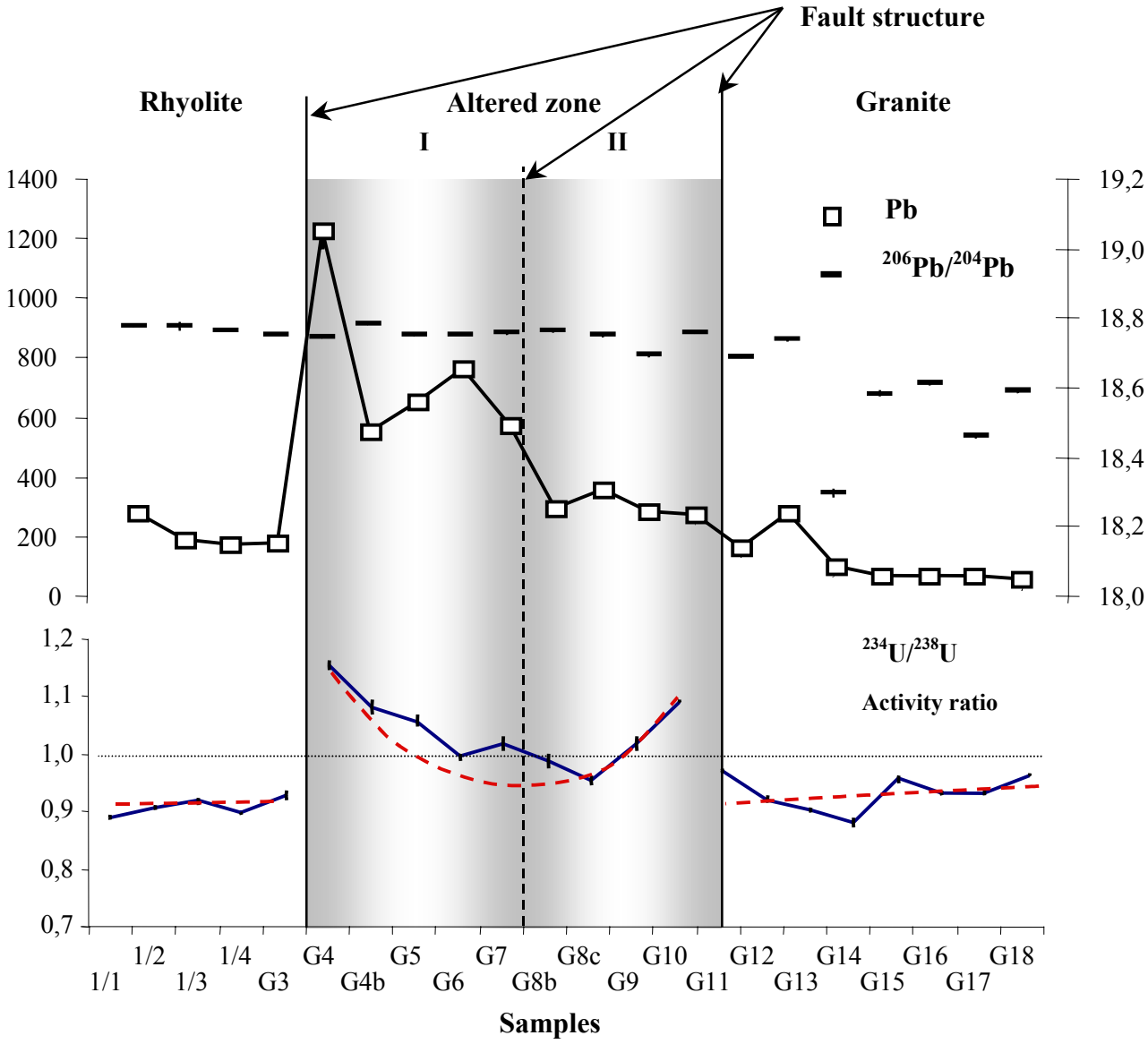

Figure 5.2: The rhyolite samples and especially the altered zones samples have a high lead content. These samples have the same isotopic ratios. The granite zone does not have a perturbed lead signature.

The disequilibrium profile reveals that all the samples are in Th excess. The samples of the altered zones show a symmetric anomalous activity sequence due to an exchange with the aqueous phase.

5.2.1 The late Jurassic event

The granite zone of the sampling profile has underwent an event which set up a new Rb-Sr isotopic composition and reset the Rb/Sr system which originatly corresponded to the Carboniferous intrusion ages. The Rb-Sr data of the granite samples produce a whole rock isochron of 152 ± 5,7 Ma (2σ error) in good agreement with the well-known late Jurassic hydrothermal event (135-160 Ma). Only the granite reflect clearly this alteration event. The fault structure could have acted as permeable boundary. The high kaolinite content of altered zone II, evidence for a high fluid circulation, may have slow down the hydrothermal fluids coming from the granite. But the hydrothermal process was able to reset the whole rock composition of the granite and should have also affected the rhyolite. To explain this difference, it can also be suppose that the preexisting fault, probably acquired during granite uplift by decompression and cooling, was not tectonically active. The rhyolite was not fissured and so more preserved from the alteration processes, contrary to the faulted underlying granite.

5.2.2 Tertiary rifting

The rhyolite and the altered zones samples have high lead contents with homogeneous stable Pb isotopic ratios (fig. 5.2). The rhyolite seems to be the source for the lead enrichment in the altered zones. The rocks evolution lines for Pb support a Tertiary hydrothermal event (54 Ma ± 16), potentially connected with the development of the Rhine Graben. This rifting reactivated old weak tectonic structures from the granite and initiated new fault systems with enhanced fluid circulation. Sufficient porosity and permeability was then available along the Schauenburg fault for fluid movement. The Pb enrichment gives evidence for a transport and deposition of the elements by hydrothermal fluids. Thus the hydrothermal fluid circulations connected with the Rhine Graben formation could also be responsible for the element enrichments (Sb, Cu, Ba) and the geochemical changes (fig. 5.2) identified in the altered zones. The geochemical shifts allows to distinguish the main fault boundaries with the granite and rhyolite and also the boundary between the altered zone I and II (fig. 5.1, 5.2). The two zones displays various intensity of fluid circulation due to several events of fluid circulations or due to adjacent fault sealing (induce various permeability thus various volume of circulating fluids). Only the two first granite samples on the cataclase side have been disturbed. The clay rich zone (altered zone II), by reducing the permeability, probably act as barrier.

5.2.3 Quaternary alteration

The profile samples have undergone uranium and thorium redistribution processes which have occurred within the last ~ 10^6 years. The samples of the altered zones record a more complex history of uranium exchange with the aqueous phase. On both sides of the altered zones the fault mechanisms have increased the porosity, thus the permeability (Katz and Thompson, 1987) that enable longer contact between water and rock. At this location, a higher exchange of uranium with the aqueous phase occurs. Within the altered zones, the porosity is lower in the central area, similar to the porosity of the rhyolite and granite samples situated beside the altered zone. In these segments, low volumes of circulating fluid have restricted uranium exchange between the rock and the aqueous phase. The best approximation is reached for an exchange coefficient (λ_E) for uranium ranging from 2,5 E-06 [a^{-1}] in the middle of the altered zones to 2,5 E-05 [a^{-1}] on the sides of the altered zones. The boundaries of the fault with the granite and the rhyolite are recognizable but the limit between altered zone I and II is not of importance for the recent uranium exchange, evidence for the reactivation history of the fault inducing creation and destruction of fracture permeability.

Chapter 6
Scope for further research

The Schauenburg fault zone presents an excellent chance to investigate the alteration processes of felsic magmatic rocks and other associated fluid-rock-interaction processes along fault zones. This work provides a source of data for further work on alteration processes and has implications for the investigation of the geothermal borehole of Soultz-sous-forêt (France). Due to uplift of the graben shoulders, various crustal levels are exposed at the surface today, where a wide spectrum of rock types can be sampled, reflecting a broad range of the Rhine graben history. This offers the opportunity to study rock and mineral alteration phenomena that occurred at different times of regional crustal evolution, under conditions resembling the present Earth's surface and at depth, in closely related materials and environments.

The conclusions of the isotopic systems are important for studying geological repositories for nuclear waste by improving the knowledge of the isotopes mobility. The fault and clayey barrier properties appear to be governed by the physical and structural characteristics (porosity, permeability, discontinuity) which could be the goal of further study. Concerning the Th/U disequilibrium, other materials have to be analyzed to study the range of the exchange coefficient of uranium, which could be a useful tool to understand the mobility of uranium and thus improve the U/Th dating method on systems perturbed by uranium exchange.

Appendix A
Isotopic systems and chemical separation

A1 Sample dissolution

The samples were first crushed into chips, the altered crust removed, and then powdered (< 5 µm) using an agate ball mill. Disaggregation and grinding also has the effect of homogenizing the samples. Approximately 100 µm was then weighted. The powders were dissolved with suprapur and a concentrated $HF/HNO_3/HCl$ mixture (1, 3, and 1 ml). Dissolution was carried out in closed, pressurized teflon bombs (fig. a1.1), using a microwave assistance oven (MLS Ethos with terminal M240). A description of the oven is presented in Weißhaar (2000). The oven program settings are shown in table a1.1.

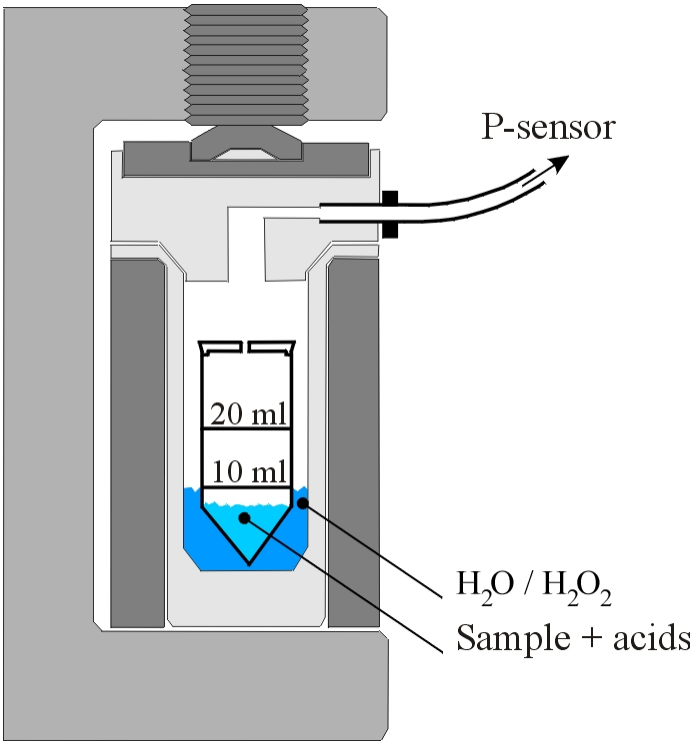

Figure a1.1: Scheme of a Teflon bomb of the oven MLS Ethos.

After evaporation, the samples dissolved for Pb chemistry were taken up in 1,5 ml HCl (2,4 N). The samples dissolved for U-Th chemistry were taken up in 10 ml HNO_3 (7N). The chemical preparation was performed in a class 100-1000 clean room.

For selected samples, potassium-feldspar, apatite, and biotite were separated from the whole rock. The individual mineral fractions were obtained by using magnetic and heavy liquid separation techniques and hand sorting.

The porosity of some samples has been measured by mercury injection porosimetry at the Centre de Géochimie de la Surface of Strasbourg by Fabrice Surma using the methodology of Surma and Geraud (2003).

The overall chemical compositions (major and trace elements) of the samples were determined by Inductively Coupled Plasma Atomic Emission Spectrometry (ICP-AES) and by Inductively Coupled Plasma Mass Spectrometry (ICP-MS) having uncertainties of 2% on the major elements and 5% on the trace elements (Samuel et al., 1985). These measurements were conducted at the Centre de Géochimie de la Surface of Strasbourg.

Table a1.1: Program settings of oven MLS Ethos.

WORK PROGRAM 1 (cleaning)

(1-20) ENT=OK

STEP	TIME	POWER	PRESS	TEMP
1	00:05:00	300W	0 B	0
2	00:01:00	0W	25 B	100
3	00:02:00	400W	25 B	100
4	00:05:00	0W	25 B	100
5	00:02:00	500W	25 B	100
6	00:20:00	0W	25 B	100
7	00:00:00	0W	0 B	0
8	00:00:00	0W	0 B	0
9	00:00:00	0W	0 B	0
10	00:00:00	0W	0 B	0

RCTRL=OFF TAT=OFF TWIST=ON VENT=00:30:00

WORK PROGRAM 2 (dissolution)

(1-20) ENT=OK

STEP	TIME	POWER	PRESS	TEMP
1	00:01:00	0W	0 B	0
2	00:05:00	300W	15 B	110
3	00:04:00	400W	15 B	110
4	00:03:00	500W	15 B	110
5	00:03:00	600W	15 B	110
6	00:12:00	350W	15 B	110
7	00:00:00	0W	0 B	0
8	00:00:00	0W	0 B	0
9	00:00:00	0W	0 B	0
10	00:00:00	0W	0 B	0

RCTRL=OFF TAT=OFF TWIST=ON VENT=00:60:00

WORK PROGRAM 3 (evaporation)

(1-20) ENT=OK

STEP	TIME	POWER	PRESS	TEMP
1	02:00:00	150W	0 B	125
2	00:00:00	0W	0 B	0
3	00:00:00	0W	0 B	0
4	00:00:00	0W	0 B	0
5	00:00:00	0W	0 B	0
6	00:00:00	0W	0 B	0
7	00:00:00	0W	0 B	0
8	00:00:00	0W	0 B	0
9	00:00:00	0W	0 B	0
10	00:00:00	0W	0 B	0

RCTRL=OFF TAT=OFF TWIST=ON VENT=00:30:00

A2 The law of radioactive decay (from Dickin, 1997)

The rate of decay of a radionuclide to a stable isotope daughter product is proportional to the number of atoms, n, present at any time t (Rutherford and Soddy, 1902):

$$-\frac{dn}{dt} = \lambda n \tag{1}$$

where λ is the constant of proportionality, which is characteristic of the radionuclide in question and is called the decay constant (expressed in unit of reciprocal time). The decay constant states the probability that a given atom of the radionuclide will decay within a stated time

The solution of equation (1) is:

$$n = n_0 e^{-\lambda t} \tag{2}$$

an useful way of referring to the rate of decay of a radionuclide is the "half-life", $t_{1/2}$, which is the time required for half of the parent atoms to decay:

$$t_{1/2} = \frac{1n2}{\lambda} = \frac{0{,}693}{\lambda} \tag{3}$$

The number of radiogenic daughter atoms formed, D*, is equal to the number of parent atoms consumed:

$$D^* = n_0 - n \tag{4}$$

Rearranging equation (2), we can substitute n_0 in equation (4). We obtain:

$$D^* = n\left(e^{\lambda t} - 1\right) \tag{5}$$

If the number of daughter atoms at time t = 0 is Do, then the total number of daughter atoms after time t is given as:

$$D = D_0 + n\left(e^{\lambda t} - 1\right) \tag{6}$$

This equation is the fundamental basis of geochronology dating tools.

A3 Rubidium (Rb) - Strontium (Sr) (from Dickin, 1997)

The alkali-earth metal Sr has four stable, naturally-occurring isotopes: ^{84}Sr, ^{86}Sr, ^{87}Sr, and ^{88}Sr. Only ^{87}Sr is radiogenic and gradually increases in minerals due to beta-decay of the radioactive alkali metal ^{87}Rb (equation 7), which has a half-life of 48.8 x10^9 years. Thus, there are two sources of ^{87}Sr in any material: that formed during primordial nucleo-synthesis along with ^{84}Sr, ^{86}Sr and ^{88}Sr, as well as that formed by radioactive decay of ^{87}Rb. Rubidium, a group 1 alkali metal, has two naturally occurring isotopes. ^{85}Rb and ^{87}Rb, whose abundances are 72,17% and 27,83% respectively. The atomic abundance ratio ^{85}Rb/^{87}Rb = 2,593 (Catanzaro et al., 1969) is a constant throughout the Earth, moon and most meteorites due to isotopic homogenization in the solar nebula. ^{87}Rb is radioactive, and decays to the stable isotope ^{87}Sr by emission of a β particle and antineutrino (ν). The decay energy (Q) is shared as kinetic energy by these two particles:

$$^{87}_{37}Rb \rightarrow ^{87}_{38}Sr + \beta^- + \bar{\nu} + Q \qquad (7)$$

the number of ^{87}Sr daughter atoms produced by decay of ^{87}Rb in a rock or mineral since its formation t years ago is given by substituting into the general decay equation (6):

$$^{87}Sr = ^{87}Sr_0 + ^{87}Rb\left(e^{\lambda t} - 1\right) \qquad (8)$$

where $^{87}Sr_0$ is the number of ^{87}Sr atoms present initially and $\lambda = 1.42 \times 10^{-11}$ [a^{-1}]. However, it is difficult to measure precisely the absolute abundance of a given nuclide. Therefore it is more convenient to convert this number to an isotope ratio by dividing through ^{86}Sr (which is not produced by radioactive decay and therefore remains constant with time). Hence we obtain:

$$\left(\frac{^{87}Sr}{^{86}Sr}\right) = \left(\frac{^{87}Sr}{^{86}Sr}\right)_0 + \frac{^{87}Rb}{^{86}Sr}\left(e^{\lambda t} - 1\right) \qquad (9)$$

The present-day Sr isotope ratio is measured by mass spectrometry, and the atomic ratio ^{87}Rb/^{86}Sr is calculated from the weight ratio of Rb/Sr. If the initial ratio (^{87}Sr/^{86}Sr)$_0$ is known or can be estimated, then t can be determined, subject to attention that the system has been closed to Rb and Sr mobility from time t until the present:

$$t = \frac{1}{\lambda}\ln\left\{1 + \frac{^{86}Sr}{^{87}Rb}\left[\left(\frac{^{87}Sr}{^{86}Sr}\right) - \left(\frac{^{87}Sr}{^{86}Sr}\right)_0\right]\right\} \qquad (10)$$

$^{87}Sr/^{86}Sr$ in minerals and rocks ranges from about 0.7 to greater than 4.0 (Faure, 1972). As a general rule, carbonates and plagioclase feldspars contain the least radiogenic Sr, whereas K-feldspars and micas contain the most radiogenic Sr.

The utility of the Rb-Sr isotope system results from the fact that different minerals in a given geologic setting can have distinctly different $^{87}Sr/^{86}Sr$ values as a consequence of different ages, original Rb/Sr values, and initial $^{87}Sr/^{86}Sr$. For example, consider the case of a simple igneous rock such as a granite that contains the Sr-bearing minerals plagioclase feldspar, K-feldspar, hornblende, muscovite and biotite. If these minerals crystallized from the same magma, each mineral had the same $^{87}Sr/^{86}Sr_{initial}$ as the parent melt, but different relative proportions of Rb to Sr depending on the lattice-site preference for these two chemically contrasting elements. Typically, Rb/Sr increases in the order plagioclase, hornblende, K-feldspar, muscovite, biotite. Therefore, given sufficient time for production of radiogenic $^{87}Sr/^{86}Sr_{present\text{-}day}$ will be different in the minerals, increasing in the same order. The evolution of variable $^{87}Sr/^{86}Sr$ in the granite minerals is shown schematically in a traditional Rb-Sr "isochron" diagram. Once in solution, Sr should behave chemically in a manner similar to that of the alkaline-earth element Ca (Elias et al., 1982).

The whole Rb-Sr chemistry and measurements use in this study, have been carried out with the assistance of Dietlinde Pingel at the Institute for Environmental Geochemistry of Heidelberg.

A4 Uranium (U) - Thorium (Th) - Lead (Pb)

(from Dickin, 1997)

Lead has four stable, naturally-occurring isotopes: ^{204}Pb, ^{206}Pb, ^{207}Pb, and ^{208}Pb. Only ^{204}Pb is non-radiogenic. The other lead isotopes are the final decay products of three complex decay chains from uranium (U) and thorium (Th), however, the intermediate members of each series are relatively short-lived, so they can usually be ignored when geological time-scales of millions of years are involved (fig. a5.1). Table a5.1 and figure a5.2 show the ultimate parent-daughter pairs, of which the highest atomic weight parent (^{238}U) decays to the lowest atomic weight daughter (^{206}Pb) and vice versa. It will be noted that the ^{238}U half-life is comparable with the age of the Earth, whereas that of ^{235}U is much shorter, so that almost all primordial ^{235}U in the Earth has now decayed to ^{207}Pb. The ^{232}Th half-life is comparable with the age of the universe.

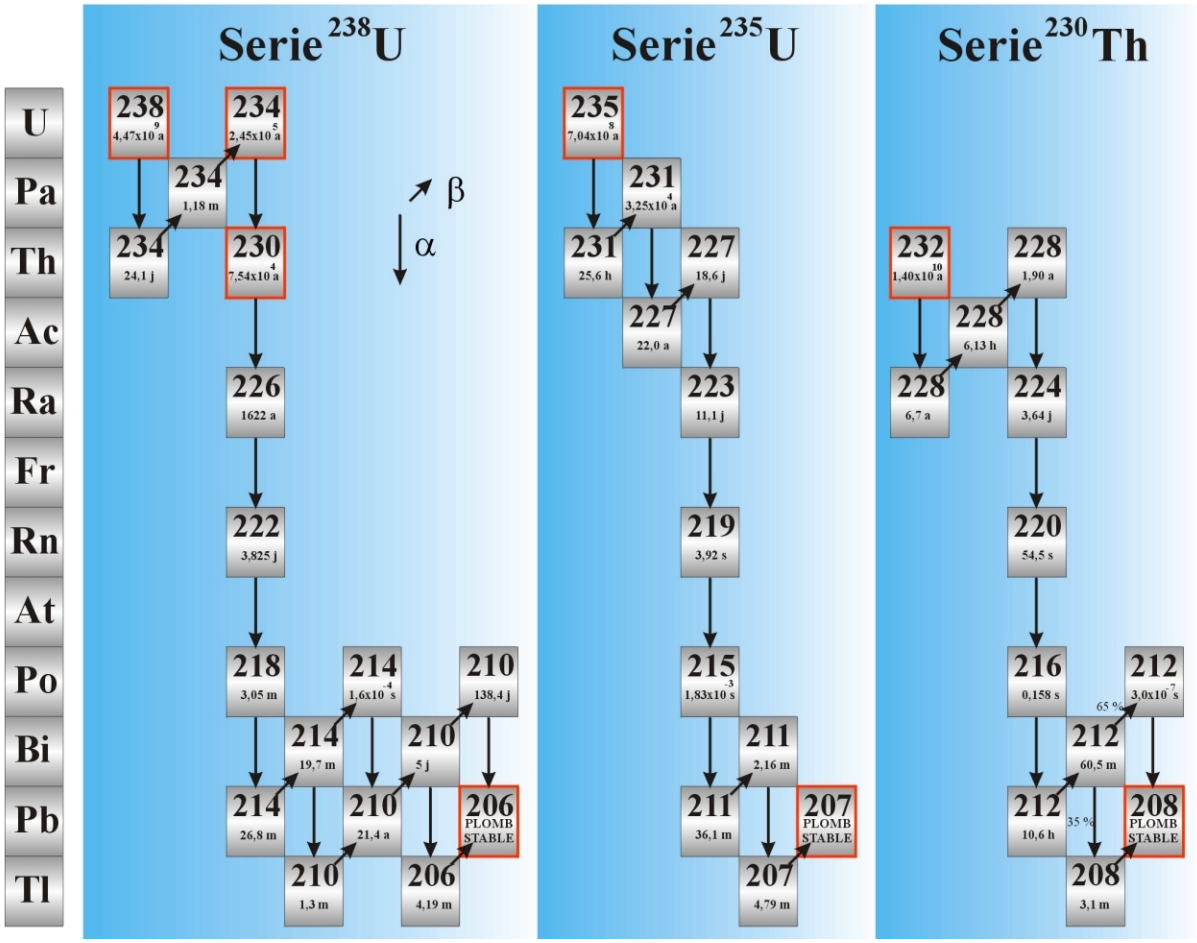

Figure a5.1: ^{238}U-, ^{235}U-, ^{232}Th decay series.

Decay route	$t_{1/2}$, Ga	Decay constant λ, a^{-1}
$^{238}U \rightarrow {}^{206}Pb$	4,47	$1{,}55125 \times 10^{-10}$
$^{235}U \rightarrow {}^{207}Pb$	0,704	$9{,}8485 \times 10^{-10}$
$^{232}Th \rightarrow {}^{208}Pb$	14,01	$0{,}49475 \times 10^{-10}$

Table a5.1: ultimate parent-daughter pairs of uranium and thorium (Jaffrey et al., 1971).

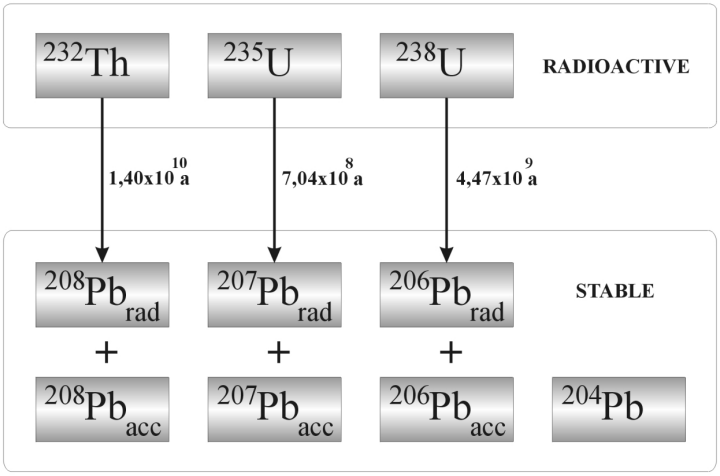

Figure a5.2: Simplified ^{238}U-, ^{235}U-, ^{232}Th decay series.

If we consider a system of age t, then we can write an equation for the nuclides involved in each decay scheme, derived from the general equation (6):

$$^{206}Pb = {}^{206}Pb_0 + {}^{238}U\left(e^{\lambda_{238}t} - 1\right) \quad (11)$$

$$^{207}Pb = {}^{207}Pb_0 + {}^{235}U\left(e^{\lambda_{235}t} - 1\right) \quad (12)$$

$$^{208}Pb = {}^{208}Pb_0 + {}^{232}Th\left(e^{\lambda_{232}t} - 1\right) \quad (13)$$

where 0 indicates the initial abundance of that nuclide. It is convenient to divide by ^{204}Pb to obtain equations containing isotope ratios rather than absolute nuclide abundances. ^{204}Pb is chosen, as it is the only non-radiogenic isotope. Hence we obtain:

$$\left(\frac{^{206}Pb}{^{204}Pb}\right)=\left(\frac{^{206}Pb}{^{204}Pb}\right)_0+\frac{^{238}U}{^{204}Pb}\left(e^{\lambda_{238}t}-1\right) \quad (14)$$

$$\left(\frac{^{207}Pb}{^{204}Pb}\right)=\left(\frac{^{207}Pb}{^{204}Pb}\right)_0+\frac{^{235}U}{^{204}Pb}\left(e^{\lambda_{235}t}-1\right) \quad (15)$$

$$\left(\frac{^{208}Pb}{^{204}Pb}\right)=\left(\frac{^{208}Pb}{^{204}Pb}\right)_0+\frac{^{232}Th}{^{204}Pb}\left(e^{\lambda_{232}t}-1\right) \quad (16)$$

in principle, the decay equation (14) to (16) can be used to construct isochron diagrams and hence to date rocks in a manner analogous to the Rb-Sr system (section A3). Th-Pb and U-Pb isochrons are subject to similar assumptions as for Rb-Sr, the most critical of which is that the samples analyzed remained closed to Th, U and Pb during the life-time of the system being dated. For U-Pb dating it is also necessary to assume that there is no interference by a ^{235}U fission chain reaction.

The ranges of isotope ratio values for the majority of geologic materials are 14.0 to 30.0 for ^{206}Pb/^{204}Pb, 15.0 to 17.0 for ^{207}Pb/^{204}Pb and 35.0 to 50.0 for ^{208}Pb/^{204}Pb (Doe, 1970), although numerous examples of values outside these ranges are reported in the literature.

The utility of the U-Th-Pb isotope system lies in the fact that in a single rock, individual minerals attain diagnostic Pb-isotope signatures due to long-lived differences in U/Pb, Th/Pb, and Th/U. Because feldspars incorporate Pb but do not have lattice positions for U and Th, they have relatively unradiogenic Pb-isotope compositions compared to those of hornblende and micas that both have lattice positions for the transuranics and incorporate U- and Th-rich trace phases. Hornblende tends to have greater Th/U, and thus greater ^{208}Pb/^{204}Pb at given ^{206}Pb/^{204}Pb than that in micas because of the preferential incorporation of trace phases such as Th-rich monazite in hornblende and U-rich zircon in biotite. Although resistant to alteration themselves, these trace phases provide radiogenic nuclides to the lattices of their ferromagnesian hosts through the alpha-particle recoil processes that accompany spontaneous decay of ^{232}Th and ^{238}U. Because U, Th and Pb behave so different geochemically, the fact that the Pb isotope composition of any material is the composite of the three independent decay chains creates the potential for greater differences in isotope values between minerals of a single rock relative to that for the Rb-Sr system.

The isotopic composition of lead in magmatic rocks is often classified as either "common Pb" or "radiogenic Pb" (Pb*). Common lead is found in minerals such as plagioclase and K-feldspar, which have low U/Pb and Th/Pb ratios and lead isotopic values that have not evolved significantly by radioactive decay since the mineral formed. Radiogenic lead is found mainly in accessory minerals that have high U/Pb and Th/Pb ratios, and are old enough so that a significant amount of Pb* has been produced by the decay of uranium and thorium. Minerals that contain Pb* are commonly used for geochronology and include zircon ($ZrSiO_4$), apatite ($Ca_5P_3O_{12}F$), epidote ($Ca_2Al_2Si_3O_{12}OH$), monazite ((Ce, La, Th)PO_4), sphene (Ca $TiSiO_5$), uraninite (UO_2), and others. Because minerals that contain most of the Pb* are generally accessory phases, mass balance dictates that lead isotope ratios in most whole rock samples are much closer to the values in plagioclase and K-feldspar than to the radiogenic accessory minerals (Erel et al., 1994). The isotopic composition of lead (and other heavy isotopes) cannot be modified by biological uptake or the formation of secondary mineral phases in soils (Blum et al., 1994).

A5 Pb separation chemistry

The applied procedure follows that which is used in the radiogenic isotope laboratory of the Environmental Geochemistry Institute of Heidelberg (Kober, unpublished). When complete dissolution has been achieved the solution is split into two weighed aliquots, so that one fraction can be "spiked" with an enriched isotope for isotope dilution analysis, while the second fraction is left "unspiked" for accurate isotope ratio analysis. On the first aliquots, 10 drops of Pb spike (appendix B4) have been added. The concentrations are only measured on the mineral samples and on some whole rock samples. This allows a comparison with the ICP-MS and ICP-AES results (appendix B5). To concentrate and extract the Pb, the following protocol has been used:

Column type: Small teflon column
Resin type: Eichrom: Sr resin SPS (50-100 mesh)

Step	Description
H_2O bi-distilled	Column leaching
HCl (6N)	
200 µl resin	Resin on column (correspond to 3-4 mm in the column)
6 x 1 ml HCl (6N)	Resin leaching
2 x 0,5 ml HCl (2,4N)	Resin to right pH
1,5 ml HCl (2,4N)	Sample on column
2 x 0,5 ml HCl (2,4N)	Resin leaching
3 x 1 ml HCl (2,4N)	
2 x 0,5 HCl (6N)	Pb fraction extracted

A6 The Thorium (Th) – Uranium (U) disequilibria method

The intermediate nuclides in the uranium and thorium decay series have very short half-lives in comparison to their parents, and are usually ignored in the Pb isotope dating methods. However, their short half-lives make these nuclides useful for dating Pleistocene geological events which are too old to be well-resolved by the radiocarbon method and too young to be well-resolved by decay schemes with long half-lives. Generally they are most useful to date events of similar age to their half-life.

A distinctive property of the U-series nuclides which sets them apart from the other dating schemes is that the radiogenic daughters are also radioactive. Hence, in a uranium-bearing system undisturbed for a few million years, a state of "secular" equilibrium becomes established between the abundances of successive parent and daughter nuclides in the U and Th decay chains, such that the decay rate (or "activity") of each daughter nuclide in the chain is equal to that of the parent:

$$\text{Activity} = \lambda_0 n_0 = \lambda_1 n_1 = \lambda_2 n_2 = \lambda_N n_N$$

Where λ_0 is the decay constant and n_0 is the number of atoms of the original parent, λ_1 and n_1 are the decay constant and abundance of the 1st daughter, and so on. It follows that the abundance of each nuclide will be directly proportional to its half-live (i.e. inversely proportional to its decay constant).

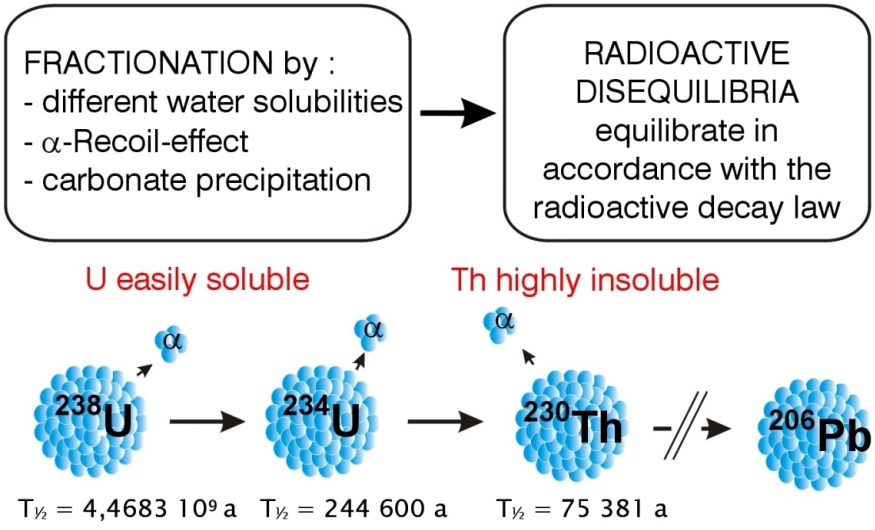

Figure a7.1: Basis of the U/Th disequilibrium method.

The U-Th series radionuclides, because of their widely different geochemical behaviors allow to characterize the diversity of physico-chemical conditions involved in alteration processes even during weak and recent alteration of host rocks (fig. a7.1). The U-series nuclides provide a unique tool in this regard because disequilibrium in this series could potentially constrain both extend and timing of elemental fractionation (Osmond and Ivanovich, 1992).

In old unaltered materials, natural decay series are in secular radioactive equilibrium. In geological processes such as erosion, sedimentation, melting or crystallization, different nuclides in the decay series can become fractionated relative to one another, due to variations in their chemistry or the structural site they occupy. This results in a state of secular disequilibrium. During alteration, U is leached and Th is highly insoluble in most natural waters at low temperatures. That produces the radioactive disequilibria in clastic particles:

$$^{234}U/^{238}U < 1 \text{ and } ^{230}Th/^{234}U > 1$$

Isotope	$t_{1/2}$, Ma	Decay constant λ, a^{-1}
^{238}U	4 470	$1{,}55125 \times 10^{-10}$
^{234}U	0,245	$2{,}826288 \times 10^{-6}$
^{230}Th	0,076	$9{,}157711 \times 10^{-6}$
^{235}U	704	$9{,}8485 \times 10^{-10}$
^{232}Th	14 010	$0{,}49475 \times 10^{-10}$

Table a6.1: Uranium and thorium isotopes decay constants (Cheng et al., 2000).

A7 U-Th separation chemistry

Before the dissolution, 500 µl U-spike and 500 µl Th-spike (appendix B4) have been added to the samples. To concentrate and extract the Pb, the following protocol has been used:

Column type: Large quartz column
Resin type: Dowex 1x8 (100 – 200 mesh)

Step	Description
10 ml resin	Resin on column (correspond to 10 cm in the column)
H_2O distilled HNO_3 (7N)	Resin to right pH
10 ml HNO_3 (7N)	Sample on column
50 ml HNO_3 (7N)	Resin leaching
50 ml HBr 20 H_2O distilled	U-Th fraction extracted.

For the next step, the U-Th fraction is evaporated and re-dissolved in 0,5 ml HNO_3 (7N)

Column type: Small quartz column
Resin type: Biorad AG 1x8 (200 – 400 mesh)

Step	Description
2 ml resin	Resin on column
H_2O distilled HNO_3 (7N)	Resin to right pH
0.5 ml HNO_3 (7N)	Sample on column
5 x 1 ml HNO_3 (7N)	Resin leaching
10 ml HBr 10 ml H_2O distilled	U-Th fraction extracted.

Appendix B
Thermal Ionization Mass Spectrometry (TIMS)

B1 General features of Solid source mass spectrometry

(from Dickin, 1997)

In order to use radiogenic isotopes as dating tools or tracer, they must be separated by mass from non-radiogenic isotopes in a "mass spectrometer". In a "magnetic sector" instrument the nuclides to be separated are ionized under vacuum and accelerated through a high potential (V) before passing between the poles of a magnet. An uniform magnetic field (H) acting on particles in the ion beam bends them into curves of different radius (r) according to the following equation:

$$r^2 = \frac{m}{e}\frac{2V}{H^2}$$

Where m/e = mass/charge fort the ion in question. Since most of the ions produced are single-charged, nuclides will be separated into a simple spectrum of masses. The relative abundance of each mass is then determined by its corresponding ion current, captured by a Faraday bucket or multiplier detector. The radiogenic elements are analyzed by solid source mass spectrometry.

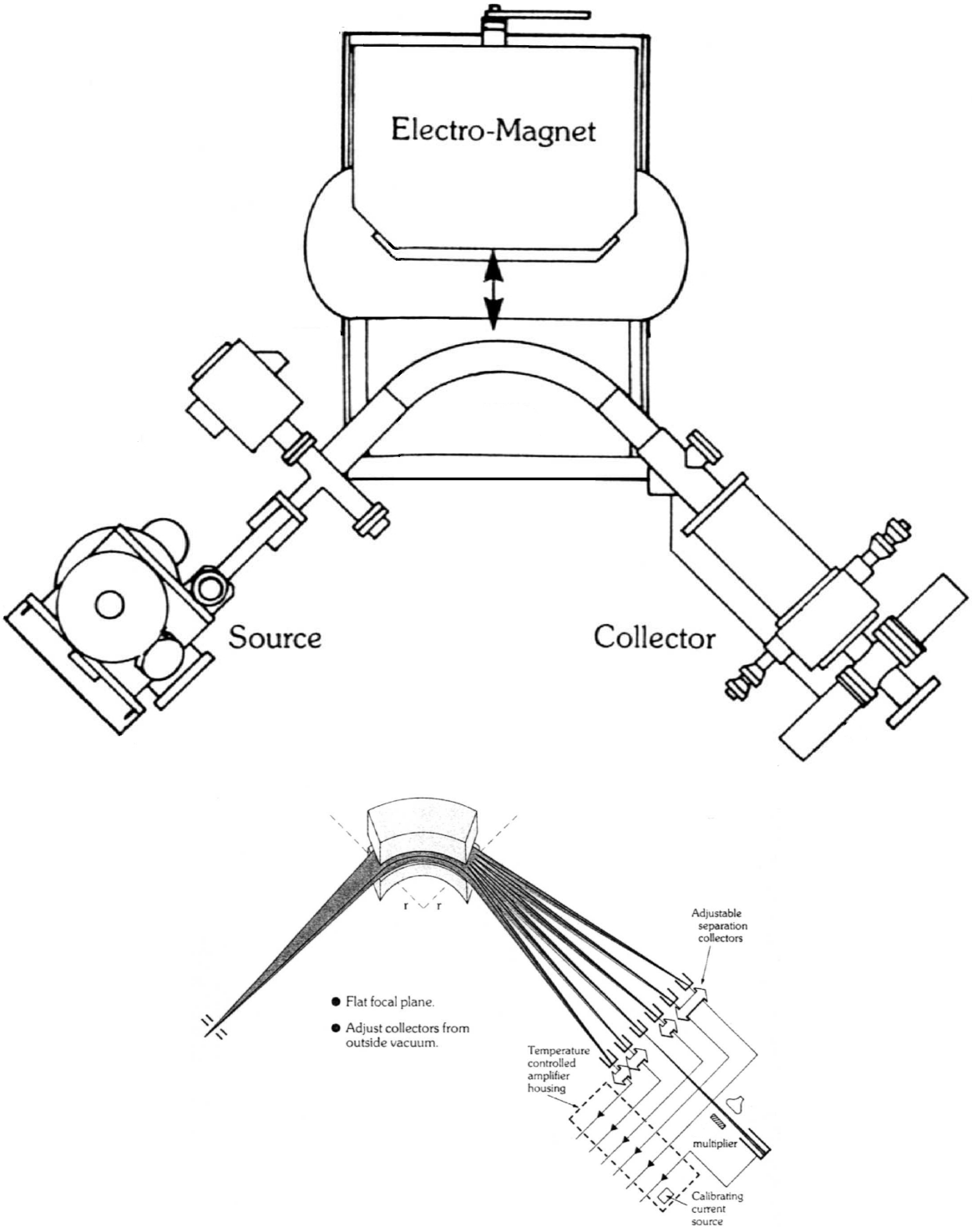

Figure b1.1: Scheme of a solid thermal ionization mass spectrometer.

The normal starting point of precise isotopic measurements by mass spectrometry is chemical separation of the element to be analyzed. This required the sample to be converted into a solution.

Sample loading

The sample (in solution) is loaded on a single filament (Re) by evaporating the solution with heating the filament. During mass spectrometry analysis, the filament current is raised to yield a temperature where effectively simultaneous volatilization and ionization of the sample occurs. The Pb samples are loaded in phosphoric acid, which seems to a) displace all other anion species to yield a uniform salt composition, b) destroy organic residues (such as ion exchange resin) mixed with the sample, and c) glue the sample to the filament. In the case of Pb, the samples are also loaded on the Re filament in a silica gel (Cameron et al., 1969). This is thought to form a blanket over the sample which effectively retards Pb volatilization so that the filament can be raised to a higher temperature (where Pb fractionation is more reproducible) without burning off the sample uncontrollably. For Uranium and Thorium the stable volatilization and ionization does not occurs at the same temperature. Therefore, a multiple source filament is used. In this configuration one filament bearing the sample load can be heated to the optimum temperature for stable volatilization, while another hotter filament can be used to ionize the atomic cloud by bombarding it with electrons.

Ion optics

The ion optic properties of an instrument determine how the cloud of ions generated at the source filament is accelerated, focused into a beam, separated by the magnetic field, and collected for measurement (fig. b1.1). Correct ion optic alignment is essential to obtain reliable results, because if parts of the ion beam hits an obstruction, different masses may be affected to different degrees, leading to a bias in the results.

Detectors

Ion beams in mass spectrometry normally range up to ca. 10^{-10} A. for beams as small as 10^{-13} A, the most suitable detector is the Faraday bucket. This is connected to electrical ground via a large resistance (e.g. 10^{11} Ohms). Electrons travel from ground through this output resistor is then amplified and converted into a digital signal. A typical ion beam of 10^{-11} generates a potential of 1 V (100 000 digital counts).

For ion beams smaller than ca. 10^{-13} A, the electrical noise of the faraday amplifier becomes significant relative to the signal size, so that some form of signal-multiplication is necessary.

Data collection

In order to achieve very high precision data, it is necessary to measure the intensity of each ion beam for an hour or more. To achieve this in a single collector machine, the magnetic field is switched to cycle round a sequence of peak positions. On switching to a new sequence of peaks there is a waiting period of 1-2 s to allow the output resistor and amplifier to reach a steady state in response to the new ion current. Then data is collected during a few seconds. In practice, each peak must normally be corrected for incomplete decay of the signal from previous peaks (termed "dynamic zero", "tau" or "resistance memory"). Before isotope ratios can be determined from the different signals, background electronic noise must be subtracted in order to determine net peak heights. This is done by measuring a baseline position in each collector channel, usually a few a.m.u. away from the mass of interest. A set of net peak ratios is extracted and collected in blocks of 10 scans.

Isotope dilution

In this technique, a sample containing an element of natural isotopic composition is mixed with a "spike" solution, which contains a known concentration of the element, artificially enriched in one of this isotopes. When known quantities of the two solutions are mixed, the resulting isotopic composition (measured by mass spectrometer) can be used to calculate the concentration of the element in the sample solution. The element in question must normally have two or more naturally occurring isotopes, one of which can be enriched on a mass separator. However, in some cases, a long-lived artificial isotope is used.

Double spiking

The double-spike isotope dilution technique can be used to allow comparison between all of the isotope ratios in a suite of samples, including those used for fractionation normalization. The theory of double spiking was first investigated in Dobson (1963). However, it is not usually possible to calculate "absolute" values of isotopic abundance because there is not normally any absolute standard to calibrate the double spike.

B2 Finnigan MAT261 TIMS

The Rb-Sr and Pb isotopic data were collected on a Finnigan MAT 261 solid source mass spectrometer at the Institute for Environmental Geochemistry of Heidelberg (fig. b2.1). As predecessor of the MAT262 model (appendix B3) the structure of the MAT261 is not substantially different. However, the MAT261 does not have mobile Faraday Cups. In Kober (1983) the configuration is described in detail.

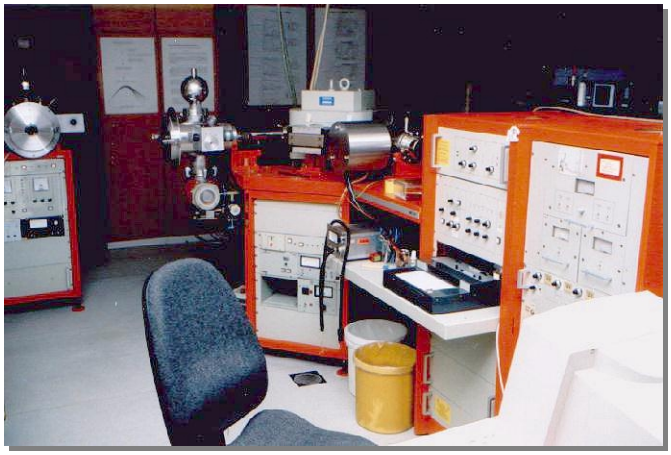

Figure b2.1: The Finnigan MAT261 solid source mass spectrometer.

The Pb analyses are accomplished with the single filament method. The samples (chemical procedure is described in appendix A5) are loaded on a rhenium filament. A Silica-gel suspension is loaded as a fine film into the center of the filament with a glass capillaries (Kober, 1983). Subsequently, the lead salt can be taken up in a micro-drop phosphoric acid and added to the silica-gel. The silica-gel is dried by a weak filament stream. The isotope dilution technique and standard procedures for Pb isotopes geochemistry are described by Kober (1983).

The samples were brought gradually in 20 min on measuring temperature (1200 ^{o} C) with assistance of an exactly specified heating procedure (appendix B2.1). The measurement is started after temperature control and focusing of the ion beam. The collection of the data takes place in the static mode in 10 blocs of 10 scans (appendix B2.1). The fractionation is determined by using the Pb standard (SRM981) as reference. The same load method and identical heating procedures are used for the SRM981 in order to achieve the same fractionation behavior. The fractionation is determined with the deviations from the desired values (Catanzaro et al., 1969) and is 1,2 ± 0,2 ‰ per amu. All the results are "fractionation" corrected following the off-line evaluation of the data.

B2.1 Lead acquisition program

Filament step heating procedure

FIL12 PROGRAMMED STEP HEATER

1	PILOT CHANNEL		FAR2
2	MONITOR	- MASS	208
3		- RANGE [mV]	1000
4	IONI	- PILOT MASS	208
5		- RANGE [mV]	10000
6		- MAXIMUM FILAMENT CURRENT [mA]	1
7	EVA	- PILOT MASS	208
8		- RANGE [mV]	1000
9		- MAXIMUM FILAMENT CURRENT [mA]	2200
10	WAITING TIME BEFORE MEASUREMENT [min]		1

FIL	Tsum [min]	Tline [min]	Pilot	Value	Slope [mA/min]	Steps	Actions
EVA	0.0	3.0	FILC	1500 mA	500	3	RP
EVA	(3.0)	6.0	FILC	1500 mA	500	3	RP
EVA	(9.0)	6.0	FILC	1500 mA	500	3	RP
EVA	(15.0)	3.0	FILC	1500 mA	500	3	RP
EVA	(18.0)	2.0	FILC	1500 mA	500	3	RP
END	(20.0)						

Data Collection

COL5 MULTICOLLECTOR STATIC MODE

1	NUMBER OF SCANS PER BLOCK		10
2	NUMBER OF BLOCKS PER RUN		10
3	ABUNDANCE MEASUREMENT (+/- mass units)		NO
4	HV-ADJUST TO OPTIMUM POINT		NO
5	REPEAT PEAK CENTER		5
6	INTERBLOCK ACTION	-BASELINE	USE OLD VALUES
7		-BASELINE MASS	NO
8		-DELAY TIME [sec]	15
9		-INTERGRATION TIME [sec]	32

10			-GAIN CALIBRATION [FAR]		USE OLD VALUES
11			-Z FOCUS		NO
12			-LENS FOCUS		NO
13	PILOT CHECK		-UPPER TOLERANZ [%]		NO
14			-LOWER TOLERANZ [%]		NO
15			-CONTROL FILAMENT		EVA
16			-MAX.CURRENT [mA]		2200
17	INTERSCAN REPORT		- 1st RATIO		204/206
18			- 2nd RATIO		207/206
19			- 3rd RATIO		208/206
20	PEAK#	MASS	TYPE	CHANNEL	T-Integration [s]
	1	208.0	ISC	FAR2	8
	2	207.0	/ISO	FAR3	
	3	206.0	/ISO	FAR4	
	4	204.0	/ISO	FAR5	

Data reduction, Step 1

RED15 MULTICOLLECTOR QUADRATIC DRIFT CORRECTION

1	1st INTERFERING ISOTOPE		-PILOT	THERE IS NO
2			-RATIO	0
3	INTERFERED MASS			THERE IS NO
4	2nd INTERFERING ISOTOPE		-PILOT	THERE IS NO
5			-RATIO	0
6	INTERFERED MASS			THERE IS NO
7	DIXON TEST			TABLE 1
8	PRINT RESULTS			YES
9	ELEMENT (FOR WEIGHT % CALC)			None
10	RATIO	PEAK#/PEAK#	MASS/MASS	CORRECTIONS
	1	3/4	206/204	1.000000 RS
	2	2/4	207/204	1.000000 RS
	3	1/4	208/204	1.000000 RS
	4	4/3	204/206	1.000000 RS

Data reduction, Step 1

RED15 NOT DEFINED

B2.2 Fractionation

The process of volatilization and ionization on the source filament of a mass spectrometer requires the breaking of chemical bonds, but the strength of these bonds is mass dependent. The continual process of fractionation starts to "use up" the lighter isotope on the filament so that the isotopic composition of the samples gets progressively heavier ("the reservoir effect"). Eberhardt et al. (1964) showed that this process follows a Rayleigh fractionation law. For elements with two or more non-radiogenic isotopes, an internal normalization for such mass-dependant fractionation can be performed by using a natural isotopic ratio to correct the measurement. These problems are much less severe for heavier mass. In the analysis of uranium, fractionation effects may be reduced by running at high temperature as the oxide. Double spiking with two artificial isotopes may be used to apply an internal fractionation correction to elements such as Pb with only one natural non-radiogenic isotope.

Measured differences in $^{87}Sr/^{86}Sr$ in different materials due to stable isotope fractionation (primarily due to thermal effects in the mass spectrometer) must be corrected for. Fortunately, the stable isotope pair $^{88}Sr/^{86}Sr$ can be used as an internal monitor of both natural and analytical fractionation. In the absence of stable isotope fractionation, $^{88}Sr/^{86}Sr$ should be identical in all materials, with an accepted value of 8.37521 (IUGS: International Union of Geological Scientists). When the Sr (and other) isotopes fractionate, the amount of fractionation between pairs of isotopes is proportional to their mass ratios. Therefore, as a standard analytical procedure, $^{87}Sr/^{86}Sr$ is measured simultaneously with $^{88}Sr/^{86}Sr$, and the measured $^{87}Sr/^{86}Sr$ is adjusted by an amount proportional to that required to correct the measured $^{88}Sr/^{86}Sr$ to the accepted value. Consequently, the reported $^{87}Sr/^{86}Sr$ is "fractionation-corrected".

However, as with the Sr isotopes, there is no stable, non-radiogenic pair of Pb isotopes that can be used as the basis for a fractionation correction. To circumvent this problem, Pb isotope analyses are typically corrected for fractionation during analysis using factors determined by repeated analyses of Pb standard N.I.S.T. SRM 981. However, there is no obvious means of correcting for possible fractionation in nature; thus, we assume that the Pb isotopes do not fractionate perceptibly in nature due to their high mass values. Although probably valid, the uncertainty associated with correcting for analytical fractionation renders Pb isotope analyses inherently less precise than those for Sr. Fortunately, the range of Pb isotope composition observed in nature is substantial.

B3 Finnigan MAT262 TIMS

U-Th isotopic measurements were performed on a Finigan MAT262 thermal ionization mass spectrometer. The Heidelberger Academy of Sciences has since 1993 a solid thermal ionization mass spectrometer from the company Finnigan (MAT262 RPQplus; fig. b3.1). Information about the structure and the start-up of the machine can be found in Bollhöffer (1996) and Frank (1997).

The analyses have been performed on whole rock samples because mineral separation methods could influence the uranium concentration. Whole rock analyses also allow a quick overview of the sampling profile and to pick out the most interesting samples for more precise investigations such as mineral separation analyses.

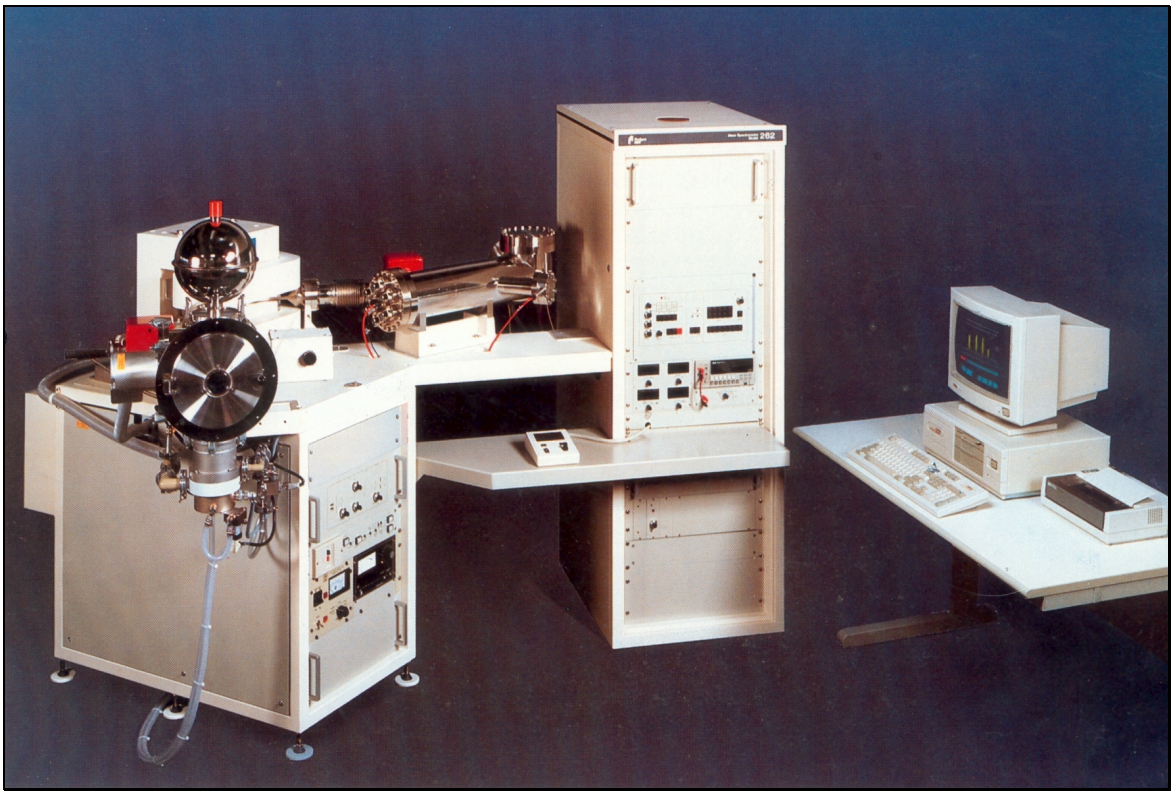

Figure b3.1: Finnigan MAT262 thermal ionization mass spectrometer.

After the chemical separation (appendix A7), the sample is loaded in nitrate form on a highly pure rhenium filament. Before the measurement, the filament is heated before the evaporation of the uranium and the thorium, in order to remove organic remainders and other impurities, which can affect the high vacuum negatively. During the measurement the sample is heated precisely and evaporated gradually at an element-specific temperature. The MAT262 works with the double filament technology, i.e. the sample evaporates from evaporation filament and ionizes trough a second, separated adjustable ionization filament. This technology makes an extremely controlled regulation possible of the ion stream and improves the probability of ionization. The combination of a rotary vane pump, a turbo-molecular pump and a cryopump produce in the ion source (fig. b3.2) a high vacuum (10^{-8} hPa).

After the thermal ionization the ions are accelerated with a high voltage of 10kV. An electromagnetic lens system makes possible the focusing and adjustment of the ion beam before it enter a water-cooled 90° sector field magnet (approx. 1 Tesla) which isolated the ions and after the specific charge (q/m). The mass spectrometer can measure only abundance ratios. For the determination of the concentrations artificial isotopes (spikes) in defined quantity are added to the sample.

For the proof of the ion stream three detector systems stand for order. Stream under 1mV are proven by a photomultiplier (SEV). The mass separation ability of this unit lies in a magnitude of 10^{-6}. A second SEV has a lens system (Retarding potential quadrupole), which increases the mass separation ability by further than two orders of magnitude ($2*10^{-8}$). Stream over 1 mV are detected with the Faraday Cups, six of it are mobile, one is fixed (fig. b3.3).

The Faraday Cups are calibrated among themselves (Gain Calibration) through a signal which is standardized on the immovable Cup. The electronic noise is corrected by the determination of the baseline. The calibration of the Cups by the SEV is done via the determination of a yield factor by putting alternately on the two detectors a signal between 5 and 10 mV. In the course of a measurement the yield can change around some percent. Therefore it is necessary to correct the drift with help of the natural $^{235}U/^{238}U$ ratio ($7{,}2527*10^{-3}$) during the data evaluation.

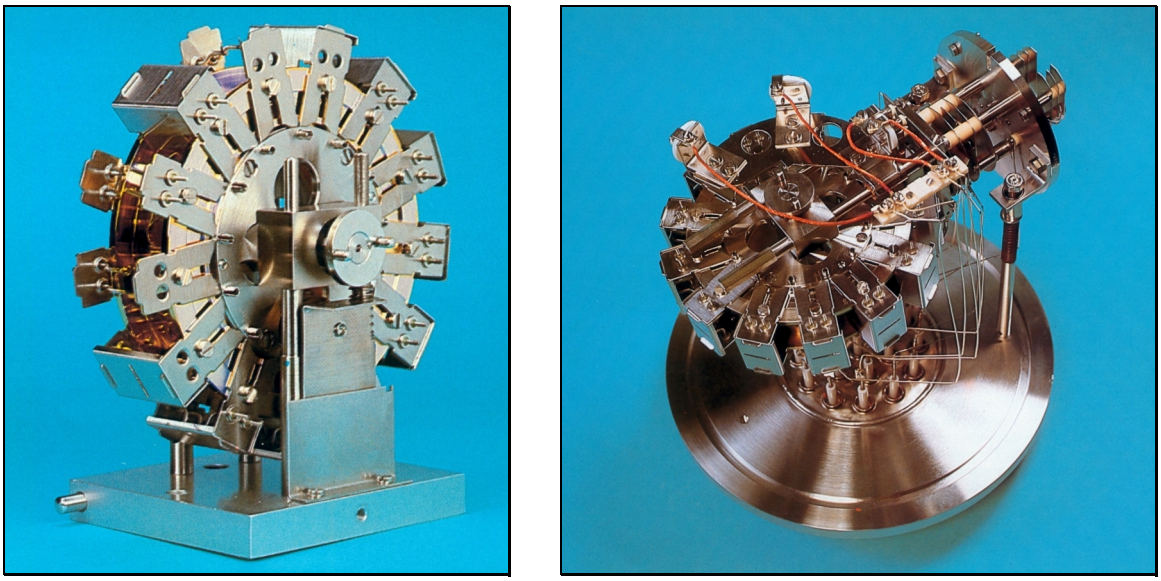

Figure b3.2: MAT262 ion source.

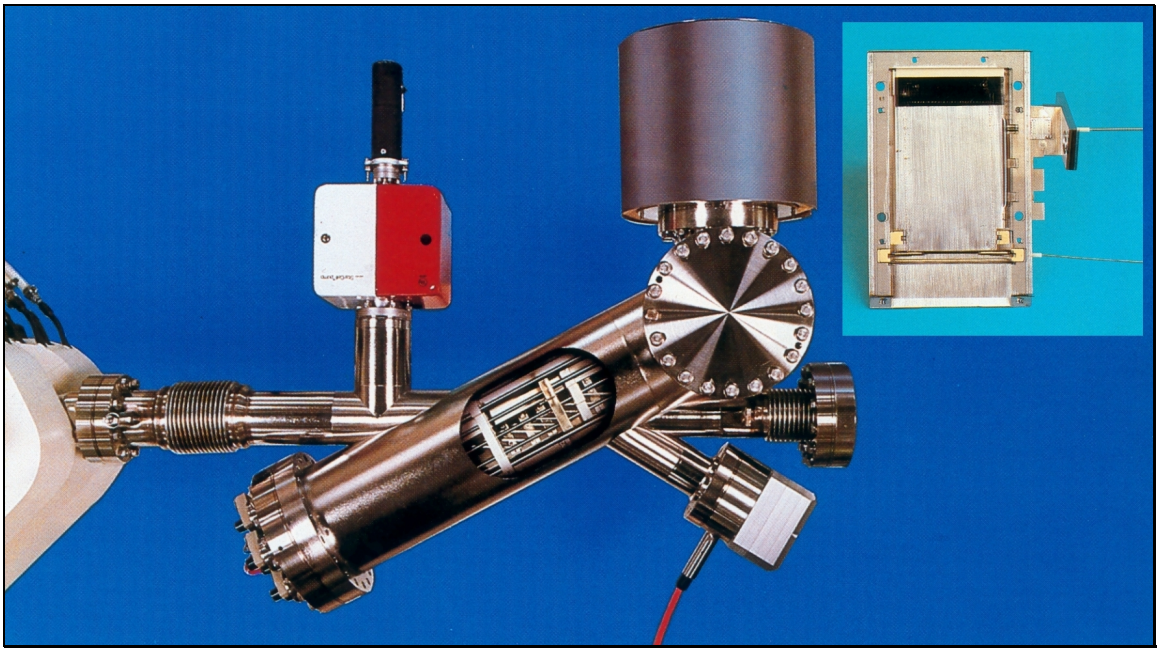

Figure b3.3: Faraday-Cups configuration of MAT262. On the right is a single Faraday-Cup to be seen.

The magnetic field is regulated by a 16-bit digital analog converter (2^{16} channels). A 10-bit DAC regulates the high voltage in steps of ± 0.5 %. The reference HV DAC of 512 value corresponds to a high voltage of 10 kV. A set of six reference masses serves for the alignment of the HV DAC values (Reference Mass Calibration). During the measurement this value is determined by adaptation of the high voltage, in order to correct the system drift.

The MAT262 can measure either in the static mode (simultaneous measurement of the isotopes on different detectors) or in the peak Jump mode (the isotopes are steered alternately on the detectors). The half-static mode combines the two methods. The acquisition programs of this work are given in appendix B3.1 and B3.2. The results are determined with the off-line evaluation of the Finnigan software by using a 2σ-Test to eliminate the outliners. Methodology for the $^{233}U/^{236}U$ double spike and the ^{229}Th spike are described in Bollhöfer (1996) and Frank (1997). The concentrations of the spikes are represented in appendix B4.

B3.1 Uranium oxide acquisition program

Filament step heating procedure

FIL1 NOT DEFINED

Data Collection

COL6 MULTICOLLECTOR JUMPING MODE

1	NUMBER OF SCANS PER BLOCK					10
2	NUMBER OF BLOCKS PER RUN					30
3	HV-ADJUST TO OPTIMUM POINT					NO
4	REPEAT PEAK CENTER			5		
5	INTERBLOCK ACTION			-BASELINE		EACH BLOCK
6				-BASELINE MASS FAR		250.5
7				-BASELINE MASS SEM		NO
8				-DELAY TIME [sec]		8
9				-INTERGRATION TIME [sec]		32
10				-GAIN CALIBRATION [FAR]		USE OLD VALUES
11				-RPQ or ICM-YIELD		5
12				-Z FOCUS		NO
13				-LENS FOCUS		NO
14	PILOT CHECK			-UPPER TOLERANZ [%]		NO
15				-LOWER TOLERANZ [%]		NO
16				-CONTROL FILAMENT		EVA
17				-MAX.CURRENT [mA]		4000
18	INTERSCAN REPORT			- 1st RATIO		251/254 (Peak#s 5/1)
19				- 2nd RATIO		249/252 (Peak#s 4/6)
20				- 3rd RATIO		250/254 (Peak#s 2/1)
21	PEAK#	MASS	TYPE	CHANNEL	T-Integration [s]	T-Idle [s]
	1	254.0	ISC	FAR2	4	2
	2	250.0	/ISO	ICM		
	3	251.0	/ISO	FAR4		
	4	249.0	ISC	ICM	4	2
	5	251.0	ISC	ICM	4	2
	6	252.0	ISC	ICM	4	2

Data reduction, Step 1

RED15 MULTICOLLECTOR QUADRATIC DRIFT CORRECTION

1	1st INTERFERING ISOTOPE	-PILOT	249
2		-RATIO	.003765
3	INTERFERED MASS		250
4	2nd INTERFERING ISOTOPE	-PILOT	249
5		-RATIO	.12285
6	INTERFERED MASS		251
7	DIXON TEST		TABLE1
8	PRINT RESULTS		YES
9	ELEMENT (FOR WEIGHT % CALC)		None

10	RATIO	PEAK#/PEAK#	MASS/MASS	CORRECTIONS	
	1	5/1	251/254	1.000000	IEC NRM RS
	2	2/1	250/254	1.000000	IEC NRM RS
	3	3/1	251/254	1.000000	IEC NRM RS
	4	4/1	249/254	1.000000	NRM RS
	5	2/4	250/249	1.000000	IEC NRM RS
	6	4/6	249/252	1.000000	IEC RS

B3.2 Thorium oxide acquisition program

Filament step heating procedure

FIL1 NOT DEFINED

Data Collection

COL6 MULTICOLLECTOR JUMPING MODE

1	NUMBER OF SCANS PER BLOCK					10
2	NUMBER OF BLOCKS PER RUN					30
3	HV-ADJUST TO OPTIMUM POINT					NO
4	REPEAT PEAK CENTER					5
5	INTERBLOCK ACTION			-BASELINE		EACH BLOCK
6				-BASELINE MASS FAR		246.5
7				-BASELINE MASS SEM		NO
8				-DELAY TIME [sec]		8
9				-INTERGRATION TIME [sec]		8
10				-GAIN CALIBRATION [FAR]		USE OLD VALUES
11				-RPQ or ICM-YIELD		5
12				-Z FOCUS		NO
13				-LENS FOCUS		NO
14	PILOT CHECK			-UPPER TOLERANZ [%]		NO
15				-LOWER TOLERANZ [%]		NO
16				-CONTROL FILAMENT		EVA
17				-MAX.CURRENT [mA]		6500
18 I	NTERSCAN REPORT			- 1st RATIO		245/248 (Peak#s 2/1)
19				- 2nd RATIO		246/245 (Peak#s 3/2)
20				- 3rd RATIO		246/248 (Peak#s 3/1)
21	PEAK#	MASS	TYPE	CHANNEL	T-Integration [s]	T-Idle [s]
	1	248.0	ISC	FAR5	2	2
	2	245.0	ISC	ICM	8	2
	3	246.0	ISC	ICM	16	2

Data reduction, Step 1

RED15 MULTICOLLECTOR QUADRATIC DRIFT CORRECTION

1	1st INTERFERING ISOTOPE		-PILOT	THERE IS NO
2			-RATIO	0
3	INTERFERED MASS			THERE IS NO
4	2nd INTERFERING ISOTOPE		-PILOT	THERE IS NO
5			-RATIO	0
6	INTERFERED MASS			THERE IS NO
7	DIXON TEST			TABLE 1
8	PRINT RESULTS			YES
9	ELEMENT (FOR WEIGHT % CALC)			None
10	RATIO	PEAK#/PEAK#	MASS/MASS	CORRECTIONS
	1	2/1	245/248	1.000000 RS
	2	3/2	246/245	1.000000 RS
	3	3/1	246/248	1.000000 RS

B3.3 Oxide correction

The samples have been measured as oxide (UO, ThO). The correction is done during the data acquisition (appendix B3.1 and B3.2)

After Karlsruher Nuklidkarte, 1974:

^{16}O: 99.756 %
^{17}O: 0.039 %
^{18}O: 0.205 %

Oxide correction:

^{230}Th:
$$\left[\frac{^{230}Th^{16}O}{^{229}Th^{16}O}\right]_{corr} = \left[\frac{^{230}Th^{16}O}{^{229}Th^{16}O}\right]_{mes} - \left[\frac{^{229}Th^{17}O}{^{229}Th^{16}O}\right]$$
$$with \frac{^{229}Th^{17}O}{^{229}Th^{16}O} = 0.00039$$

^{232}Th: no correction because ^{232}Th^{16}O >> ^{230}Th^{18}O

^{233}U: no correction because ^{232}Th and ^{231}Pa evaporated for higher temperature

^{234}U:
$$\left[\frac{^{234}U^{16}O}{^{233}U^{16}O}\right]_{corr} = \left[\frac{^{234}U^{16}O}{^{233}U^{16}O}\right]_{mes} - \left[\frac{^{233}U^{17}O}{^{233}U^{16}O}\right]$$
$$with \frac{^{233}U^{17}O}{^{233}U^{16}O} = 0.00039$$

^{235}U:
$$\left[\frac{^{235}U^{16}O}{^{238}U^{16}O}\right]_{corr} = \left[\frac{^{235}U^{16}O}{^{238}U^{16}O}\right]_{mes} - \left[\frac{^{233}U^{18}O}{^{238}U^{16}O}\right]$$

^{236}U:
$$\left[\frac{^{236}U^{16}O}{^{235}U^{16}O}\right]_{corr} = \left[\frac{^{236}U^{16}O}{^{235}U^{16}O}\right]_{mes} - 0.00039$$

B4 Spike concentration and isotopic composition

$^{233}U/^{236}U$ double spike

$^{234}U/^{233}U$:	$3{,}375*10^{-3}$	± 0,002
$^{235}U/^{233}U$:	0,1208	± 0,0002
$^{238}U/^{233}U$:	0,0271	± 0,0002
$^{233}U/^{236}U$:	0,87104	± 0,00105
c(^{233}U):	0,4163	± 0,0006 ng/g

^{229}Th spike

$^{232}Th/^{229}Th$:	$2{,}67*10^{-3}$	$\pm 1{,}4*10^{-4}$
$^{230}Th/^{229}Th$:	$4{,}7*10^{-5}$	$\pm 3*10^{-6}$
c(^{229}Th):	0,10294	± 0,00020 ng/g

Pb spike

c(Pb):	1,0375 µg/g	
^{208}Pb:	99,14 %	± 0,10 %
^{207}Pb:	0,69 %	± 0,05 %
^{206}Pb:	0,17 %	± 0,05%
^{204}Pb:	<0,05 %	

B5 Standard and reproducibility

Pb standard SRM 981

	$^{206}Pb/^{204}Pb$	1σ	$^{207}Pb/^{204}Pb$	1σ	$^{208}Pb/^{204}Pb$	1σ	$^{208}Pb/^{206}Pb$	1σ	$^{207}Pb/^{206}Pb$	1σ
	16,907	2,E-03	15,444	2,E-03	36,534	5,E-02	2,16102	7,E-05	0,91354	2,E-05
	16,899	4,E-03	15,432	4,E-03	36,498	9,E-03	2,15978	5,E-05	0,91319	2,E-05
	16,903	3,E-03	15,438	3,E-03	36,516	3,E-02	2,16040	6,E-05	0,91336	2,E-05
	16,917	4,E-03	15,455	4,E-03	36,565	9,E-03	2,16141	7,E-05	0,91359	4,E-05
	16,910	3,E-03	15,447	3,E-03	36,541	3,E-02	2,16091	6,E-05	0,91348	2,E-05
	16,906	4,E-03	15,442	4,E-03	36,528	9,E-03	2,16065	7,E-05	0,91342	4,E-05
	16,906	3,E-03	15,442	3,E-03	36,526	3,E-02	2,16053	6,E-05	0,91338	2,E-05
	16,903	4,E-03	15,438	4,E-03	36,516	9,E-03	2,16040	7,E-05	0,91336	4,E-05
	16,901	3,E-03	15,435	3,E-03	36,507	3,E-02	2,16009	6,E-05	0,91328	2,E-05
	16,910	4,E-03	15,447	4,E-03	36,541	9,E-03	2,16091	7,E-05	0,91348	4,E-05
mean	16,906		15,442		36,5273		2,16061		0,91341	
Catanzaro, 1968	16,937		15,491		36,721		2,1681		0,9146	
Deviation	1,00183		1,00316		1,00530		1,00347		1,00130	

The isotopes concentrations have only been measured with TIMS method on the mineral samples and on some whole rock sample allowing a comparison with the ICP-MS and ICP-AES results for Rb, Sr, Pb, U and Th. There is an excellent agreement between the TIMS and the ICP-MS values (fig. b5.1).

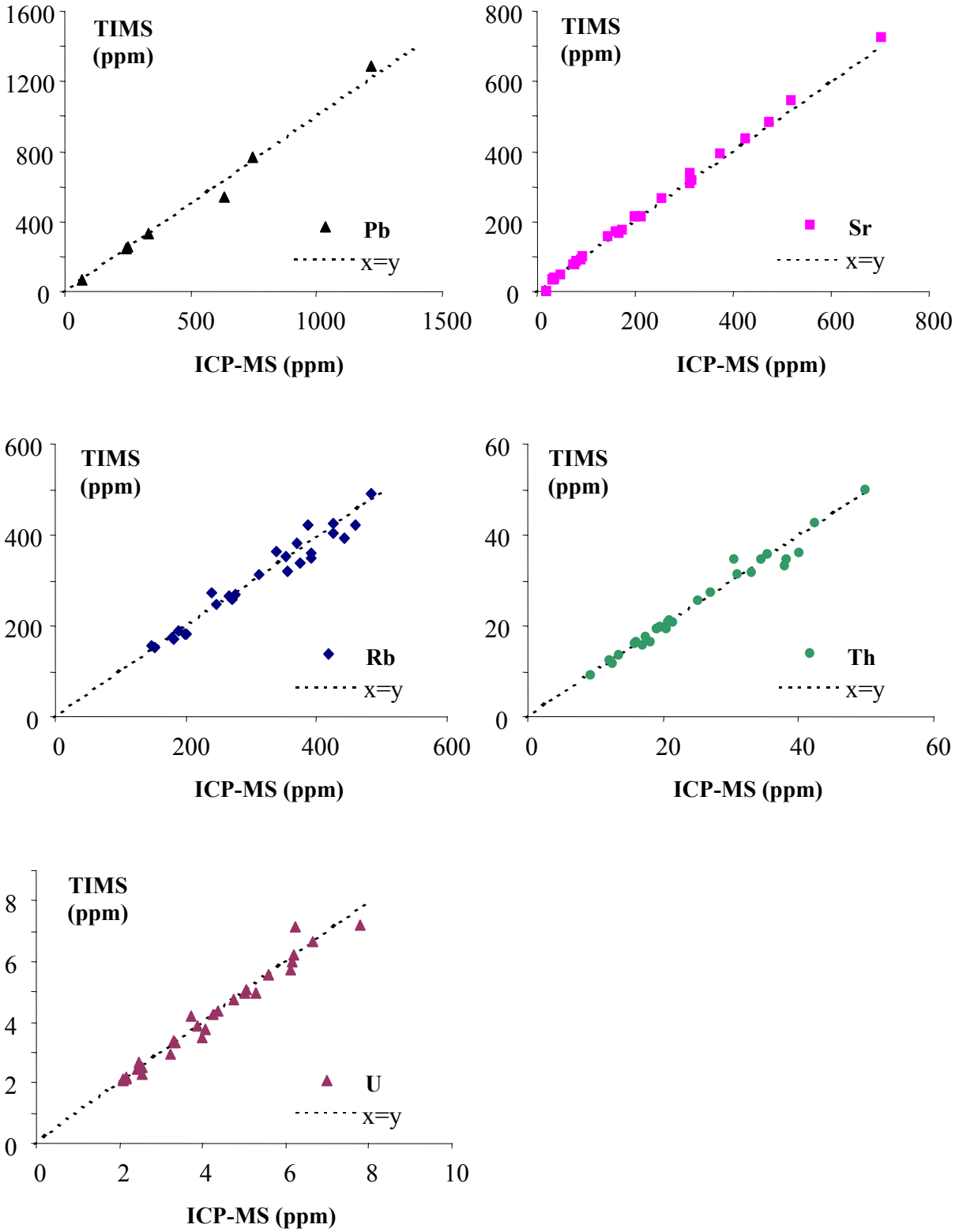

Figure b5.1: Comparison between TIMS and ICP-MS element measures for Rb, Sr, Pb, U and Th

B6 Blanks

U-Th blanks

^{238}U [ng]	error [ng]	^{235}U [pg]	error [pg]	^{234}U [pg]	error [pg]	^{232}Th [ng]	error [ng]	^{230}Th [fg]	error [fg]
0,303	0,004	25,988	0,429	0,926	0,282	0,700	0,000	5,320	0,000
1,352	0,003	35,264	0,194	0,804	0,014	0,339	0,056	7,897	1,647
16,348	0,178	142,883	2,006	2,022	0,099	1,339	0,102	13,250	2,916
0,773	0,007	32,072	0,802	1,047	0,128	0,860	0,000	6,120	0,000
0,717	0,002	30,248	0,266	0,905	0,045	0,627	0,004	4,840	3,032
0,874	0,001	30,869	0,068	0,777	0,005	0,339	0,056	7,897	1,647
0,795	0,002	30,559	0,167	0,841	0,025	0,483	0,030	6,369	2,339

Pb and Rb-Sr blanks

Description	Pb [ng]	Pb [pg/g solution]	Pb [pg/g solution]
Resin blank	4,662		
Total blank	5,105	61	348,5
Total blank	5,527	10	166,3
Total blank	7,279	12,8	89,37

Appendix C
Data

C1 TIMS

C1.1 Lead

Reference samples

Sample	$^{206}Pb/^{204}Pb$	error 1σ abs	$^{207}Pb/^{204}Pb$	error 1σ abs	$^{208}Pb/^{204}Pb$	error 1σ abs	$^{208}Pb/^{206}Pb$	error 1σ abs	$^{207}Pb/^{206}Pb$	error 1σ abs
G1F2	18,365	5,E-03	15,617	5,E-03	38,533	1,E-02	2,09814	1,E-04	0,85031	3,E-05
G1F1	18,571	6,E-03	15,634	6,E-03	38,764	1,E-02	2,08727	1,E-04	0,84184	3,E-05
GB	18,599	2,E-02	15,635	1,E-02	38,757	3,E-02	2,08379	1,E-04	0,84057	5,E-05
G1W2	18,598	3,E-02	15,750	3,E-02	38,998	7,E-02	2,09690	2,E-04	0,84682	2,E-04
QV	18,770	2,E-01	15,649	2,E-02	38,949	5,E-02	2,07493	1,E-04	0,83351	5,E-05
QS	18,802	9,E-03	15,642	7,E-03	38,993	2,E-02	2,07390	3,E-05	0,83188	3,E-05
vitriol	18,930	2,E-03	15,713	2,E-03	39,129	5,E-03	2,06723	8,E-05	0,82987	2,E-05

Description page 31.

Profile samples

Sample	$^{206}Pb/^{204}Pb$	error 1σ abs	$^{207}Pb/^{204}Pb$	error 1σ abs	$^{208}Pb/^{204}Pb$	error 1σ abs	$^{208}Pb/^{206}Pb$	error 1σ abs	$^{207}Pb/^{206}Pb$	error 1σ abs
1/1	18,7792	3,E-03	15,6268	3,E-03	38,909	6,E-03	2,07182	1,E-04	0,83208	3,E-05
1/2	18,7778	1,E-02	15,6309	1,E-02	38,915	2,E-02	2,07239	2,E-04	0,83238	5,E-05
1/3	18,7639	8,E-04	15,6150	9,E-04	38,883	2,E-03	2,07214	7,E-05	0,83214	1,E-05
1/4	18,7542	3,E-03	15,6069	2,E-03	38,852	7,E-03	2,07165	1,E-04	0,83216	2,E-05
G3	18,7448	2,E-03	15,6379	1,E-03	38,907	3,E-03	2,07559	1,E-04	0,83423	2,E-05
G3	18,7587	7,E-04	15,6483	7,E-04	38,914	2,E-03	2,07469	5,E-05	0,83403	1,E-05
G4	18,7863	1,E-03	15,6654	1,E-03	39,016	4,E-03	2,07685	1,E-04	0,83385	2,E-05
G5	18,7535	1,E-03	15,6532	1,E-03	38,942	3,E-03	2,07649	6,E-05	0,83466	2,E-05
G6	18,7506	2,E-03	15,6357	2,E-03	38,902	5,E-03	2,07471	7,E-05	0,83386	1,E-05
G7	18,7551	1,E-03	15,6464	1,E-03	38,931	3,E-03	2,07571	4,E-05	0,83422	1,E-05
G8	18,7614	2,E-03	15,6584	2,E-03	38,966	5,E-03	2,07689	5,E-05	0,83460	1,E-05
G9	18,7510	9,E-03	15,6526	8,E-03	38,903	2,E-02	2,07468	5,E-05	0,83483	2,E-05
G10	18,6928	2,E-03	15,6546	2,E-03	38,920	7,E-03	2,08208	2,E-04	0,83744	4,E-05
G11	18,7599	2,E-03	15,6369	2,E-03	38,881	5,E-03	2,07249	3,E-04	0,83348	2,E-05
G12	18,6894	1,E-03	15,6368	1,E-03	38,859	5,E-03	2,07917	1,E-04	0,83664	3,E-05
G13	18,7368	1,E-03	15,6433	1,E-03	38,914	3,E-03	2,07688	4,E-05	0,83488	1,E-05
G13	18,7365	1,E-03	15,6402	7,E-04	38,883	3,E-03	2,07546	3,E-05	0,83459	1,E-05
G14	18,2980	1,E-02	15,5841	9,E-03	38,329	2,E-02	2,09473	1,E-04	0,85168	1,E-04
G14	18,3015	7,E-03	15,5689	5,E-03	38,260	1,E-02	2,09062	1,E-04	0,85069	4,E-05
G15	18,5836	8,E-03	15,6027	7,E-03	38,368	2,E-01	2,06460	7,E-05	0,83956	3,E-05
G16	18,6109	5,E-03	15,6181	4,E-03	38,433	1,E-02	2,06492	1,E-04	0,83914	2,E-05
G17	18,4624	5,E-03	15,6047	4,E-03	38,375	5,E-03	2,07811	7,E-05	0,84519	3,E-05
G18	18,9228	1,E-01	15,8851	9,E-02	39,192	2,E-01	2,07190	7,E-04	0,83946	2,E-04

Mineral samples

Sample	$^{206}Pb/^{204}Pb$	error 1σ abs	$^{207}Pb/^{204}Pb$	error 1σ abs	$^{208}Pb/^{204}Pb$	error 1σ abs	$^{208}Pb/^{206}Pb$	error 1σ abs	$^{207}Pb/^{206}Pb$	error 1σ abs
mx1	18,306	2,E-02	15,620	2,E-02	38,375	5,E-02	2,09655	2,E-04	0,85339	1,E-04
mx2	18,296	9,E-02	15,397	7,E-02	37,736	2,E-01	2,06353	5,E-04	0,84128	3,E-04
mx3	18,656	1,E-01	15,492	1,E-01	38,157	3,E-01	2,04547	9,E-04	0,83036	5,E-04
mx4	18,173	9,E-03	15,613	7,E-03	38,310	2,E-02	2,10798	1,E-04	0,85900	5,E-05
mx5	26,617	3,E-01	15,924	2,E-01	39,063	4,E-01	1,46757	8,E-04	0,59817	4,E-04
mx6	18,179	4,E-03	15,599	4,E-03	38,259	1,E-02	2,10449	6,E-05	0,85803	2,E-05
mx7	24,122	1,E-01	16,056	1,E-01	39,906	2,E-01	1,65449	2,E-04	0,66552	9,E-05
mx8	19,145	3,E-03	15,675	3,E-03	39,089	1,E-02	2,04171	2,E-04	0,81872	3,E-05
mx9	19,263	8,E-03	15,688	7,E-03	39,138	2,E-02	2,03184	2,E-04	0,81445	6,E-05
mx10	18,243	3,E-03	15,614	2,E-03	38,214	6,E-03	2,09463	2,E-05	0,85583	1,E-05
mx11	28,641	6,E-02	16,223	3,E-02	42,663	9,E-02	1,48939	1,E-04	0,56640	5,E-05
mx12	19,273	1,E-02	15,655	1,E-02	39,056	3,E-02	2,02635	7,E-05	0,81231	3,E-05
mx13	19,144	1,E-02	15,653	9,E-03	38,958	2,E-02	2,03504	2,E-04	0,81760	6,E-05
KFG4	18,370	6,E-03	15,591	5,E-03	38,324	1,E-02	2,08617	1,E-04	0,84862	2,E-05
KFG12	18,184	1,E-02	15,570	9,E-03	38,224	2,E-02	2,10199	3,E-04	0,85622	7,E-05

Sample	Description		Pb [ppm]
mx1	whole rock	G1F2	31
mx2	Biotite 100-200 µm		13
mx3	Biotite 200-315 µm		15
mx4	K-feldspar		107
mx5	Apatite		14
mx6	K-feldspar	G1W2	63
mx7	Apatite		23
mx8	Biotite 100-200 µm		64
mx9	Biotite 200-315 µm		74
mx10	K-feldspar	G13	87
mx11	Apatite		20
mx12	Biotite 100-200 µm		16
mx13	Biotite 200-315 µm		13
KFG4	K-feldspar	G4	87
KFG12	K-feldspar	G12	57

C1.2 Rb-Sr

Profile samples

Sample	$^{87}Sr/^{86}Sr$	error 2σ abs	$^{84}Sr/^{88}Sr$	error 2σ abs	$^{87}Rb/^{86}Sr$	error 2σ abs	Sr [ppm]	error 2σ abs	Rb [ppm]	error 2σ abs
1/1	0,83976	7,E-05	0,4152	3,E-03	27,41	8,E-01	33,9	7,E-01	318,2	7,E+00
1/2	0,87553	6,E-05	0,3011	2,E-03	34,80	1,E+00	35,5	7,E-01	422,1	9,E+00
1/3	0,85874	8,E-05	0,3332	3,E-03	31,56	9,E-01	33,4	7,E-01	360,1	7,E+00
1/4	0,87951	8,E-05	0,4708	8,E-03	34,28	1,E+00	33,7	7,E-01	394,4	8,E-01
G3	0,72490	6,E-05	0,0363	3,E-04	3,87	1,E-01	261,2	5,E+00	350,3	7,E+00
G4	0,73485	8,E-05	0,0766	9,E-04	5,84	2,E-01	171,5	4,E+00	346,7	7,E+00
G5	0,72738	1,E-04	0,0279	2,E-04	3,88	1,E-01	251,7	5,E+00	338,2	7,E+00
G6	0,75455	7,E-05	0,1339	9,E-04	12,65	4,E-01	96,8	2,E+00	423,1	9,E+00
G7	0,74688	8,E-05	0,2049	3,E-03	9,45	3,E-01	87,3	2,E+00	285,2	6,E+00
G8	0,74606	8,E-05	0,1363	2,E-03	10,12	3,E-01	74,0	2,E+00	258,6	5,E+00
G9-1	0,73014	8,E-05	0,0419	3,E-04	9,06	3,E-01	128,6	3,E+00	403,3	8,E+00
G9-2	0,73014	8,E-05	0,0419	3,E-04	9,04	3,E-01	128,6	3,E+00	402,4	8,E+00
G10	0,74184	7,E-05	0,1122	7,E-04	7,34	2,E-01	101,2	2,E+00	257,1	5,E+00
G11-1	0,74233	6,E-05	0,0877	1,E-03	15,10	4,E-01	73,5	2,E+00	383,5	1,E+01
G11-2	0,74233	6,E-05	0,0877	1,E-03	21,01	6,E-01	73,5	2,E+00	533,6	1,E+01
G12	0,71192	1,E-04	0,0287	9,E-05	1,01	3,E-02	542,5	1,E+01	189,8	4,E+00
G13	0,71371	5,E-05	0,0159	2,E-04	1,78	5,E-02	436,6	9,E+00	269,4	6,E+00
G14-1	0,72576	6,E-05	0,1009	4,E-04	3,25	9,E-02	158,5	3,E+00	178,5	4,E+00
G14-2	0,72576	1,E-04	0,0737	6,E-04	7,21	2,E-01	109,4	2,E+00	273,1	6,E+00
G14-3	0,72576	1,E-04	0,0737	6,E-04	7,33	2,E-01	109,4	2,E+00	277,5	6,E+00
G15	0,71458	1,E-04	0,0504	3,E-04	2,31	7,E-02	267,1	6,E+00	213,5	4,E+00
G16	0,71118	7,E-05	0,0940	5,E-04	0,43	1,E-02	1150,0	2,E+01	172,5	4,E+00
G17	0,71235	2,E-04	0,0363	1,E-04	1,23	4,E-02	337,8	7,E+00	143,7	3,E+00
G18-1	0,71527	6,E-05	0,0513	2,E-04	1,91	6,E-02	214,5	4,E+00	142,2	3,E+00
G18-2	0,71538	8,E-05	0,0667	2,E-03	2,47	7,E-02	211,7	4,E+00	181,0	4,E+00

Reference samples

Sample	$^{87}Sr/^{86}Sr$	error 2σ abs	$^{84}Sr/^{88}Sr$	error 2σ abs	$^{87}Rb/^{86}Sr$	error 2σ abs	Sr [ppm]	error 2σ abs	Rb [ppm]	error 2σ abs
G1F2	0,71251	9,E-05	0,02244	8,E-05	1,27	4,E-02	391,2	8,E+00	173	4,E+00
G1F1	0,71108	7,E-05	0,02060	3,E-04	0,93	3,E-02	481,9	1,E+01	156	3,E+00
GB	0,70912	5,E-05	0,02264	9,E-05	0,49	1,E-02	723,5	1,E+01	123	3,E+00
G1W2	0,71348	7,E-05	0,03168	1,E-03	1,70	5,E-02	305,5	6,E+00	180	4,E+00
QV	0,87177	1,E-04	0,28884	2,E-02	39,57	1,E+00	36,4	8,E-01	492	1,E+01
QS	0,79470	8,E-05	0,24787	1,E-02	22,05	6,E-01	47,8	1,E+00	362	7,E+00

Description page 31.

Mineral samples

Sample	$^{87}Sr/^{86}Sr$	error 2σ abs	$^{84}Sr/^{88}Sr$	error 2σ abs	$^{87}Rb/^{86}Sr$	error 2σ abs	Sr [ppm]	error 2σ abs	Rb [ppm]	error 2σ abs
mx1	0,71184	7,E-05	0,0947	4,E-04	1,046	3,E-02	468,2	1,E+01	169,8	3,E+00
mx2			0,5138	8,E-03	168,77	5,E+00	14,2	3,E-01	773,0	2,E+01
mx3			0,6542	1,E-02	226,50	7,E+00	11,1	2,E-01	787,6	2,E+01
mx4	0,71123	9,E-05	0,0184	2,E-04	0,906	3,E-02	933,9	2,E+01	293,6	6,E+00
mx5	0,70702	8,E-05	0,2386	2,E-03	0,106	3,E-03	393,7	8,E+00	14,5	3,E-01
mx6	0,71172	8,E-05	0,2789	2,E-03	0,903	3,E-02	1066,2	2,E+01	333,8	7,E+00
mx7	0,70733	6,E-05	0,2133	2,E-01	0,089	3,E-03	406,8	8,E+00	12,5	3,E-01
mx8			0,1792	1,E-03	24,609	7,E-01	38,1	8,E-01	321,9	7,E+00
mx9			0,2088	1,E-03	24,970	7,E-01	37,3	8,E-01	319,9	7,E+00
mx10	0,72071	2,E-04	0,1272	6,E-04	3,058	9,E-02	348,3	7,E+00	369,0	8,E+00
mx11	0,70644	3,E-04	0,6309	1,E-02	0,285	8,E-03	184,9	4,E+00	18,3	4,E-01
mx12			0,8649	1,E-02	305,394	9,E+00	12,7	3,E-01	1252,1	3,E+01
mx13			1,1654	3,E-02	180,135	5,E+00	17,0	3,E-01	990,0	2,E+01
KFG4	0,71607	9,E-05	0,1484	9,E-04	2,322	7,E-02	449,5	9,E+00	361,8	7,E+00
KFG12	0,70877	9,E-05	0,0448	3,E-04	0,467	1,E-02	1418,0	3,E+01	229,5	5,E+00

C1.3 Th-U

Sample	^{238}U [ppm]	error 2σ abs	^{238}U [dpm/g]	error 2σ abs	^{234}U [ppb]	error 2σ abs	^{234}U [dpm/g]	error 2σ abs	deltaAU [o/oo]	error 2σ abs
1/1	7,188	0,019	5,363	0,014	0,347	0,001	4,794	0,019	-106	4
1/2	6,027	0,012	4,497	0,009	0,296	0,001	4,092	0,014	-90	3
1/3	5,094	0,010	3,801	0,008	0,253	0,002	3,501	0,024	-79	6
1/4	5,721	0,008	4,268	0,006	0,278	0,001	3,837	0,012	-101	3
G3	3,060	0,011	2,283	0,008	0,154	0,002	2,125	0,022	-69	10
G4	4,947	0,023	3,691	0,017	0,309	0,002	4,276	0,024	158	8
G4b	3,775	0,020	2,817	0,015	0,221	0,002	3,060	0,032	86	12
G5	3,485	0,016	2,600	0,012	0,200	0,002	2,759	0,026	61	11
G6	4,625	0,014	3,451	0,011	0,249	0,001	3,446	0,018	-1	6
G7	2,933	0,011	2,189	0,008	0,162	0,002	2,234	0,027	21	13
G8b	1,599	0,005	1,193	0,004	0,085	0,001	1,180	0,015	-11	13
G8c	4,954	0,019	3,697	0,014	0,256	0,002	3,536	0,024	-43	7
G9	1,999	0,012	1,492	0,009	0,110	0,001	1,521	0,018	20	13
G10	2,064	0,003	1,540	0,002	0,122	0,000	1,686	0,005	95	3
G11	2,570	0,002	1,918	0,002	0,135	0,000	1,867	0,006	-27	3
G12	3,037	0,008	2,266	0,006	0,151	0,001	2,092	0,014	-77	7
G13	3,215	0,005	2,399	0,004	0,157	0,000	2,172	0,005	-95	2
G14	1,754	0,004	1,309	0,003	0,084	0,001	1,158	0,010	-115	8
G15	3,335	0,010	2,488	0,007	0,173	0,001	2,389	0,015	-40	7
G16	4,631	0,012	3,455	0,009	0,234	0,001	3,236	0,013	-63	4
G17	2,529	0,004	1,887	0,003	0,128	0,001	1,767	0,008	-63	4
G18	2,659	0,004	1,984	0,003	0,139	0,000	1,918	0,006	-33	3
Reference samples (description page 31)										
G1F2	1,794	0,007	1,338	0,005	0,094	0,001	1,295	0,014	-32	11
GB	3,407	0,006	2,542	0,004	0,179	0,001	2,470	0,011	-28	5
G1W2	2,115	0,005	1,578	0,003	0,107	0,001	1,477	0,008	-64	5
QV	6,213	0,022	4,636	0,017	0,307	0,002	4,241	0,029	-85	7
QS	3,137	0,012	2,341	0,009	0,145	0,001	2,001	0,015	-145	7

Sample	^{232}Th [ppm]	error 2σ abs	^{232}Th [dpm/g]	error 2σ abs	^{230}Th [ppb]	error 2σ abs	^{230}Th [dpm/g]	error 2σ abs
1/1	34,55	0,43	8,435	0,106	0,147	0,0026	6,70	0,12
1/2	35,98	0,30	8,784	0,074	0,116	0,0014	5,28	0,06
1/3	29,91	0,43	7,301	0,106	0,125	0,0031	5,68	0,14
1/4	34,52	0,27	8,427	0,067	0,099	0,0013	4,49	0,06
G3	23,52	0,30	5,742	0,072	0,073	0,0015	3,33	0,07
G4	15,66	0,16	3,824	0,039	0,112	0,0020	5,10	0,09
G4b	11,68	0,15	2,851	0,036	0,084	0,0014	3,82	0,06
G5	16,30	0,19	3,979	0,046	0,076	0,0015	3,47	0,07
G6	8,64	0,08	2,110	0,020	0,091	0,0010	4,14	0,04
G7	16,25	0,12	3,968	0,029	0,119	0,0016	5,42	0,07
G8b	14,28	0,09	3,487	0,023	0,037	0,0007	1,67	0,03
G8c	9,18	0,06	2,242	0,014	0,085	0,0010	3,89	0,05
G9	10,26	0,04	2,505	0,009	0,039	0,0003	1,78	0,01
G10	14,67	0,10	3,582	0,025	0,047	0,0005	2,13	0,02
G11	13,00	0,05	3,417	0,011	0,051	0,0002	2,30	0,01
G12	24,06	0,22	5,873	0,055	0,061	0,0009	2,77	0,04
G13	25,90	0,24	6,322	0,058	0,058	0,0009	2,66	0,04
G14	15,21	0,15	3,714	0,038	0,043	0,0008	1,95	0,04
G15	19,84	0,38	4,844	0,092	0,084	0,0025	3,84	0,11
G16	14,97	0,14	3,654	0,034	0,082	0,0011	3,76	0,05
G17	19,45	0,12	4,749	0,028	0,051	0,0007	2,34	0,03
G18	29,44	0,59	7,188	0,145	0,059	0,0015	2,69	0,07
Reference samples (description page 31)								
QV	31,46	0,35	7,681	0,086	0,111	0,0011	5,08	0,05
GB	20,78	0,11	5,072	0,026	0,070	0,0007	3,20	0,03
QS	27,74	0,22	6,772	0,054	0,066	0,0010	2,99	0,04
G1F2	9,43	0,05	2,302	0,011	0,035	0,0003	1,59	0,01
G1W2	16,35	0,09	3,993	0,023	0,042	0,0004	1,92	0,02

C2 ICP-MS and ICP-AES

C2.1 Major elements (%)

Samples	Total	SiO_2	Al_2O_3	MgO	CaO	Fe_2O_3	MnO	TiO_2	Na_2O	K_2O	P_2O_5
1/1	99,12	82,7	8,3	0,03	0,09	1,1	0,006	0,05	0,39	5,77	0,04
1/2	100,41	81,8	9,5	0,01	0,11	1,2	0,009	0,05	0,66	6,42	0,03
1/3	100,23	83,2	8,6	0,03	0,08	1,1	0,007	0,05	0,39	6,26	0,03
1/4	98,95	80,3	9,4	0,03	0,1	1,2	0,008	0,05	0,53	6,59	0,02
G 3	100,88	70,6	15,7	0,49	0,04	1,4	0,015	0,31	0,31	10,55	0,09
G 4	100,51	71,3	14,6	0,46	0,06	2,0	0,006	0,39	0,08	10,21	0,08
G4B	100,03	75,0	12,7	0,42	0,05	1,0	0,004	0,32	0,11	9,11	0,08
G5	100,43	73,0	13,9	0,68	0,04	1,9	0,055	0,32	0,22	9,01	0,03
G6	100,77	76,9	12,0	0,43	0,05	1,4	0,017	0,29	0,06	8,34	0,04
G7	100,78	79,9	10,5	0,32	0,04	1,7	0,008	0,23	0,03	6,94	0,05
G8B	99,97	83,0	8,6	0,25	0,04	1,5	0,006	0,16	0,01	5,21	0,04
G8C	100,76	82,6	8,2	0,29	0,03	2,0	0,004	0,14	0,00	5,28	0,09
G9	100,64	72,9	14,1	0,37	0,04	2,0	0,007	0,26	0,18	9,41	0,06
G10	99,79	75,5	13,4	0,23	0,03	0,6	0,009	0,26	0,07	7,28	0,04
G11	99,88	72,6	13,7	0,51	0,04	2,5	0,012	0,36	0,00	7,95	0,04
G12	98,70	68,6	15,1	0,96	1,41	2,6	0,025	0,47	2,75	5,61	0,18
G13	100,68	68,6	15,3	1,09	1,08	2,9	0,039	0,50	2,42	6,91	0,22
G14	100,05	74,8	13,6	0,08	0,49	0,5	0,003	0,08	2,61	7,29	0,02
G15	99,72	70,0	14,8	0,87	1,40	2,5	0,038	0,33	3,00	5,29	0,10
G16	99,09	69,9	14,9	0,71	2,00	3,0	0,062	0,31	3,39	3,61	0,15
G17	100,07	70,9	15,1	0,57	1,77	1,9	0,052	0,23	3,54	5,02	0,10
G18	99,40	73,0	12,9	0,85	1,27	2,5	0,038	0,38	2,56	4,45	0,11
Reference samples (description page 31)											
G1F1	99,32	72,9	13,9	0,44	0,84	1,1	0,019	0,20	3,57	5,18	0,22
G1W1	100,87	70,7	15,2	1,11	0,39	2,5	0,021	0,37	2,31	5,76	0,14
G1F2	101,06	71,6	15,4	1,09	0,78	2,2	0,032	0,40	3,47	4,74	0,19
G1W2	99,20	69,5	14,9	1,20	0,45	2,3	0,019	0,37	2,15	5,48	0,15
GB	99,86	68,2	15,6	1,29	2,26	2,8	0,050	0,54	4,08	3,92	0,20
QV	100,16	81,7	8,9	0,02	0,11	1,2	0,011	0,05	0,57	6,84	0,01
QS	100,67	81,7	9,2	0,08	0,09	0,6	0,009	0,04	0,00	7,88	0,07
Po1W	99,88	79,0	10,0	0,08	0,08	2,0	0,007	0,07	0,17	6,94	0,03
Po1F	100,22	80,8	9,8	0,05	0,09	0,8	0,006	0,06	0,19	7,61	0,02

C2.2 Trace elements (ppm)

Samples	Co	Rb	Nb	Mo	Sn	Sb	Cs	Hf	Ta	W	Pb	Th	U
1/1	1,0	357	18,6	0,7	1,5	8,8	16,7	4,7	2,7	4,7	254	38,4	7,8
1/2	0,0	459	23,0	0,5	1,7	14,3	23,5	5,2	3,1	4,1	161	40,2	6,2
1/3	0,0	393	19,5	0,5	1,3	12,3	19,0	4,6	2,8	3,2	147	34,6	5,1
1/4	1,0	444	23,1	0,5	1,4	11,9	23,9	5,3	3,1	4,7	152	42,5	6,1
G 3	3,3	393	12,8	0,5	2,4	5,9	49,9	3,2	1,0	5,9	1220	15,9	2,2
G 4	2,7	427	14,3	0,5	2,5	11,3	61,6	4,2	1,3	8,1	533	17,1	5,3
G4B	1,7	340	16,8	0,5	2,2	11,3	37,9	4,6	1,1	7,0	491	12,7	4,1
G5	7,3	376	12,3	0,6	2,1	17,2	174	5,0	1,3	3,8	635	18,1	4,0
G6	3,2	387	14,4	1,2	2,0	36,5	36,8	3,4	1,2	5,0	749	12,2	5,6
G7	2,1	353	10,1	0,6	1,9	26,1	44,3	3,0	1,1	4,6	552	19,2	3,3
G8B	1,6	270	6,9	0,4	1,7	18,4	43,3	2,4	0,6	4,7	267	17,6	2,1
G8C	1,5	270	9,2	1,5	1,4	27,6	31,0	2,5	0,6	4,0	671	9,4	5,0
G9	2,1	426	9,7	0,4	1,9	22,4	95,5	2,9	1,1	7,1	333	13,6	2,4
G10	1,8	312	11,8	0,5	1,9	16,1	30,2	4,9	0,9	3,2	256	31,1	3,9
G11	4,5	370	12,1	0,4	2,0	14,2	85,4	5,1	1,4	5,8	246	19,5	3,3
G12	6,3	247	8,3	0,4	2,0	5,0	46,3	6,2	1,0	1,3	132	35,6	4,3
G13	7,0	276	8,8	0,4	2,0	4,0	55,2	6,0	1,0	2,4	252	38,0	4,4
G14	0,6	240	4,0	0,2	1,5	2,5	15,9	2,5	0,7	0,7	70	21,1	2,5
G15	5,6	266	8,6	0,5	2,2	2,7	63,2	3,6	1,3	1,0	39	27,1	4,8
G16	5,9	181	7,9	0,3	2,0	1,4	54,7	3,7	1,4	1,1	40	20,8	6,7
G17	5,8	188	6,7	0,0	1,7	1,4	28,9	3,1	0,9	1,1	38	20,6	2,5
G18	8,5	198	12,9	0,7	4,9	7,9	50,6	3,5	1,7	4,5	25	25,3	2,5
Reference samples (description page 31)													
G1F1	2,3	148	5,7	0,2	2,1	0,2	10,6	3,2	0,8	3,5	45	16,2	2,6
G1W1	4,3	229	10,5	1,3	2,5	1,1	37,9	4,3	1,0	8,9	37	19,1	1,9
G1F2	3,7	178	8,6	0,0	2,7	0,1	24,6	4,4	0,7	1,7	30	19,2	2,2
G1W2	4,4	201	10,2	0,7	2,7	1,1	38,9	4,6	0,9	9,3	38	19,7	2,1
GB	5,2	153	8,9	0,2	2,5	0,1	13,8	5,7	0,9	0,4	37	21,5	3,3
QV	0,0	485	23,3	1,2	2,8	26,7	23,7	4,4	2,9	3,3	109	33,1	6,2
QS	0,3	339	27,0	0,4	11,6	24,8	11,6	4,4	4,5	3,4	203	29,9	3,3
Po1W	1,4	353	24,0	2,9	3,9	14,8	17,7	5,1	3,2	5,2	151	49,9	6,2
Po1F	0,1	503	27,7	1,1	3,1	5,1	17,2	4,8	3,1	4,7	45	30,6	3,7

Samples	Sr	Ba	V	Ni	Cr	Zn	Cu	Sc	Y	Zr
1/1	34	156	10	9	30	58	18	10,2	79,2	94
1/2	37	102	8	6	6	29	17	12,7	44,2	103
1/3	32	166	7	5	5	37	18	11,1	25,7	92
1/4	33	122	8	7	5	31	17	12,9	39,8	105
G 3	214	2869	24	5	37	82	25	5,2	21,9	98
G 4	162	1023	30	6	19	75	45	6,4	33,9	143
G4B	146	1163	24	5	21	46	27	7,7	87,4	157
G5	174	2310	29	7	16	104	51	5,3	11,8	163
G6	77	742	28	6	15	54	44	5,9	7,1	108
G7	82	772	26	5	13	39	21	4,4	13,1	88
G8B	73	322	23	5	10	25	10	4,5	14,7	69
G8C	89	211	24	6	15	90	42	5,4	15,7	86
G9	168	2023	27	6	42	41	11	5	8	79
G10	94	430	23	5	19	36	19	6,6	9,6	119
G11	89	546	35	9	25	88	15	6,7	6,3	150
G12	518	1362	46	9	18	96	6	5,1	8,7	193
G13	425	1405	50	12	22	125	7	5,9	10,5	189
G14	146	562	11	3	6	24	5	1,5	3,7	43
G15	255	802	35	11	18	107	6	3,9	8,9	101
G16	316	676	40	11	19	129	10	4,3	10,4	107
G17	313	1114	31	28	25	86	14	3,2	9	103
G18	200	399	39	12	29	95	11	5,1	10,5	119
Reference samples (description page 31)										
G1F1	474	968	19	56	7	32	11	2,4	11,7	115
G1W1	353	1353	45	10	20	96	15	4,1	8,6	162
G1F2	375	1276	45	9	14	61	12	4,3	10,7	181
G1W2	312	1175	47	11	22	93	12	3,9	10,4	166
GB	704	1166	48	8	18	63	12	4,9	10	218
QV	35	104	8	5	5	30	20	12,6	59,8	97
QS	47	100	10	5	6	27	19	8,5	157	83
Po1W	20	244	17	7	4	101	20	16,4	64,4	120
Po1F	20	224	10	13	16	27	14	12,3	26,2	114

C2.3 Rare Earth elements (ppm)

Samples	La	Ce	Pr	Nd	Sm	Eu	Gd	Tb	Dy	Ho	Er	Tm	Yb	Lu
1/1	18,3	48,9	7,1	31,8	12,06	0,25	11,05	2,28	14,21	3,03	7,33	1,23	7,09	1,16
1/2	16,3	33,9	4,8	19,8	6,60	0,11	6,33	1,30	8,54	1,82	4,82	0,90	5,70	0,93
1/3	7,6	16,4	2,6	11,2	4,26	0,11	3,80	0,80	5,25	1,18	3,08	0,58	3,90	0,62
1/4	15,4	30,0	4,4	17,9	6,07	0,11	5,63	1,17	8,10	1,80	4,65	0,84	5,24	0,84
G 3	49,6	76,9	11,9	46,5	9,37	0,45	5,98	0,90	3,98	0,70	1,62	0,23	1,37	0,20
G 4	176,0	232,0	38,3	152,6	16,80	0,47	8,23	1,18	5,54	1,06	2,65	0,35	1,87	0,28
G4B	176,0	224,0	30,1	97,3	11,50	0,39	9,54	1,93	12,20	2,71	6,48	0,92	4,78	0,71
G5	37,1	62,6	9,1	34,3	7,30	0,42	4,14	0,55	2,42	0,44	1,06	0,16	1,01	0,16
G6	25,0	30,4	5,0	17,2	3,87	0,27	2,71	0,34	1,61	0,28	0,61	0,09	0,60	0,09
G7	34,5	43,7	7,1	26,1	5,51	0,39	3,54	0,52	2,42	0,46	1,06	0,14	0,77	0,13
G8B	122,3	102,0	22,0	71,2	10,13	0,66	4,92	0,66	3,01	0,56	1,40	0,18	0,95	0,15
G8C	147,0	117,0	20,4	63,1	8,48	0,53	5,12	0,59	2,52	0,50	1,25	0,16	0,98	0,12
G9	131,6	114,0	24,9	90,3	11,40	0,96	5,51	0,60	2,33	0,38	0,92	0,11	0,67	0,11
G10	67,8	76,0	14,2	50,2	7,48	0,69	3,71	0,51	2,46	0,44	1,17	0,18	1,20	0,18
G11	36,9	52,5	7,7	26,6	4,22	0,46	2,50	0,32	1,63	0,29	0,78	0,12	0,82	0,14
G12	89,6	165,0	17,9	60,5	9,47	1,91	5,11	0,56	2,29	0,40	1,03	0,13	0,79	0,13
G13	46,8	175,0	12,4	44,8	7,70	1,31	4,32	0,53	2,63	0,47	1,21	0,19	1,07	0,16
G14	11,4	22,4	2,6	8,3	1,45	0,51	0,96	0,16	0,81	0,17	0,44	0,08	0,52	0,08
G15	49,8	87,2	9,9	31,8	4,17	0,88	2,80	0,37	1,97	0,40	1,07	0,18	1,01	0,19
G16	47,7	78,7	9,4	31,7	5,73	1,24	3,68	0,52	2,56	0,49	1,16	0,19	1,16	0,17
G17	34,7	61,8	6,4	21,4	3,62	0,69	2,27	0,32	1,60	0,33	0,85	0,13	0,94	0,14
G18	31,7	63,3	7,5	26,8	5,16	0,88	2,87	0,41	1,86	0,39	1,04	0,17	1,07	0,15
Reference samples (description page 31)														
G1F1	32,2	62,8	7,00	23,2	3,42	0,81	2,40	0,34	1,86	0,36	1,00	0,15	0,89	0,13
G1W1	67,2	135	13,6	46,9	5,90	0,95	3,80	0,41	1,65	0,31	0,85	0,10	0,74	0,11
G1F2	57,1	110	11,8	39,2	6,28	0,97	4,00	0,46	1,88	0,32	0,84	0,11	0,80	0,12
G1W2	60,7	116	12,6	43,7	5,67	1,02	3,83	0,44	1,88	0,38	0,88	0,13	0,80	0,10
GB	33,6	64,8	6,88	23,1	3,41	0,83	2,22	0,30	1,49	0,29	0,81	0,12	0,94	0,13
QV	12,0	24,0	3,10	12,4	4,85	0,06	5,68	1,34	9,46	2,35	6,04	1,01	6,37	0,98
QS	16,8	33,0	4,22	15,8	5,71	0,20	10,3	3,11	23,1	5,76	14,2	2,13	12,5	1,88
Po1W	21,9	329	9,88	43,4	16,1	0,35	14,8	2,28	12,2	2,37	5,98	0,92	5,99	0,90
Po1F	6,13	19,0	1,54	5,94	2,39	0,03	2,65	0,61	4,51	1,06	2,80	0,46	3,09	0,51

Appendix D
Others

D1 Geological time scale

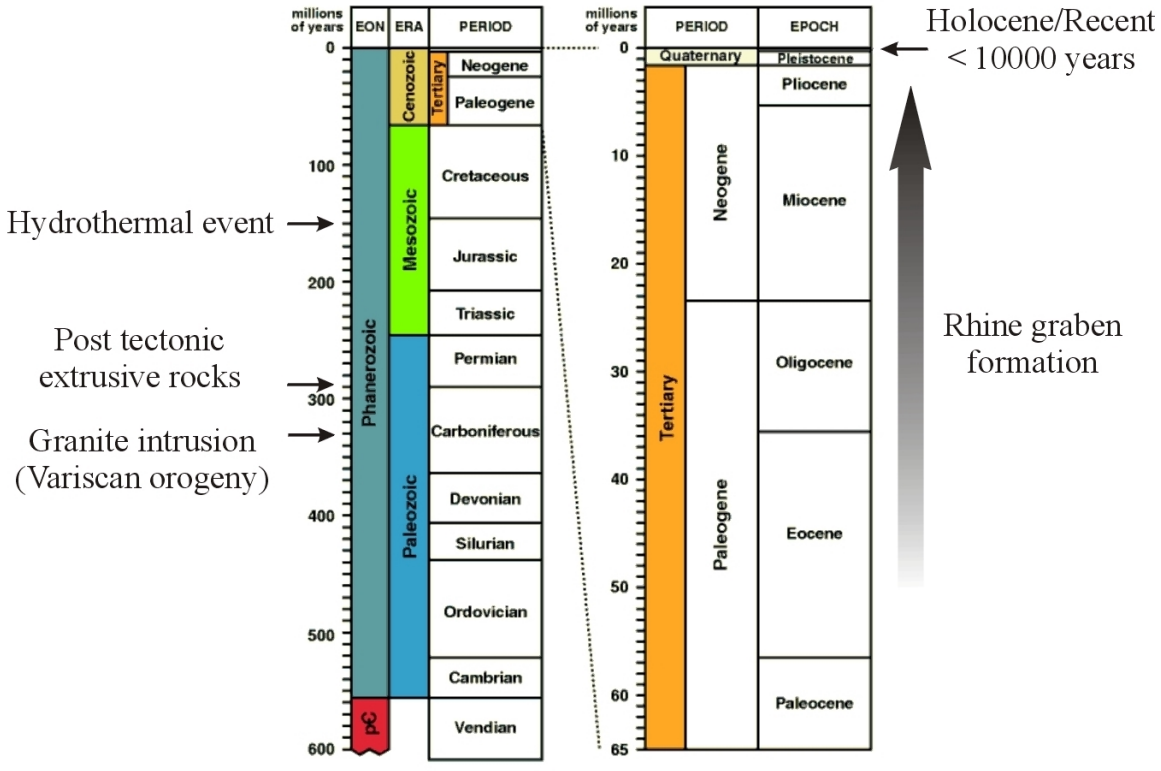

Source: http://www.nearctica.com/paleo/tectonic.htm

D2 Geological map

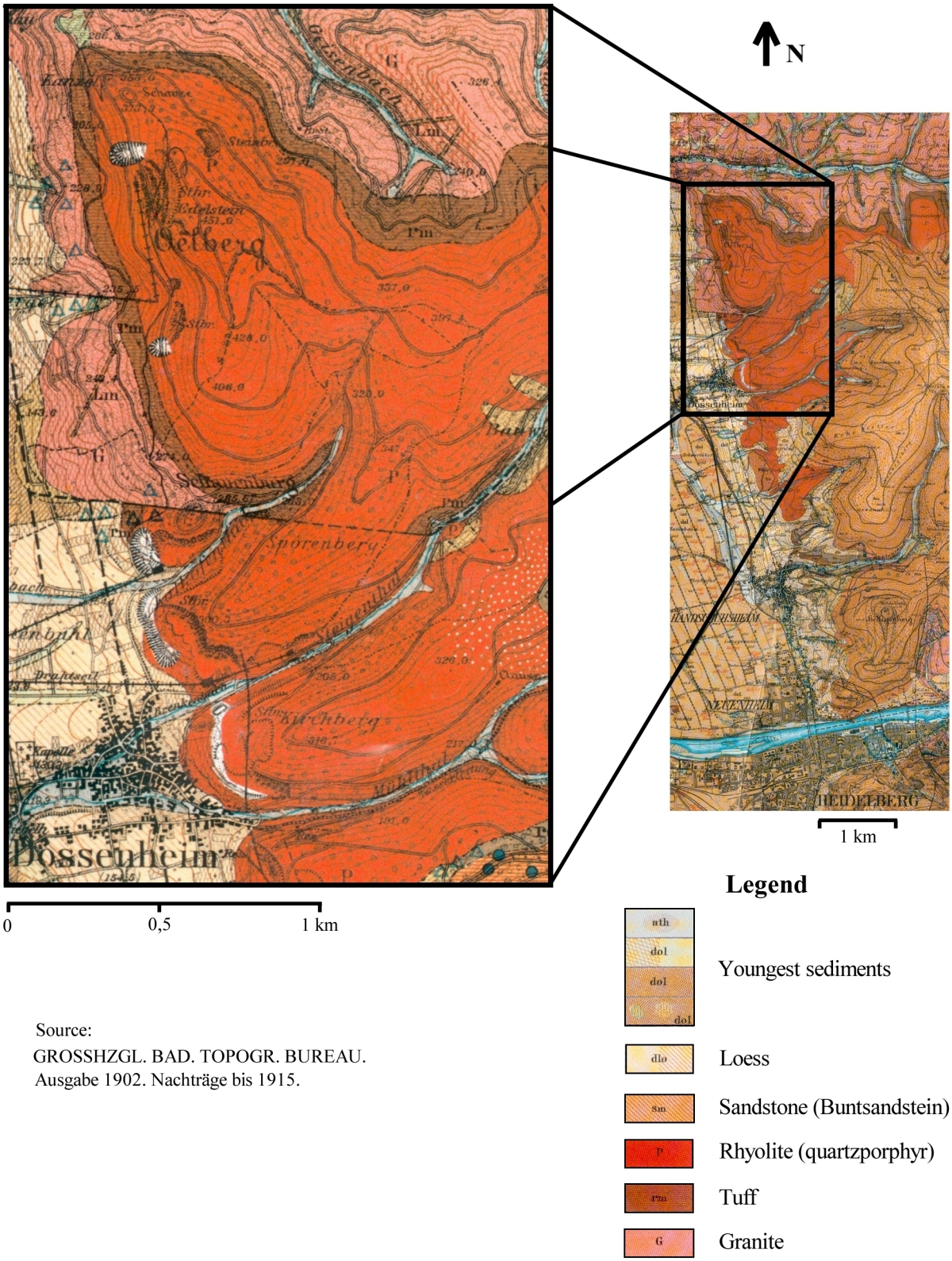

Source:
GROSSHZGL. BAD. TOPOGR. BUREAU.
Ausgabe 1902. Nachträge bis 1915.

D3 The Schauenburg castle

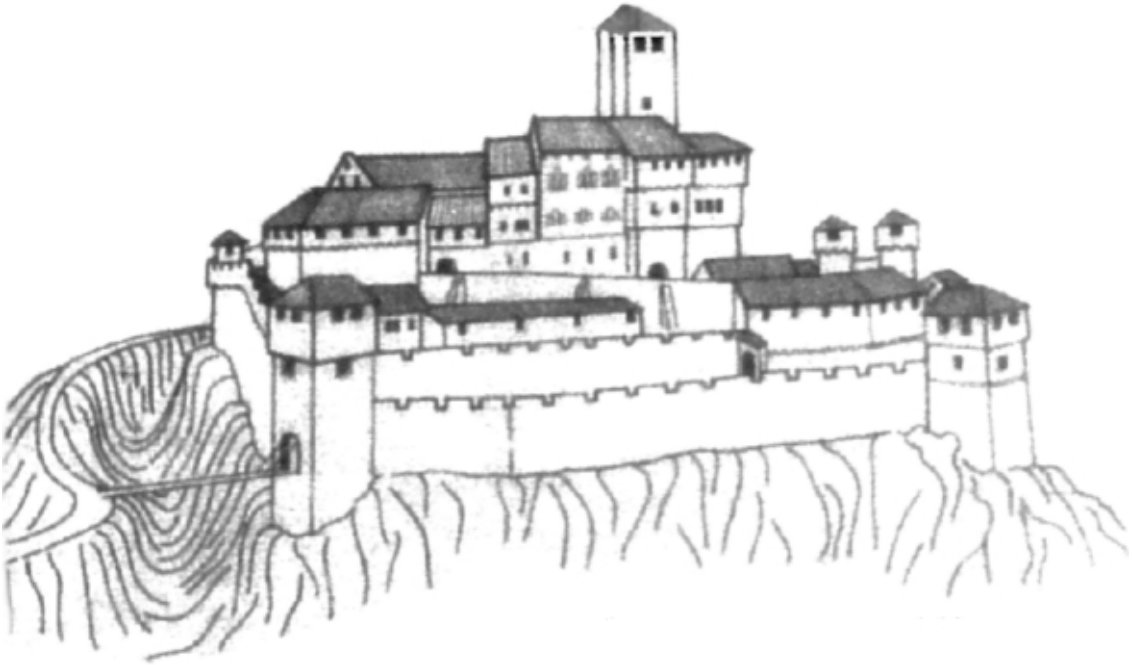

(modified from Mannheimer Geschichtsblätter)

The castle Schauenburg was built around the year 1100 by the monastery Lorsch for the safeguarding and administration of the tenures. The castle beneficiary is "Gerhard von Schauenburg", which descendants got the dominion over the communities Dossenheim, Handschuhsheim and Seckenheim. Around 1280 dies the Schauenburg stock and the castle belongs thereby to the episcopate Speyer. The episcopate Mainz acquires the castle in 1320. The castle undergoes the quarrels between Mainz and the Kurpfalz. In the middle of the 15th century, Friedrich I allows the castle break down after the surrender of the garrison. Since then lies the castle open and the stones are used for the construction of the neighbors houses (Mannheimer Geschichtsblätter).

The silver exploitation in Schriesheim and surroundings began around the year 1470 and the Dossenheim and Schriesheim very steeler rhyolite was already employs by the roman for the road construction.

D4 The Odenwald

The Odenwald is further subdivided into two zones, based mainly on petrological and geochronological constraints. In the eastern segment is the Buntsandstein Odenwald with the Rotliegenden, Zechstein and Buntsandstein layers. In the west lies the crystalline Odenwald (fig. d4.1). On basis of lithologic, structural, and tectonic features, the crystalline Odenwald can be subdivided into four units (Krohe, 1991; Krohe and Willner, 1995). The "Böllstein Odenwald" forms the northeastern separate unit IV (fig. d4.1). It forms a dome-like structure with a core of granitic to granodioritic gneisses and an envelope of predominantly metapsammitic schists, both with intercalations of metabasites (Chatterjee, 1960; Nickel, 1975). The "Bergsträsser Odenwald" is divided in unit I to III and lies between Heidelberg and Darmstadt (fig. d4.1). Unit III is influenced by many SSW-NNE disturbances. Three main intrusive bodies are situated in unit III, which are the Trommgranit (TP), the Weschnitzpluton (Granodiorit, WP) and the Heidelberg granite pluton (HIC) which contains the working area.

The Heidelberg Intrusive Complex (HIC) consists of gabbros and diorites which were successively intruded by granodiorites and granites. The mafic types are composed of variable amounts of plagioclase, amphibole, clinopyroxene, biotite, and, in places, secondary muscovite (Okrusch et al., 2000). The Heidelberg granite contains euhedral phenocrysts of K-feldspar in a medium grained matrix of plagioclase (An_{30-12}), quartz and biotite, with accessory titanite, apatite, zircon, magnetite, and rare tourmaline (Maggetti, 1975). An intrusion depth of about 15 km was estimated for a quartz-diorite and granite of the HIC. The HIC magma presumably originates from a metabasaltic to metatonalitic source (Altherr et al., 1999).

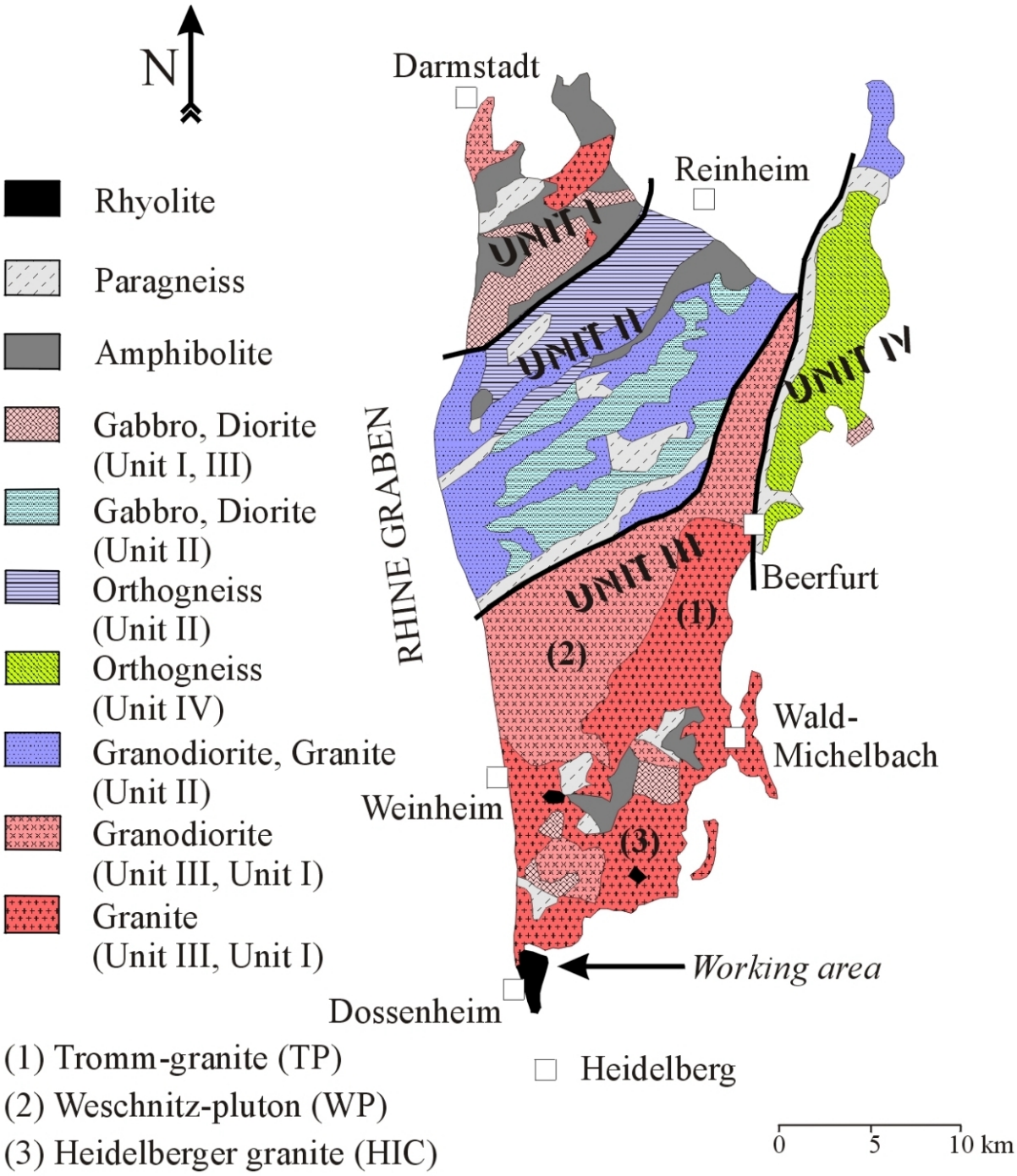

Figure d4.1: Geological map of the crystalline Odenwald (modified after Okrusch et al., 2000).

D5 The Variscan orogeny

Late Devonian 370 Ma

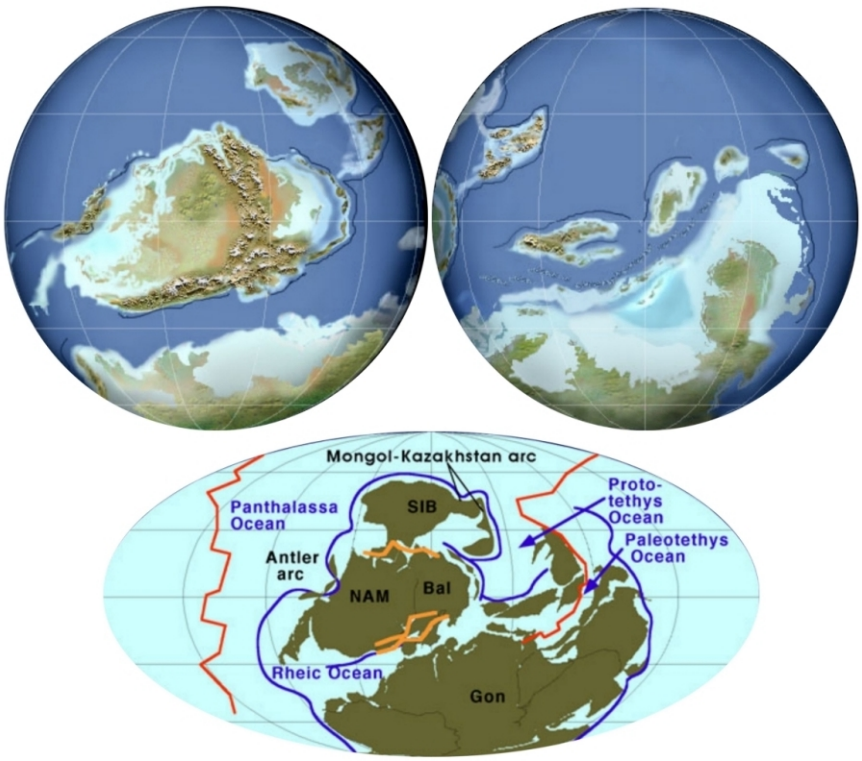

Early Mississippian 340 Ma

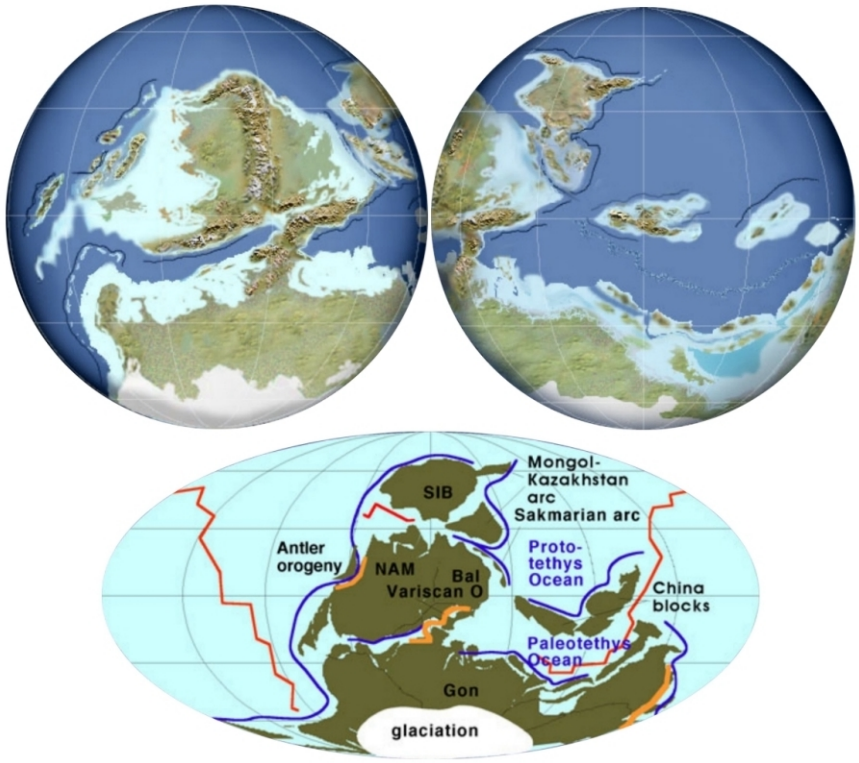

Source: http://www.nearctica.com/paleo/tectonic.htm
Comment: page 13

Late Pennsylvanian 300 Ma

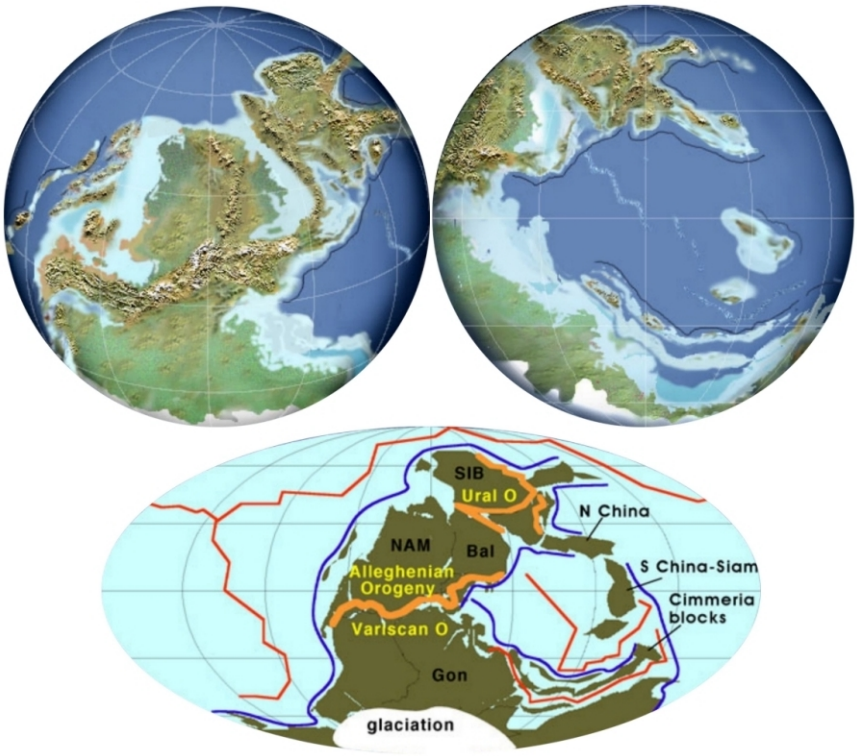

Early Permian 270 Ma

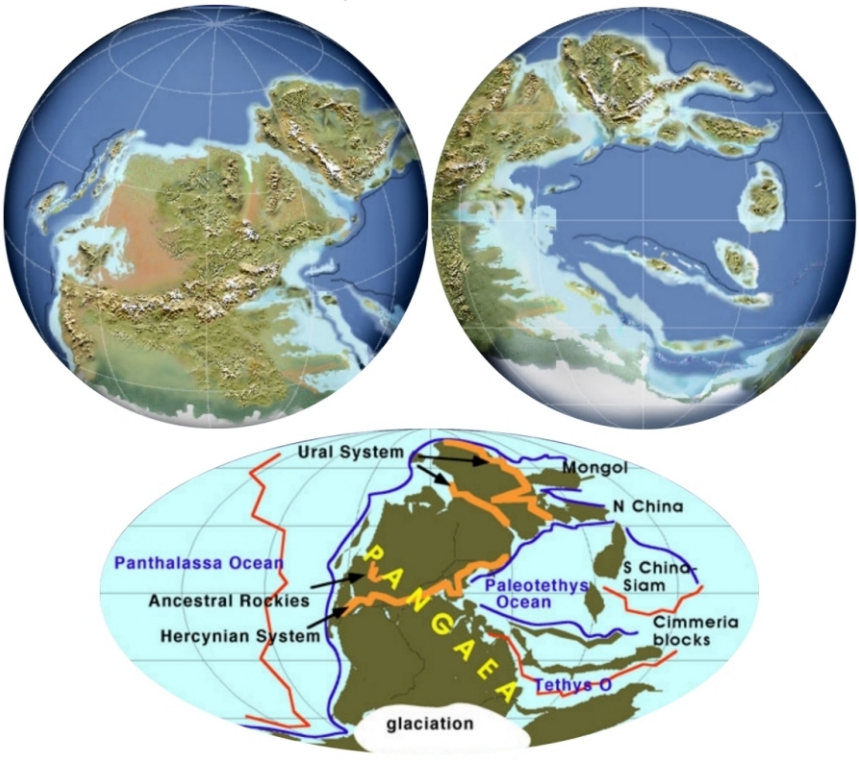

References

- ALTHERR R., HENES-KLAIBER V., HEGNER E., SATIR M. AND LANGER C. (1999) Plutonism in the Variscan Odenwald (Germany): from subduction to collision. *Int. Jour. Earth Sciences* **88**, 422-433.
- ANDERS E. AND GREVESSE N. (1989) Abundances of the elements: Meteoritic and solar. *Geochim. Cosmochim. Acta* **53**, 197-214.
- ANDRAE A. AND OSANN A. (1893) Erläuterungen zur Geologie des Blattes Heidelberg. 5. Auflage von Hans Thürach (1995) *Mitt. Bad. Geol. L.-Anst.* **2**, 345-388.
- AUDÉTAT A., GÜNTHER D. AND HEINRICH C. A. (2000) Magmatic-hydrothermal evolution in a fractionating granite: A microchemical study of the Sn-W-F-mineralized Mole Granite (Australia). *Geochim. Cosmochim. Acta* **64**, 3373-3393.
- BATZLE M. L. AND SIMMONS (1977) Geothermal systems: rocks, fluids, fractures. *American Geophysical Union Monograph* **20**, 233-242.
- BAU M. (1996) Controls on the fractionation of isovalent trace elements in magmatic and aqueous systems :evidence from Y/Ho, Zr/Hf and lanthanide tetrad effect. *Contrib. Mineral. Petrol.* **123**, 323-333.
- BLUM J. D., EREL Y. AND BROWN K. (1994) $^{87}Sr/^{86}Sr$ ratios of Sierra Nevada stream waters: Implications for relative mineral weathering rates. *Geochim. Cosmochim. Acta* **58**, 5019-5025.
- BOLLHÖFER A., EISENHAUER A., FRANK N., PECH D. AND MANGINI A. (1996) Th- and U-isotopes in a Mn-nodule from the Peru Basin determined by alpha spectrometry and Thermal Ionisation mass spectrometry: Are manganese supply and growth related to climate? *Geol. Rundschau*. **85**, 577-585.
- BROOKS C. (1968) Relationship between feldspar alteratio and the precise post-crystallization movement of rubidium and strontium isotopes in a granite. *Journal of Geophysical Research* **73**, 4751-4757.

- CAMERON A. E., SMITH D. H. AND WALKER R. L. (1969) Mass spectometry of nanogram-size samples of lead. *Anal. Chem.* **41**, 525-526.
- CATANZARO E. J. (1968) Absolute isotopic abundance ratios of three common lead reference samples. *Earth and Planetary Science Letters* **3**, 343-346.
- CATANZARO E. J., MURPHY T. J., GARNER E. L. AND SCHIELDS W. R. (1969) Absolute isotopic abundance ratio and atomic weight of terrestrial rubidium. *J. Res NBS* **73A**, 511-516.
- CHATTERJEE N. D. (1960) Geologische Untersuchungen im Kristallin des Böllsteiner Odenwaldes. *Neues Jahrb. Geol. Paläont. Abhandl.* **37**, 223-256.
- CHEN J. H., EDWARDS R. L. AND WASSERBURG G. J. (1986) ^{234}U, ^{238}U and ^{232}Th in seawater. *Earth Planet. Sci. Lett.* **80**, 241-251.
- CHENG H., EDWARDS R. L., HOFF J., GALLUP C. D., RICHARDS D. A. AND ASMEROM Y. (2000) The half-lives of uranium-234 and thorium-230. *Chemical geology* **169**, 17-33.
- CHESWORTH W. (1992) Weathering systems. *Weathering, Soils and Paleosols* (ed. I. P. Martini and W. Chesworth), 19-40, New York, Elsvier.
- CLAUER N., ZWINGMANN H. AND CHAUDHURI S. (1996) Extent and importance of the liassic hydrothermal activity in Western Europe based on isotopic constraints from contemporaneous mica-type minerals. *Clay Min*. **31**, 301-318.
- DICKIN A. P. (1997) Rodiogenic Isotope Geology. *Cambridge University Press*, 490 pages.
- DODSON M. H. (1963) A theoretical study of the use of internal standards for precise isotopic analysis by the surface ionisation technique: Part I – General first-order algebraic solutions. *J. Sci. Instrum.* **40**, 289-295.
- DOE B. R. (1970) Lead isotopes. *Springer-Verlag*, Berlin, Heidelberg, and New York, 137 pages.
- EBERHARDT A., DELWICHE R. AND GEISS Z. (1964) Isotopic effects in single filament thermal ion sources. *Z. Natur* **19a**, 736-740.
- EDWARDS R. L., BECK J. W., BURR G. S. ET AL. (1993) A large drop in atmospheric $^{14}C/^{12}C$ and reduced melting in the Younger Dryas, documented with ^{230}Th ages of corals. *Science* **260**, 962-968.
- EDWARDS R. L., CHEN J. H. AND WASSERBURG G. J. (1987) ^{238}U-, ^{234}U-, ^{230}Th-, ^{232}Th systematics and the precise measurement of time over the past 500,000 years. *Earth Planet. Sci. Lett.* **81**, 175-192.
- EISBACHER G. H. (1991) Einführung in die Tektonik. *Ferdinand Enke Verlag*, Stuttgart, 310 pages.

- EISENHAUER A., WASSERBURG G. J., CHEN J. H. ET AL. (1993) Holocene sea-level determination relative to the Australian continent: U/Th (TIMS) and ^{14}C (AMS) dating of coral cores from the Aborlhos Islands. *Earth Planet. Sci. Lett.* **114**, 529-547.
- ELIAS R. W., HIRAO Y. AND PATTERSON C. C. (1982) The circumvention of the natural biopurification of calcium along nutrient pathways by atmospheric inputs of industrial lead. *Geochim. et Cosmochim. Acta*, **46**, 2561-2580.
- EREL Y., HARLAVAN Y. AND BLUM J. D. (1994) Lead isotope systematics of granitoid weathering. *Geochim. Cosmochim. Acta* **58**, 5299-5306.
- FARMER G. L. AND DEPAOLO D. J. (1987) Nd and Sr isotope study of hydrothermally altered granite at San Manuel, Arizona; implications for element migration paths during the formation of porphyry copper ore deposits. *Economic Geology and the Bulletin of the Society of Economic Geologists* **82**, 1142-1151.
- FAURE G. (1991) Principles and Applications of inorganic Geochemistry. *Macmillan Publ. Co*.
- FAURE G. AND POWELL J. L. (1972) Strontium isotope geology. *Springer-Verlag*, Berlin, New York, 188 pages.
- FRANK N. (1997) Anwendung der Thermionen Massenspektrometrie zur Uranreihen Datierung von pleistozänen mitteleuropäischen Travertinen. *Ph. D. Thesis*, University of Heidelberg.
- GAUPP R., MATTER A., PLATT J., RAMSEYER K. AND WALZEBRUCK J. (1993) Diagenesis and fluid evolution of deeply buried Permian (Rotliegend) Gas Reservoirs, Northwest Germany. *Am. Assoc. Petrol. Geol. Bull.* **77**, 1111-1128.
- GEYER O. F. AND GWINNER M. P. (1991) Einführung in die Geologie von Baden Württemberg. *Schweizerbartsche Verlagsbuchhandlung Stuttgart*, 482 pages.
- GOLDICH S. S. (1938) A study in rock-weathering. *Agricultural and Mechanical College of Texas*, 17-58.
- GROMET L. P., SILVER L. T. (1983) Rare earth element distributions among minerals in a granodiorite and their petrogenetic implications. *Geochimica et Cosmochimica Acta* **47**, 925-940
- GU Z. Y., LAI D., LIU T. S., GUO Z. T., SOUTHON J. AND CAFFEE M. W. (1997) Weathering histories of Chinese loess deposits based on uranium and thorium series nuclides and cosmogenic ^{10}Be. *Geochim. Cosmochim. Acta* **61**, 5221-5231.
- HAN KECHONG AND WANG XUEMENG (1983) Argillitization in fault zones. *Diqiu Huaxue = Geochimica* **1983**, 213-220.

- HARLAVAN Y., EREL Y. (2002) The release of Pb and REE from granitoids by the dissolution of accessory phases. *Geochim. Cosmochim. Acta* **66**, 837-848.
- HESS J. C. AND LIPPOLT H. J. (1996) Numerische Stratigraphie permokarbonischer Vulkanite Zentraleuropas. Teil III: Odenwald. *Geol. Jb Hessen* **124**, 39-46.
- HOOPER E. C. D. (1991) Fluid migration along growth faults in compacting sediments. *Journal of Petroleum Geology* **14**, 161-180.
- IRBER W. (1999) The lanthanide tetrad effect and its correlation with K/Rb, Eu/Eu*, Sr/Eu, Y/Ho, and Zr/Hf of evolving peraluminous granite suites. *Geochim. Cosmochim. Acta* **63**, 489-508.
- IVANOVICH M. AND HARMON R. S. (1992) Uranium-series Disequilibrium. *Oxford Science Publications*, **2nd edn.**, 899 pages.
- JAFFREY A. H., FLYNN K. F., GLENDENIN L. E., BENTLEY W. C. AND ESSLING A. M. (1971) Precision measurement of the half-lives and specific activities of ^{235}U and ^{238}U. *Phys. Rev.* **C4**, 1889-1907.
- KATZ A. J., THOMPSON A. H. (1987) Quantitative prediction of permeability and electrical conductivity in porous rock. *Geophysics* **52**, 378 pages
- KIRSCH H. (1989) $^{40}Ar/^{39}Ar$-chronologische und mineralogische Untersuchungen zur Sericitisierung von Plagioklasen. *Ph. D. Thesis*, University of Heidelberg, 232 pages.
- KIRSCH H., KOBER B. AND LIPPOLT H. J. (1988) Age of intrusion and rapid cooling of the Frankenstein gabbro (Saxothuringian zone) evidenced by $^{40}Ar/^{39}Ar$ and single zircon $^{207}Pb/^{206}Pb$ measurements. *Geol.Rundsch.* **77**, 693-711.
- KOBER B. (1983) Gesteins- und Mineral- Analysen des südlichen Schwarzwaldes. *Ph. D. Thesis*, University of Heidelberg, 206 pages.
- KOMNINOU A., AND YARDLEY W. D. (1996) Fluid-rock interactions in the Rhine Graben: A thermodynamic model of the hydrothermal alteration observed in deep drilling. *Geochim. Cosmochim. Acta* **61**, 515-531.
- KOSTITSYN Y. A. AND KREMENETSKIY A. A. (1995) Time span between whole rock and mineral isochrone ages for the youngest Eldjurta granite body, and ist sense implying from Sr and O isotopic data. *Terra Abstracts* **17**, 155.
- KROHE A. (1991) Emplacement of synkinematic plutons in the Variscan Odenwald (Germany) controlled by trans tensional tectonics. *Geol. Rundschau* **80**, 391-409.
- KROHE A. AND WILLNER A. P. (1995) The Odenwald Crystalline Complex. In: Dallmeyer R. D., Franke W. and Weber K. (eds). *Pre-Permian geology of central and eastern Europe*, *ICP*, **233**, 174-181.

- LIPPOLT H. J., KISCH H. AND PLEIN E. (1990) Karbonische und permische Vulkanite aus dem Untergrund des nördlichen Oberrheingrabens: Art, Alterbestimmung und Konsequenz. *Jber. Mitt. oberrhein. geol.* **72**, 227-242.
- MAGGETTI M. (1975) Dir Tiefengesteine des Bergsträßer Odenwaldes. *Aufschluss*, **Sonderband 27** (Odenwald), 87-107, Heidelberg.
- MCKAY G. A. (1989) Partitioning of rare earth elements between major silicate minerals and basaltic melts. *Reviews in Mineralogy* **21**, 45-77.
- MERTZ D. (1987) Isotopengeochemische und mineralogische Untersuchungen an postvariscischen hydrothermalen Silikaten. *Ph. D. Thesis*, University of Heidelberg, 207 pages.
- NEFF U., BOLLHÖFER A., FRANK N. AND MANGINI A. (1999) Explaining discrepant depth of $^{234}U/^{238}U$ and $^{230}Th_{exc}$ in Mn-crusts. *Geochimica et Cosmochimica Acta* **63**, 2211-2218.
- NESBITT H. W., YOUNG G. M. (1982) Early Proterozoic climates and plate motions inferred from major element chemistry of lutites. *Nature (London)* **299**, 715-717.
- NICKEL E. (1975) Geologische Position und Petrogenese des Kristallinen Odenwaldes-Aufschluß, **Sdbd. 27**, 1-25, Heidelberg
- OKRUSCH M., SCHBERT W. AND STÄHLE V. (2000) The Odenwald, Germany: Variscan metamorphic evolution and igneous events. *Beih. Z. Eur. J. Mineral.* **12**, 45-89.
- OSMOND J. K. AND COWART J. B. (1982) Ground water. *Uranium series disequilibrium: applications to environmental problems*, **1st** edn. (eds. M. Ivanovich and R. S. Harmon), 202-245.
- OSMOND J. K. AND IVANOVICH M. (1992) Uranium series mobilization and surface hydrology. Uranium series Disequilibrium: Applications to Earth. *Marine and Environmental Sciences,* **2nd Ed**., 260-289.
- POWER W. L., TULLIS T. E., BROWN S., BOITNOTT G. N. AND SCHOLZ C. H. (1987) Roughness of natural fault surfaces. *Geophysical Research Letters* **14**, 29-32.
- PRIBNOW D. AND CLAUSER C. (1999) Heat- and fluid-flow at the Soultz hot-dry-rock system in the Rhine Graben. *Journal of Conference Abstracts*, **4**, 846 pages.
- RECIO C., FALLICK A. E., UGIDOS J. M. AND STEPHENS W. E. (1997) Characterization of multiple fluid-granite interaction processes in the episyenites of Avila-Bejar, central Iberian Massif, Spain. *Chemical Geology* **143**, 127-144.
- RUTHERFORD E. AND SODDY F. (1902) The radioactivity of thorium compounds II. The cause and nature of radioactivity. *Nature* **307**, 245-247.

- SAMUEL J., ROUAULT R. AND BESNUS Y. (1985) Analysis multi-élémentaire standardisée des matériaux géologiques en spectrométrie d'émission par plasma à couplage inductif. *Analysis* **13**, 312-317.
- SAUSSE J. (2002) Hydromechanical properties and alteration of natural fracture surfaces in the Soultz Granite (Bas-Rhin, France). *Tectonophysics* **348**, 169-185.
- SAUSSE J., JACQUOT E., FRITZ B., LEROY J. AND LESPINASSE M. (2002) Evolution of crack permeability during fluid-rock interaction; example of the Brezouard Granite (Vosges, France). *Tectonophysics* **336**, 199-214.
- SAWKA W. N., CHAPPELL B. W. (1988) Fractionation of uranium, thorium and rare earth elements in a vertically zoned granodiorite; implications for heat production distributions in the Sierra Nevada Batholith, California, U.S.A. *Geochimica et Cosmochimica Acta*, **52**, 1131-1143.
- SCHALTEGGER U. (1990) Post-magmatic resetting of Rb-Sr whole rock ages; a study in the Central Aar Granite (Central Alps, Switzerland). *Geologische Rundschau* **79**, 709-724.
- SCHLEICHER A. (2001) Niedrig temperierte Alterationsprodukte in felsischen Gesteine am Beispiel der Schauenburgstörung, östliche Rheingrabenschulter bei Heidelberg. *Master of Science*, University of Heidelberg, 115 pages.
- SCHUMACHER M. E. (2002) Upper Rhine Graben: Role of preexisting structures during rift evolution. *Tectonics* **21**, 1-17.
- SCHWEIZER V. (1996) Kraichgau und südlicher Odenwald. *Sammlung geolog. Führer* **72**, 202 pages.
- SENGÖR A. M. C., BURKE K. AND DEWEY J. F. (1978) Rifts at high angles to orogenic belts: Tests for their origin and the upper Rhine Gragen as an example. *Amer. J. Sci.* **278**, 24-40.
- SIBSON R. H. (1994) Crustal stress, faulting and fluid flow. *Geological Society Special Publication* **78**, 69-84.
- SIMON K. (1990) Hydrothermal alteration of Variscan granites, southern Schwarzwald, Federal Republik of Germany. *Contributions to Mineralogy and Petrology* **105**, 177-196.
- SITTLER C. (1992) Illustration de l'histoire géologique du Fossé rhénan et de l'Alsace. *N. Jb. Geol. Palaeont.* **Abh. 186**, 255-282.
- SMITH D. A. (1980) Sealing and non sealing faults in Louisiana Gulf Coast Salt Basin. *American Association of Petroleum Geologists Bulletin* **64**, 145-172.
- STILLE P. AND SHIELDS G. (1997) Radiogenic Isope Geochemistry of Sedimentary and Aquatic Systems. *Lecture Notes in Earth Sciences* **68**, 217 pages.

- STILLE P., GAUTHIER-LAFAYE F., LOUVAT D., BRACKE G. AND SALAH S. (1999) REE migration in groundwater close to the natural fission reactor of Bangombe (Gabon); evidence from Sm-Nd isotope data. *Journal of Conference Abstracts* **4**, 521 pages.
- STURCHIO N. P. (1994) Uranium-Series Ages of Travertines and Timing of the Last Glaciation in the Northern Yellowstone Area, Wyoming-Montana. *Quarter. Res.* **41**, 265-277.
- SURMA F. AND GERAUD Y. (2003) Porosity and thermal conductivity of the Soultz-Sous- Forêts granite, *Pageoph* **160**, N° 5-6 (in press).
- Taylor S. R. and Mclennan S. M. (1985) The Continental Crust: Its Composition and Evolution. *Blackwell Scientific Publications*, London.
- TECHER I., LANCELOT J., CLAUER N., LIOTARD J. M. AND ADVOCAT T (2001) Alteration of a basaltic glass in an argillaceous medium: The Salagou dike of the Lodève Permian Basin (France). Analogy with an underground nuclear waste repository. *Geochim. Cosmochim. Acta* **65**, 1071-1086.
- THIEL K., VORWERK R., SAAGER R. AND STUPP H. D. (1983) ^{235}U fission tracks and ^{238}U-series disequilibria as a means to study recent mobilization of uranium in Archaean pyritic conglomerates. *Earth and Planetary Science Letters* **65**, 249-262.
- VELDE B. (1992) Introduction to clay minerals. *Chapman and Hall*, 198 pages.
- VIDAL P. (1998) Géochimie, *Dunod*, 190 pages.
- VILLEMIN T., ALVAREZ F. AND ANGELIER J. (1986) The Rhine graben : Extension, subsidence and shoulder uplift. *Tectonophysics* **128**, 47-59.
- WALTER R. (1992) Geologie von Mitteleuropa. *Schweizerbartsche Verlagsbuchhandlung Stuttgart* **22-33**, 348-352.
- WARR L. N. (2000) the Variscan Orogeny: the welding Pangaea, 271-294. In: Woodcock N. and Strachan R. (ed), Geological History of Britain and Ireland, *Blacwell Science*, 411 pages.
- WEIßHAAR R. (2000) Isotopengeochemie des Heidelberger Neckarschwemmfächers. *Ph. D. Thesis*, 113 pages, University of Heidelberg.
- WHITE A. F., BULLEN T. D., SCHULZ M. S., BLUM A. E., HUNTINGTON T. G. AND PETERS N. E. (2001) Differential rates of feldspar weathering in granitic regoliths. *Geochim. Cosmochim. Acta* **65**, 847-869.
- ZIELINSKI R. A., PETERMAN, Z. E., STUCKLESS J. S., ROSHOLT J. N. AND NKOMO I. T. (1981) The chemical and isotopic record of rock-water interaction in the Sherman Granite, Wyoming and Colorado. *Contributions to Mineralogy and Petrology* **78**, 209-219.

♦ ZWINGMANN H., CLAUER N., AND GAUPP R. (1999) Structure-related geochemical (REE) and isotopic (K-Ar, Rb-Sr, $\delta^{18}O$) characteristics of clay minerals from Rotliegend sandstone reservoirs (Permian, northern Germany). *Geochim. Cosmochim. Acta* **63**, 2805-2823.

Epilog

Acknowledgements – Danksagung – Remerciements

Here, I would like to thank all people, who have continuously supported me during the course of this thesis and who have helped me in the successful completion of this work

Herrn Prof. Dr. Augusto Mangini danke ich für die Ermöglichung dieser Arbeit. Durch seine Vorschläge und Anregung gab er mir immer wieder Impulse, die mich voranbrachten und zum Gelingen der Dissertation beitrugen. Er ließ mir zudem immer völlig freie Hand bei der Arbeit.

Herrn Priv. Doz. Dr. Laurence Warr danke ich für die freundliche Übernahme der Begutachtung. Außerdem war er trotz seines zunehmendes Berges an Arbeit, spontan bereit mir bei der englische Fassung der Ausarbeitung zu helfen. Ich danke ihm auch für die hilfreichen Diskussionen und kritischen Anmerkungen.

Mein besonderer Dank gilt Herrn Dr. Bernd Kober. Er zeigte stets Begeisterung für mein Thema und hatte viele Ideen und wertwollen Ratschläge auf lager zur Interpretation der Messergebnisse. Ich danke ihm auch für dir motivierenden Gespräche und seine wohlwollende Unterstützung.

Didi Pingel aus dem Institut für Umweltgeochemie, herzlichen Dank für die Unterstützung bei den Rubidium-Strontium Isotopenanalysen.

Mein Dank gebührt auch Diplom Geol. Anja Schleicher. Die Zusammenarbeit habe ich als äußerst angenehm empfunden. Ohne ihre „geologischen-mineralogische“ Hilfe hätte ich niemals die Untersuchung so erfolgreiche durchführen können. An dieser Stelle danke ich auch Sven Traxel, der die Mineral Separat gemacht hat.

Je tiens également à remercier les amis et collègues du Centre de Géochimie de la Surface de Strasbourg, notamment Fabrice Surma, Céline Tomachot et monsieur Yves Géraud pour les mesures de porosité. Un grand merci à monsieur Peter Stille pour les intéressantes discussions et l'aide qu'il a pu m'apporter. Je voudrais également remercier Jean Samuel et Robert Rouault pour l'aide apportée durant les mesures ICP-AES et ICP-MS et monsieur François Chabaux pour m'avoir permis d'effectuer ces mesures à Strasbourg.

Alle Freunden und Kollegen in meiner Arbeitsgruppe danke ich besonders für das hervorragende Arbeitsklima. Um euch kennen zu lernen und neue Freundschaften zu entwickeln hat es sich gelohnt die Doktorarbeit zu schreiben. Vive les Palaeos!!! Besonders zu nennen sind :

Steffen der mir als Korrekturleser sehr geholfen hat, Clemens W-ioda crossing the gangues, Stephan (DOASele im Angebot), Marcus (Druckerexperte), Denis (virtual correction!), Sibylle, Andrea, Dirk, Elke, Margarita, René, Uli, Chrisi, Rainer. Bestimmt habe ich jemand vergessen, bitte nicht ärgern!

Le meilleur je l'ai gardé pour la fin. Je tiens à remercier de tout cœur mes parents, ma sœur Stéphanie, mon frère Gilles, ainsi que toute ma famille et mes amis (la liste serait, par bonheur, trop longue à citer) qui avec leur intérêt pour mon travail et mes études, m'ont continuellement motivé et soutenu. C'est à vous que je dédie ma thèse.

Die Arbeit wurde finanziell gefördert von der Deutschen Forschungsgemeinschaft (DFG) im Rahmen des Graduiertenkolleg 237, Einwirkung Fluider Phasen auf Locker- und Festgesteine.